Mineralogy of phosphate accumulations in the Huber stock, Krásno ore district, Slavkovský les area, Czech Republic

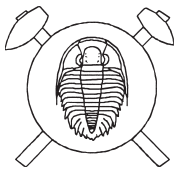

Mineralogie akumulací fosfátů oblasti Huberova pně, rudní revír Krásno, Slavkovský les, Česká republika

(91 figs, 31 tabs)

JIŘÍ SEJKORA[1] – RADEK ŠKODA[2] – PETR ONDRUŠ[3] – PAVEL BERAN[4] – CTIBOR SÜSSER[5]

[1] *Department of Mineralogy and Petrology, National Museum, Václavské nám. 68, CZ-115 79 Praha 1, Czech Republic*
[2] *Institute of Geological Sciences, Masaryk University, Kotlářská 2, CZ-611 37, Brno, Czech Republic*
[3] *Biskupský dvůr 2, CZ-110 00 Praha 1, Czech Republic*
[4] *Regional Museum Sokolov, Zámecká 1, Sokolov, CZ-356 00, Czech Republic*
[5] *Karla Čapka 1357, Sokolov, CZ-356 01, Czech Republic*

The present detailed research is focused on minerals of phosphate accumulations collected in the Huber open pit and at the 5th level of the Huber shaft, Krásno ore district, Slavkovský les area, Czech Republic. The following minerals have been identified at the studied localities: benyacarite, beraunite, cacoxenite, chalcosiderite, crandallite, dufrénite, earlshannonite, fluellite, fluorapatite, frondelite, goyazite, isokite, kolbeckite, leucophosphite, morinite, natrodufrénite, phosphosiderite, rockbridgeite, strengite, triplite, turquoise, vivianite, wavellite, waylandite, whitmoreite and zwieselite. A brief review of evolution of the phosphate mineral associations at the two studied localities is presented.

Key words: Huber stock; Krásno near Horní Slavkov; Slavkovský les area; greisen; phosphate minerals; mineralogy; X-ray powder diffraction data; chemical data.

Introduction

Phosphate accumulations of variable size represent a relatively common minor component of greisen bodies and associated quartz veins (Beran – Sejkora 2006). Their occurrence in greisen is localized in masses of white compact quartz, showing at places coarse-grained structure. Our research included a detailed study of phosphate accumulations exposed at various places of the floor of the Huber open pit. The accumulations vary in size from several millimetres up to 30 cm. Late hydrothermal to probably supergene alterations are a characteristic feature.

The second set of samples studied comes from a well-documented phosphate accumulation encountered at the 5th level of the Huber shaft of the Stannum mine. No indications of historical mining have been found in this subarea. The crossing of P-5025030 and M-5025034 galleries exposed an irregular mass of white compact quartz. The observed part of this quartz body was triangular in plan, with dimensions of 10 by 5 to 6 m, sited in greisen and in greisenized granite. One meter wide mass of coarse-grained topaz greisen, at places replaced by hematite and carrying oxidic Bi minerals, was exposed in the margin of the quartz mass in the M-5025034 gallery. Phosphate masses consisting of dominant fluorapatite and triplite from 10 cm to 1 m in size were excentrically located in white quartz mass at the right side of the same gallery. Aggregates of dark Fe-Mn phosphates with predominating frondelite occurred along contacts of phosphate accumulations with white quartz and cavernous corroded portions carrying crystals of younger phosphates (strengite, turquoise-chalcosiderite etc.). For comparison, two historical museum samples have been studied: *NMCR* P1N 18.583 collected by F. X. Zippe before 1842 and sample 18.585 collected by V. Wraný before 1902). The samples with original labels "triplite, Horní Slavkov" probably come from the Gellnauer vein system, as indicated by the time of collection.

Beran (1999) described other large phosphate accumulations from the VIIIth level of the Schnöd stock. At this place, white quartz carried 1 m large triplite blocks associated with fluorapatite. The phosphate masses were deformed and partly brecciated. At the Xth level of the same mine triplite aggregates (up to some dm in size) occurred in association with fluorapatite and siderite. However, no samples were available for our study from these occurrences.

Methods of mineral identification

The surface morphology of samples was studied with the optical microscope Nikon SMZ1500 in combination with the digital camera Nikon DXM1200F, used for photography in incadescent light. Detailes of surface morphology were studied in secondary electron images using the scanning electron microscopes Jeol JSM T-20 (Z. Mach, Institute of fine ceramics, Karlovy Vary) and Jeol JSM-6380 (J. Sejkora and J. Plášil, Faculty of Science, Charles University, Prague).

If not stated otherwise, all minerals described in this paper were identified by X-ray powder diffraction analysis. To minimize complicated shape of background due to classic glass sample holder, the samples studied were placed on the surface of flat silicon wafer from suspension in ethanol. Step-scanned powder diffraction data were collected using following instruments:

HZG4-AREM/Seifert diffractometer (National Museum, Prague) with a copper tube was operated at high-voltage 50 kV and tube current of 40 mA; and Philips X'Pert MPD diffractometer (Czech Geological Survey, Prague) with a metallo-ceramic copper tube was operated at high-voltage of 40 kV and tube current of 40 mA. A graphite secondary monochromator has been used to produce Cu$K\alpha_1\alpha_2$ radiation. The results were processed using X-ray analysis software ZDS for DOS (Ondruš 1993), Bede ZDS Search/Match ver. 4.5 (Ondruš – Skála 1997); unit-cell parameters were refined by program of Burnham (1962) and by program FullProf (Rodríguez – Carvajal 2005).

Quantitative chemical data were collected with the electron microprobe Cameca SX 100 (J. Sejkora and R. Škoda, Laboratory of electron microscopy and microanalysis of Masaryk University and Czech Geological Survey, Brno). Studied samples were mounted in the epoxide resin discs and polished. The polished surfaces were coated with carbon layer 250 Å thick. Wavelength dispersion mode and operating voltage of 15 kV were used in all analyses. The beam current and diameter were adjusted to stability of analyzed phases under the electron beam. Stable phases were analyzed using 20 nA current and 2 μm beam diameter. Less stable and highly hydrated minerals were analyzed using 10–4 nA and 10–30 μm beam diameter. For smaller aggregates (< 10 μm) of unstable minerals the beam diameter was as large as possible and the applied beam current was only 1–2 nA. The sequence of analyzed elements was adjusted to particular composition of the analyzed mineral. Volatile and major elements were analyzed first, followed by stable, minor and trace elements. Elevated analytical totals of minerals containing a large amount of hydroxyl group or crystal water are generally caused by two factors: a) water evaporation under high vacuum conditions, well documented by collapsed crystals; b) water evaporation due to heating of the analyzed spot by electron beam. The dehydrated domain is seen as a notably brighter spot in backscattered electron images. Lower analytical totals for some samples are primarily caused by their porous nature or by poorly polished surface of soft or cryptocrystalline minerals.

In order to minimize peak overlapping the following analytic lines and crystals were selected: Kα lines: F (PC1, fluorapatite/topaz), Mg (TAP, forsterite), Na (TAP, albite), Al (TAP, sanidine), As (TAP, InAs), Si (TAP, sanidine), Cu (TAP, dioptase), K (PET, sanidine), P (PET, fluorapatite) Ca (PET, andradite), S (PET, barite), Ti (PET, TiO), Cl (PET, vanadinite), Fe (LIF, andradite), Mn (LIF, rhodonite), Ni (LIF, NiO), Zn (LIF, ZnO); Lα lines: Y (TAP, YAG), Sr (PET, $SrSO_4$), La (PET, LaB_6), Ce (PET, $CeAl_2$), Sm (LIF, SmF_3); Lß lines: Ba (PET, benitoite), Pr (LIF, PrF_3), Nd (LIF, NdF_3); Mα lines: Th (PET, ThO_2), Pb (PET, vanadinite); Mß lines: Bi (PET, metallic Bi), U (PET, metallic U). Peak counting times (CT) were 10 to 20 s for main elements and 30 to 60 s for minor and trace elements. CT for each background was ½ of peak time. In case that background was measured only one side of the peak, the counting time was the same as counting on the peak. As far as possible, elements present in minor and trace abundances were measured with highly sensitive crystals LPET a LLIF. Raw intensities were converted to the concentrations using automatic PAP (Pouchou – Pichoir 1985) matrix correction software package.

Accurate determination of fluorine content in some of the studied phases is important. Where possible, determination of fluorine was verified by measuring peak area (integrated intensity); however, this procedure cannot be applied to triplite-like and apatite-like minerals. This control was done irrespective of the note by Raundsep (1995) that with multilayer crystal monochomators (PC1) the effect of matrix is minimal. Fluorine contents measured by the two methods are closely similar.

Review of identified mineral species

Benyacarite $KMn^{2+}_2Fe^{3+}_2Ti(PO_4)_4(OH,F)_3 \cdot 15H_2O$

The rare mineral has been found in small cavities in frondelite from phosphate acumulation at the 5th level of the Huber shaft. Benyacarite forms small brittle and imperfectly developed crystals 0.1 mm in maximum size. The mineral shows one perfect cleavage (Fig. 1) and a greasy lustre.

Owing to small size of the crystals, the Ti-rich Fe-Mn phosphate from Krásno has been identified as a mineral close to benyacarite only on the basis of quantitative chemical analyses (Table 1). After including the theoretical content of H_2O (c. 32 wt.%) the chemical analyses show high totals in the range of 116–120 wt.%. Fransolet *et al*. (1984) found in the course of analysis of the structurally related mineral mantienneite dehydration in

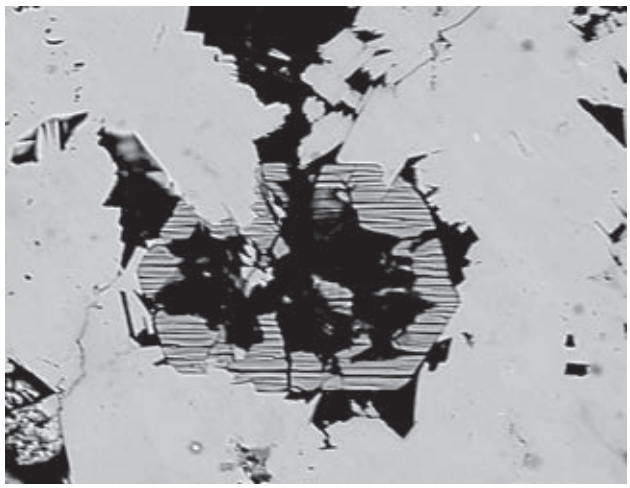

Fig. 1 Imperfect benyacarite crystals in a cavity in frondelite aggregate; dehydration in vacuum resulted in fracturing of the crystal along a single set of perfect cleavages. Width of photo 200 μm. Cameca SX100, BSE photograph by J. Sejkora and R. Škoda.

Table 1 Chemical composition of benyacarite (in wt. %)

	Krásno*1				Cerro Blanco	Hagendorf	Chelyabinsk	theor.
	1	2	3	mean	Argentina*2	Germany*3	Russia*4	*5
Na_2O	0.12	0.02	0.05	0.06	0.20			
K_2O	4.75	4.21	3.58	4.18	1.60	3.91	2.11	4.66
MnO	14.03	15.55	15.89	15.16	11.20	9.63	8.06	14.05
CaO					0.10	0.34		
PbO	0.14	0.00	0.09	0.08				
CuO	0.00	0.07	0.08	0.05				
BaO	0.32	0.03	0.23	0.19				
MgO	0.69	0.52	0.45	0.55	0.30		3.51	
ZnO	0.10	0.00	0.33	0.15				
FeO*	0.73	0.90	0.49	0.71	3.38	5.01	0.00	
Fe_2O_3*	9.98	10.97	11.74	10.90	10.32	9.91	9.18	15.81
Al_2O_3	3.59	2.43	2.32	2.78	0.70	1.60	4.25	
As_2O5	0.00	0.00	0.06	0.02				
P_2O_5	35.14	35.10	36.68	35.64	28.10	28.12	29.37	28.11
TiO_2	14.05	14.85	15.63	14.84	12.30	11.32	8.54	7.91
F	0.35	0.23	0.28	0.29	1.50			
$O\text{-}F_2$	-0.15	-0.10	-0.12	-0.12	-0.63	0.00	0.00	
H_2O**	31.86	31.88	32.18	31.98	29.51	30.21	31.41	29.45
total	115.70	116.65	119.95	117.44	98.58	100.05	96.43	100.00
Na	0.032	0.005	0.012	0.016	0.065	0.000	0.000	
K	0.815	0.723	0.588	0.707	0.343	0.838	0.433	
total M^{1+}	0.847	0.728	0.601	0.723	0.408	0.838	0.433	
Ca	0.000	0.000	0.000	0.000	0.018	0.061	0.000	
Ba	0.017	0.001	0.012	0.010	0.000	0.000	0.000	
Mg	0.138	0.104	0.086	0.109	0.075	0.000	0.842	
Pb	0.005	0.000	0.003	0.003	0.000	0.000	0.000	
Cu	0.000	0.007	0.008	0.005	0.000	0.000	0.000	
Mn^{2+}	1.598	1.773	1.732	1.701	1.595	1.371	1.098	
Zn	0.010	0.000	0.031	0.014	0.000	0.000	0.000	
Fe^{2+}	0.082	0.102	0.052	0.078	0.476	0.705		
total M^{2+}	1.850	1.987	1.924	1.920	2.164	2.136	1.940	
Al	0.569	0.386	0.351	0.434	0.139	0.317	0.806	
Fe^{3+}	1.010	1.111	1.137	1.087	1.306	1.253	1.111	
Ti^{4+}(in M^{3+})	0.421	0.503	0.512	0.479	0.555	0.430	0.033	
total M^{3+}	2.000	2.000	2.000	2.000	2.000	2.000	1.950	
Ti^{4+} (all)	1.421	1.503	1.512	1.479	1.555	1.430	1.033	
Ti^{4+} (in M^{4+})	1.000	1.000	1.000	1.000	1.000	1.000	1.000	
As^{5+}	0.000	0.000	0.004	0.001	0.000	0.000	0.000	
P^{5+}	4.000	4.000	3.996	3.999	4.000	4.000	4.000	
total P+As	4.000	4.000	4.000	4.000	4.000	4.000	4.000	
F	0.148	0.098	0.115	0.120	0.798	0.000	0.000	
H	32.820	33.109	32.842	32.929	32.495	33.541	32.192	
OH	2.820	3.107	2.845	2.923	2.494	3.541	2.197	
OH+F	2.967	3.206	2.960	3.043	3.291	3.541	2.197	
H_2O	15.000	15.001	15.000	15.003	15.001	15.000	14.998	

*1 – this paper; *2 – Demartin *et al.* (1993); *3 – Pollmann *et al.* (1998); *4 – Kydryashova – Rozhdestvenskaya (1991); *5 – theoretical composition of benyacarite $KMn_2Fe_2Ti(PO_4)_4(OH)_3 \cdot 15H_2O$

Empirical formulas were calculated on the basis of P+As = 4.00.

* – Fe_{tot} calculated to FeO and Fe_2O_3 on the basis of M^{3+} and M^{2+} occupancy of the general formula

** – H_2O content calculated from the general formula (H_2O = 15.00) and charge balance

the vacuum of electron microanalyzer; at the same time, dehydration thermal analysis indicates that H_2O begins to escape under relatively low temperatures, including loss of 15 wt. % H_2O below 180 °C. The high totals of analyses, after inclusion of the theoretical content of H_2O, can be explained by dehydration of the studied mineral during preparation of the sample for analysis in vacuum. These conclusions are supported by the presence of regular "dehydration" fractures in the studied sample (Fig. 1).

Data published by Fransolet *et al*. (1984) and Peacor *et al*. (1984) can be used to define a general formula $M^{1+}M^{2+}{}_2M^{3+}{}_2M^{4+}(PO_4)_4(OH,F)_3 \cdot 15H_2O$ for benyacarite and related minerals (mantienneite, paulkerrite). The M^{1+} position of benyacarite from Krásno contains K (0.59–0.82 *apfu*) and minor Na. Demartin *et al.* (1993) supposed on the basis of crystal structure study of benyacarite that K occupies cavities existing within the network of octahedra and tetrahedra, in a similar way as H_2O molecules, and he proposed, in difference with other authors, two M^{1+} positions *pfu* (with H_2O > K). However, no mineral related to benyacarite contains in the M^{1+} position (K+Na) higher than 1 *apfu* (the known maximum is 0.95

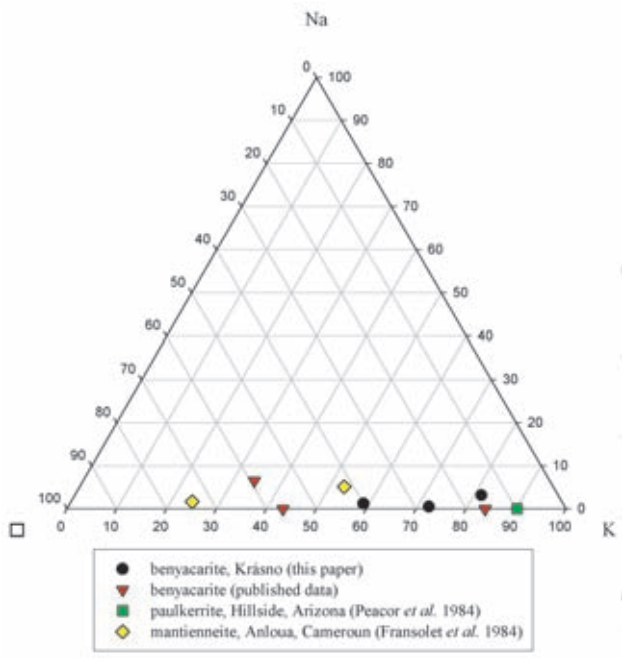

Fig. 2 Ternary plot of M^{1+} site occupancy (atomic ratio) in benyacarite-related minerals; □ – vacancy or H_2O. The published benyacarite data are from Cerro Blanco, Argentina (Demartin *et al.* 1993); Hagendorf, Germany (Pollmann *et al*. 1998); Chelyabinsk, Russia (Kydryashova – Rozhdestvenskaya 1991).

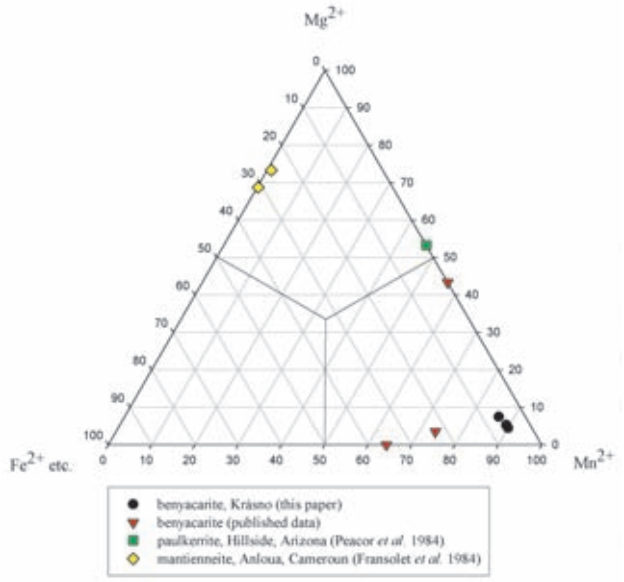

Fig. 3 Ternary plot of M^{2+} site occupancy (atomic ratio) in benyacarite-related minerals; published benyacarite data are from Cerro Blanco, Argentina (Demartin *et al.* 1993); Hagendorf, Germany (Pollmann *et al*. 1998) and Chelyabinsk, Russia (Kydryashova –Rozhdestvenskaya 1991).

apfu). Alternatively, besides the H_2O content (derived solely from the crystal structure study), Fransolet *et al*. (1984) and Peacor *et al*. (1984) prefer the role of vacancies. According to the current rules of the mineralogical system two additional mineral species (Table 2) would be possible to define on the basis of occupancy of the M^{1+} site (Fig. 2). Benyacarite from Krásno exhibits K contents in the M^{1+} position similar to the mineral from Hagendorf (Pollmann *et al*. 1998). The other published analyses of this mineral contain only 0.41–0.43 *apfu* K+Na.

In contrast to published benyacarite analyses (Fig. 3), the material from Krásno has the M^{2+} site strongly dominated by Mn (1.60–1.78) *apfu* (paulkerrite and mantienneite are Mg-dominated). Other elements occur in minor quantities – Mg 0.09–0.14 *apfu*, Fe^{2+} 0.05–0.10 *apfu*, Zn 0–0.03 *apfu*, and Ba, Pb, Cu less than c. 0.01 *apfu*. In the site M^{3+}, occupied mainly by Fe^{3+} (1.01–1.14 *apfu*), significant quantities of Al (range of 0.35–0.57 *apfu*) and Ti^{4+} (0.42–0.51 *apfu*) were found. The site M^{4+} is occupied exclusively by Ti in all benyacarite-related minerals. Surplus Ti contents, reported in majority of published analyses of benyacarite-related minerals, enter the site M^{3+} as indicated above (Fig. 4).

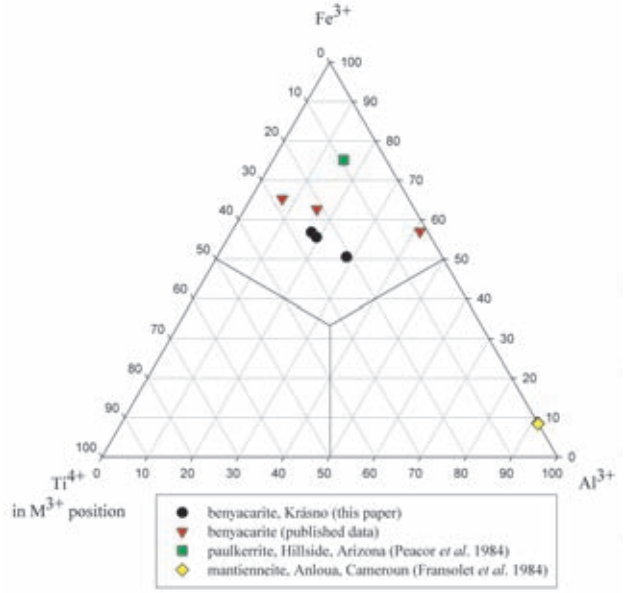

Fig. 4 Ternary plot of M^{3+} position occupancy (atomic ratio) in benyacarite-related minerals; published benyacarite data are from Cerro Blanco, Argentina (Demartin *et al*. 1993); Hagendorf, Germany (Pollmann *et al*. 1998) and Chelyabinsk, Russia (Kydryashova – Rozhdestvenskaya 1991).

Table 2 Possible new mineral species related to benyacarite

		M^{1+}	M^{2+}	M^{3+}	M^{4+}
benyacarite	Demartin *et al.* (1998), Kydryashova – Rozhdestvenskaya (1991)	□ or H_2O	Mn	Fe	Ti
new	Pollmann *et al.* (1998); this paper	K	Mn	Fe	Ti
paulkerrite	Peacor *et al.* (1984)	K	Mg	Fe	Ti
mantienneite	Fransolet *et al.* (1984) – part of analyses	K	Mg	Al	Ti
new	Fransolet *et al.* (1984) – part of analyses	□	Mg	Al	Ti

The anion group in benyacarite-related minerals contains almost exclusively P. The studied sample from Krásno contains minor local As to max. of 0.004 *apfu*. Fluorine substitutes for a part of (OH) anions in some benyacarite-related minerals (Fig. 5). In the sample from Krásno F contents correspond to 0.10 to 0.15 *apfu*.

On the basis of site occupancy, the empirical formula of benyacarite from Krásno on the 4 (P+As) *pfu* content correspond to $(K_{0.71}Na_{0.02}\square_{0.27})_{\Sigma 1.00}(Mn_{1.70}Mg_{0.11}Fe_{0.08}Zn_{0.01}Ba_{0.01}Cu_{0.01})_{\Sigma 1.92}(Fe_{1.09}Ti_{0.48}Al_{0.43})_{\Sigma 2.00}Ti_{1.00}(PO_4)_{4.00}(OH_{2.92}F_{0.12})_{\Sigma 3.04} . 15H_2O$.

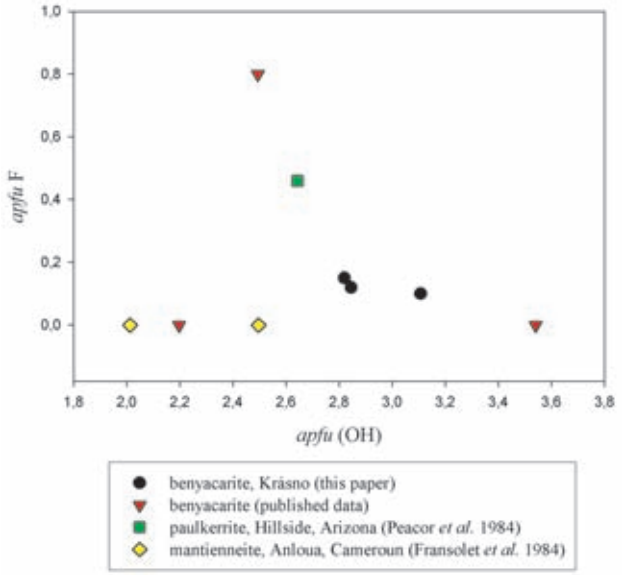

Fig. 5 A plot of *apfu* (OH) *vs. apfu* F in benyacarite-related minerals. The published benyacarite data are from Cerro Blanco, Argentina (Demartin *et al*. 1993); Hagendorf, Germany (Pollmann *et al*. 1998) and Chelyabinsk, Russia (Kydryashova – Rozhdestvenskaya 1991).

Fig. 6 Aggregates of acicular crystals of Zn- and Al-rich beraunite; Huber open pit, Krásno. Width of photo 5 mm Nicon SMZ1500 microphotography (J. & E. Sejkora)

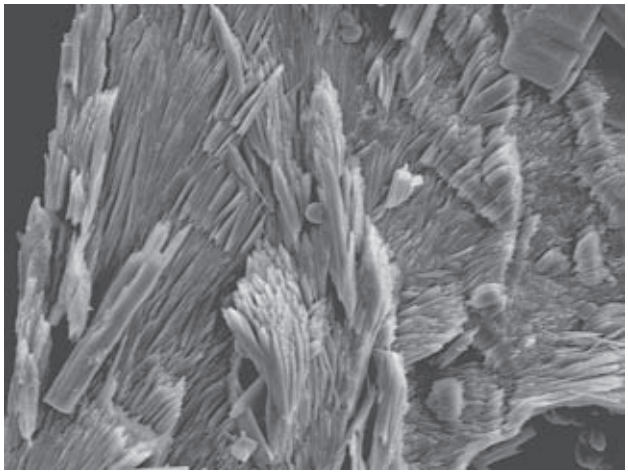

Fig. 7 Fibrous aggregate of Zn- and Al-rich beraunite, Huber open pit, Krásno. Width of photo 75 µm. SEM photograph by J. Sejkora.

Beraunite $Fe^{2+}Fe^{3+}_5(PO_4)_4(OH)_5 \cdot 6\ H_2O$

Beraunite was first described from Krásno (Huber open pit) by Korbel (1991) as spheroidal radiating aggregates, up to 3 mm in diameter, showing a dirty green colour. The study cited gives also X-ray powder diffraction data and spectral analysis. Minor contents of Si, Al, As and Zn are notable.

In the course of our study, Zn- and Al-rich beraunite have been found as long acicular crystals (Fig. 6), partly grouped in radiating aggregates up to 1 cm in size on samples from the Huber open pit. The mineral has a silvery to olive grey-green colour, grading to brown, and pearly lustre (with indications of cat's eye effect). Other samples carry porous, dark green aggregates with indistinct radiating and fibrous structure (Fig. 7), overgrown by abundant K-deficient leucophosphite, fluorapatite and microscopic aggregates of UNK3 (Sejkora *et al.* 2006). Brownish radiating aggregates up to 4 mm in diameter,

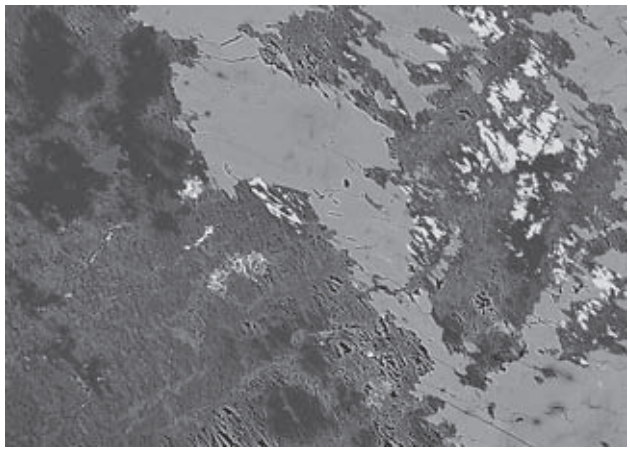

Fig. 8 Fibrous Mn-beraunite (grey) replacing older Zn-rich rockbridgeite (light) and triplite (white). Mn-beraunite is itself partly altered to younger phoshosiderite (the darkest mineral). 5th level of the Huber shaft. Width of photo 400 µm. Cameca SX100, BSE photograph by J. Sejkora and R. Škoda.

Table 3 X-ray powder diffraction pattern of Zn- and Al-rich beraunite from Krásno

I_{rel}	d	h	k	l	I_{rel}	d	h	k	l	I_{rel}	d	h	k	l
100	10.295	2	0	0	1	2.3079	4	2	0	1	1.7328	8	2	3
5	9.594	0	0	2	2	2.2991	-4	2	1	1	1.7297	-8	2	4
17	7.250	-2	0	2	3	2.2838	4	2	1	1	1.7215	-6	0	10
3	6.808	2	0	2	1	2.2695	6	0	6	1	1.7158	12	0	0
12	5.147	4	0	0	2	2.2584	-4	2	2	1	1.7093	-1	3	1
1	4.865	-1	1	1	2	2.2062	2	2	4	1	1.7077	1	3	1
2	4.797	0	0	4	1	2.2062	7	1	4	1	1.7046	6	2	6
2	4.468	-1	1	2	2	2.0924	-9	1	1	1	1.6837	10	0	6
1	4.422	4	0	2	1	2.0917	9	1	0	2	1.6757	-8	2	5
2	4.412	1	1	2	1	2.0756	7	1	5	2	1.6696	3	3	0
1	4.247	2	0	4	8	2.0632	6	2	0	1	1.6546	1	3	3
1	4.126	3	1	0	3	2.0596	-6	2	1	4	1.6491	-3	3	2
1	3.914	1	1	3	1	2.0329	-6	2	2	2	1.6439	0	2	9
8	3.740	3	1	2	1	1.9877	10	0	2	2	1.6358	-2	2	9
1	3.625	-4	0	4	2	1.9856	-6	2	3	1	1.6214	11	1	4
1	3.529	-3	1	3	1	1.9572	2	2	6	1	1.6095	3	3	3
29	3.438	1	1	4	1	1.9536	4	2	5	1	1.6005	-10	2	2
1	3.432	6	0	0	1	1.9509	1	1	9	1	1.5885	-4	2	9
15	3.298	-6	0	2	2	1.9422	6	2	3	1	1.5607	5	3	2
2	3.220	5	1	0	1	1.9367	-10	0	4	1	1.5345	-2	2	10
2	3.188	-3	1	4	3	1.9239	-3	1	9	1	1.5187	-5	3	4
8	3.169	6	0	2	2	1.9080	-2	0	10	1	1.49630	-4	2	10
16	3.150	5	1	1	2	1.8970	-4	2	6	1	1.48939	-3	3	6
3	3.110	-2	0	6	1	1.8794	0	2	7	1	1.48017	-5	3	5
2	3.071	3	1	4	1	1.8698	6	2	4	1	1.47885	-7	1	11
5	3.069	-1	1	5	1	1.8631	-2	2	7	2	1.47082	3	3	6
1	3.024	1	1	5	2	1.8504	10	0	4	1	1.46112	7	3	2
3	2.865	-3	1	5	2	1.8469	4	2	6	1	1.44172	-2	2	11
1	2.796	-4	0	6	1	1.8204	7	1	7	1	1.43633	-5	3	6
3	2.714	-1	1	6	1	1.8192	-5	1	9	1	1.43569	-3	3	7
1	2.712	6	0	4	1	1.8124	-8	0	8	1	1.43229	-6	2	10
2	2.677	1	1	6	1	1.8056	-8	2	2	1	1.43202	-7	3	4
3	2.582	0	2	0	1	1.8010	-1	1	10	1	1.43066	-12	2	1
15	2.575	-3	1	6	1	1.7892	6	2	5	1	1.42905	12	2	0
1	2.574	8	0	0	1	1.7829	-10	0	6	1	1.41082	-4	2	11
3	2.528	-5	1	5	1	1.7827	1	1	10	1	1.39868	-1	3	8
1	2.4476	8	0	2	1	1.7763	8	2	2	1	1.39177	1	3	8
1	2.4142	2	2	2	1	1.7655	-3	1	10	1	1.39010	-7	1	12
1	2.3690	-2	0	8	1	1.7643	-6	2	6	1	1.37565	-9	3	1
1	2.3442	-2	2	3	1	1.7572	0	2	8	1	1.36738	-5	1	13
1	2.3299	7	1	3	1	1.7493	-11	1	2					
1	2.3240	-3	1	7	1	1.7414	4	2	7					

Table 4 Unit-cell parameters of beraunite (for monoclinic space group *C*2/*c*)

colour	beraunite green this paper	beraunite green Moore – Kampf (1992)	Mn-beraunite red di Cossato *et al*. (1989)	beraunite green Moore (1970)	beraunite red Fanfani – Zanazzi (1967)
a [Å]	20.630(6)	20.953(5)	20.760(3)	20.80(3)	20.646(5)
b [Å]	5.164(2)	5.171(1)	5.153(1)	5.156(3)	5.129(7)
c [Å]	19.225(8)	19.226(4)	19.248(2)	19.22(6)	19.213(5)
β [°]	93.61(4)	93.34(2)	93.55(1)	93.3(4)	93.62(8)
V [Å^3]	2044.0	2083.89	2055.13	2057.8	2030.5

megascopically similar to frondelite, represent a rare example. The X-ray diffraction pattern obtained for Zn- and Al-rich beraunite (Table 3) and its refined unit-cell parameters (Table 4) are close the published data for this mineral.

Numerous samples from the 5th level of the Huber mine carry fibrous aggregates, up to 200 μm, which extensively replace older rockbridgeite and triplite (Fig. 8). They in turn show alteration of variable intensity to the youngest phosphosiderite (Fig. 9). Fluorapatite and members of the rockbridgeite – frondelite series closely associated. This mineral phase could not be examined by X-ray powder diffraction due to its small size. The similarity in chemical composition of the studied phase to Mn-rich beraunite, described by di Cossato *et al.* (1989) from Mangualde, Portugal, and its fibrous character, suggest that the mineral is probably Mn-rich beraunite. The chemical composition could also correspond to anomalously Mn-rich ludlamite, but this mineral is tabular, compact or granular.

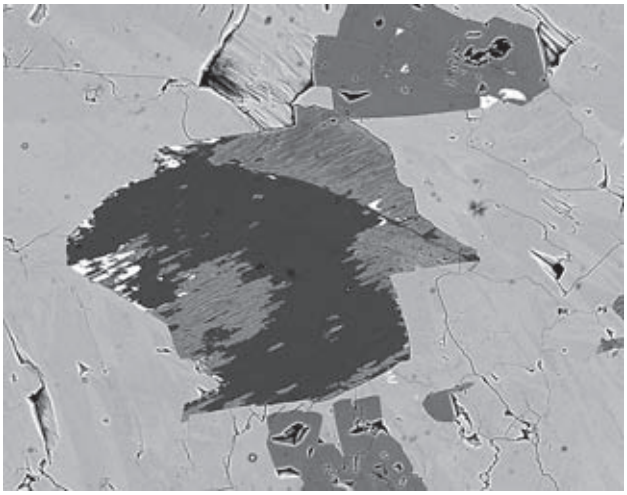

Fig. 9 Relics of fibrous Mn-rich beraunite aggregates (grey) intensively replaced by phosphosiderite (dark), intergrown in aggregates of Zn-rich rockbridgeite (light); the homogeneous, clearly bound aggregates (light grey) are fluorapatite; minute white inclusions are Fe oxi-hydroxides. 5th level of the Huber shaft. Width of photo 300 μm. Cameca SX100, BSE photograph by J. Sejkora and R. Škoda.

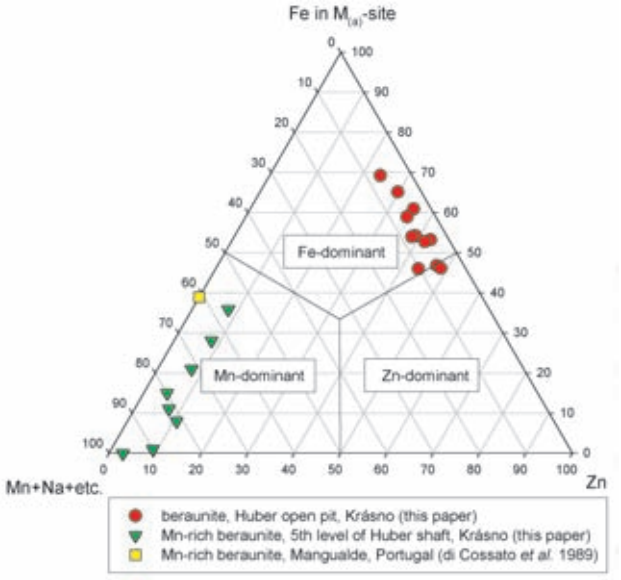

Fig. 10 Ternary plot of $M_{(a)}$-site occupancy of beraunites from Krásno and Mn-rich beraunite from Mangualde (di Cossato *et al.* 1989).

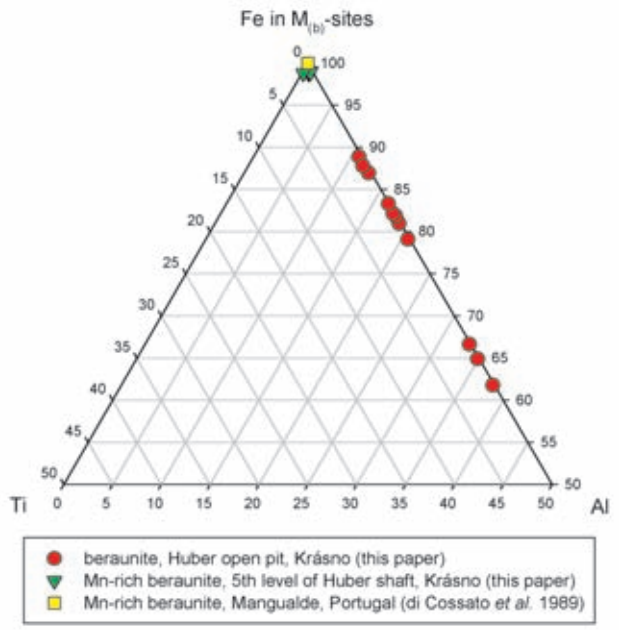

Fig. 11 Part of ternary plot of $M_{(b)}$-sites occupancy of beraunites from Krásno and Mn-rich beraunite from Mangualde (di Cossato *et al.* 1989).

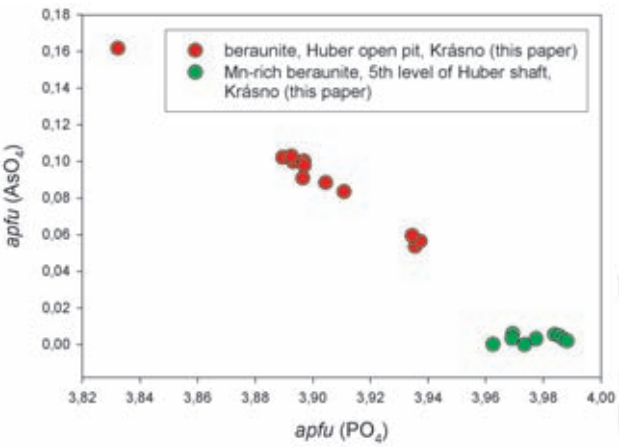

Fig. 12 A plot of (PO_4) *vs.* (AsO_4) (*apfu*) in beraunites from Krásno.

These two types of beraunite from Krásno (Table 5) clearly show a wider range of compositional variation than indicate data in the available literature. The general formula of beraunite can be written as $M_{(a)}M_{(b)5}(PO_4)_4(OH)_5 . 6\ H_2O$. The results of structure analysis (Fanfani – Zanazzi 1967; di Cossato *et al.* 1989; Moore – Kampf 1992) show Fe^{2+} (greenish black beraunite), Fe^{3+} (yellow, orange and red beraunite) and partly also Mn^{2+} (Mn-bearing beraunite) are present in the octahedral site $M_{(a)}$. The five octahedral sites $M_{(b)}$ (one M(2) site and two M(3) and M(4) sites, following the symbols of Moore – Kampf 1992), are occupied mainly by Fe^{3+} and small amounts of Al^{3+} and Mn^{2+} (or Mn^{3+}?) in the known minerals related to beraunite. The preferential occupation of $M_{(b)}$-sites by Mn was described by di Cossato *et al.* (1989); however, Moore – Kampf (1992) proposed a disorder in Mn occupation of these sites using the same set of data. The chemical analyses of both types of beraunite from Krásno were recalculated on the basis of (P+As+Si+S) = 4 and interpreted using the assumption that all the following cations – Mn, Zn, Ca etc. and Fe^{2+} – enter the $M_{(a)}$ site (the content of Fe^{2+} was calculated to the ideal occupancy of 1.00 *apfu* in the site). The $M_{(b)}$-sites, not individually specified, are occupied by Fe^{3+}, Al and Ti^{4+}. The indicated water content was calculated from the theoretical content of 6.00 H_2O in beraunite and charge balance.

In Zn- and Al-rich beraunite from Krásno (Fig. 10) the $M_{(a)}$-site is dominated by Fe (probably Fe^{2+}), corresponding to 0.46–0.69 *apfu*. Two spot-analyses show a slight predominance of Zn (the whole range is 0.24–0.48 *apfu*) and the total of other elements (Na, Mn, Ca etc.) does not exceed 0.1 *apfu*. The $M_{(b)}$-sites are dominated by Fe^{3+} (Fig. 11) ranging from 2.91 to 4.36 *apfu*. Also significant is the Al content (0.53–1.79 *apfu*); the total for $M_{(b)}$-sites is 4.59–4.97 *apfu*. In the anion group (Fig. 12), P is strongly

Table 5 Chemical composition of beraunites from Krásno (in wt. %)

	1	2	3	4	5	6	7	8	9	10
Na_2O	0.09	0.10	0.14	0.16	0.13	0.07	0.48	0.35	0.55	0.78
K_2O	0.00	0.00	0.00	0.00	0.00	0.00	0.16	0.18	0.16	0.13
CaO	0.05	0.00	0.10	0.16	0.00	0.03	0.38	0.41	0.44	0.30
FeO*	4.59	5.43	4.45	3.73	3.77	3.76	1.22	2.98	0.93	0.00
BaO	0.04	0.07	0.02	0.00	0.08	0.00	0.05	0.00	0.09	0.13
SrO	0.00	0.00	0.00	0.00	0.00	0.00	0.03	0.12	0.00	0.02
MgO	0.02	0.01	0.01	0.04	0.00	0.03	0.05	0.00	0.10	0.08
CuO	0.07	0.00	0.11	0.15	0.00	0.00	0.02	0.00	0.03	0.00
MnO	0.11	0.14	0.06	0.04	0.14	0.16	4.44	3.01	4.28	5.60
ZnO	3.51	2.80	3.59	4.02	4.37	4.46	0.69	0.75	0.69	0.29
Al_2O_3	5.88	5.17	10.49	9.87	3.03	3.35	0.18	0.18	0.23	0.03
Fe_2O_3*	34.57	34.86	26.75	28.73	39.16	39.42	44.00	42.09	44.51	45.11
SiO_2	0.05	0.08	0.02	0.04	0.06	0.05	0.08	0.07	0.13	0.11
TiO_2	0.09	0.07	0.08	0.08	0.14	0.22	0.21	0.19	0.07	0.50
As_2O_5	1.16	0.71	1.33	1.27	1.33	1.30	0.04	0.03	0.00	0.04
P_2O_5	31.56	32.35	31.79	31.22	31.16	31.27	32.73	32.94	32.09	31.91
SO_3	0.00	0.00	0.00	0.00	0.00	0.00	0.07	0.00	0.17	0.10
H_2O**	16.88	16.62	16.67	16.98	16.91	17.22	17.00	16.38	17.07	17.39
total	98.66	98.41	95.59	96.50	100.27	101.34	101.84	99.66	101.52	102.53
Na^+	0.026	0.029	0.040	0.045	0.037	0.021	0.135	0.096	0.155	0.222
K^+	0.000	0.000	0.000	0.000	0.000	0.000	0.029	0.033	0.030	0.025
Ca^{2+}	0.007	0.000	0.015	0.025	0.000	0.004	0.059	0.062	0.069	0.048
Fe^{2+}	0.561	0.653	0.539	0.460	0.465	0.463	0.146	0.356	0.113	0.000
Ba^{2+}	0.002	0.004	0.001	0.000	0.005	0.000	0.003	0.000	0.005	0.008
Sr^{2+}	0.000	0.000	0.000	0.000	0.000	0.000	0.002	0.010	0.000	0.002
Mg^{2+}	0.003	0.001	0.003	0.009	0.000	0.007	0.010	0.000	0.021	0.017
Cu^{2+}	0.008	0.000	0.011	0.017	0.000	0.000	0.002	0.000	0.003	0.000
Mn^{2+}	0.013	0.016	0.007	0.005	0.017	0.020	0.540	0.365	0.529	0.697
Zn^{2+}	0.379	0.297	0.384	0.438	0.476	0.484	0.073	0.079	0.074	0.032
$M_{(a)}$ site	1.000	1.000	1.000	1.000	1.000	1.000	1.000	1.000	1.000	1.050
Al^{3+}	1.013	0.876	1.789	1.715	0.526	0.581	0.030	0.030	0.039	0.005
Fe^{3+}	3.800	3.769	2.914	3.187	4.344	4.362	4.753	4.528	4.885	4.987
Ti^{4+}	0.010	0.008	0.008	0.009	0.016	0.024	0.022	0.021	0.007	0.055
$M_{(b)}$ site	4.824	4.653	4.712	4.911	4.887	4.968	4.806	4.579	4.931	5.047
As^{5+}	0.088	0.054	0.100	0.098	0.102	0.100	0.003	0.002	0.000	0.003
P^{5+}	3.904	3.936	3.897	3.897	3.890	3.893	3.978	3.988	3.963	3.969
S^{6+}	0.000	0.000	0.000	0.000	0.000	0.000	0.008	0.000	0.019	0.011
Si^{4+}	0.007	0.011	0.003	0.005	0.008	0.007	0.012	0.010	0.019	0.017
T sites	4.000	4.000	4.000	4.000	4.000	4.000	4.000	4.000	4.000	4.000
OH	4.448	3.927	4.103	4.692	4.630	4.899	4.275	3.620	4.616	5.042
H_2O	6.003	6.002	6.000	6.003	6.001	5.998	6.002	6.002	5.997	6.000

Zn- and Al-rich beraunite: 1 – mean of 12 spot analyses; 2–6 – representative spot analyses;
Mn-rich beraunite: 7 – mean of 8 spot analyses; 8-10 – representative spot analyses.
Empirical formulas were calculated on the basis of (P+As+Si+S) = 4.00;
* – calculation of Fe_{tot} to Fe^{2+} and Fe^{3+} is based on the assumption that Fe^{2+} (together with M^{1+} and M^{2+} elements) completely fills the $M_{(a)}$ position and only the surplus Fe (above 1 *pfu*) enters the sites M(b) as Fe^{3+};
** – H_2O content is calculated from the general formula (H_2O = 6.00) and charge balance.

dominating, As is low (0.05–0.16 *apfu*) and Si is below 0.01 *apfu*. The average empirical formula (12 spot analyses) of the Zn- and Al-rich beraunite from Krásno, based on 4 (P+As+S+Si) and the above noted assumptions, is $(Fe_{0.56}Zn_{0.38}Na_{0.03}Mn_{0.01}Ca_{0.01}Cu_{0.01})_{\Sigma 1.00}(Fe_{3.80}Al_{1.01}Ti_{0.01})_{\Sigma 4.82}$ $[(PO_4)_{3.90}(AsO_4)_{0.09}(SiO_4)_{0.01}]_{\Sigma 4.00}(OH)_{4.45} \cdot 6.00H_2O$.

The $M_{(a)}$-site in Mn-rich beraunite from Krásno (Fig. 10) is dominated by Mn (0.36–0.70 *apfu*). In addition, the site contains significant Fe^{2+} (max. 0.36 *apfu*) and increased Na in the range of 0.09 to 0.22 *apfu*. The group of $M_{(b)}$-sites (Fig. 11) is filled dominantly by Fe^{3+} (4.53–4.99 *apfu*), while Al and Ti contents are minor (max. 0.05 *apfu*). The tetrahedral sites are almost exclusively occupied by P (Fig. 12), As, Si and S contents reach max. 0.01 *apfu.* The average empirical formula (8 spot analyses) for Mn-rich beraunite from Krásno can be presented on the basis of 4 (P+As+S+Si) and the above assumptions as $(Mn_{0.54}Fe_{0.14}Na_{0.13}Zn_{0.07}Ca_{0.06}K_{0.03}Mg_{0.01})_{\Sigma 0.98}(Fe_{4.75}Al_{0.03}$ $Ti_{0.02})_{\Sigma 4.80}[(PO_4)_{3.98}(SiO_4)_{0.01}(SO_4)_{0.01}]_{\Sigma 4.00}(OH)_{4.27} \cdot 6.00H_2O$. The complicated composition of Mn-rich beraunite from Krásno can be demonstrated by comparison with the empirical formula (calculated on the same basis) of Mn-rich beraunite from Mangualde (di Cossato *et al.* 1989) $(Mn_{0.54}Fe_{0.38}Na_{0.04}Ca_{0.03}Li_{0.01})_{\Sigma 1.00}Fe_{5.18}(PO_4)_{4.00}(OH)_{5.54} \cdot 4.92H_2O$.

Cacoxenite $Fe^{3+}_{24}Al(PO_4)_{17}O_6(OH)_{12} \cdot 75\ H_2O$

It has been found as tufts or radiating aggregates (Fig. 13), up to 5 mm in diameter, of typical golden yellow colour in samples from the Huber open pit. A similar material occurs in cavities in phosphate accumulations at the 5th level of the Huber mine. At this place, cacoxenite belongs to the youngest minerals. The mineral was identified by X-ray powder diffraction.

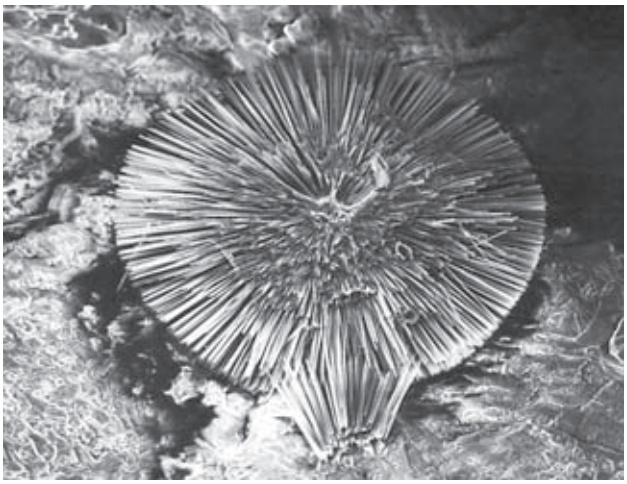

Fig. 13 A radiating fibrous aggregate of cacoxenite, Huber open pit, Krásno. Width of photo 500 μm. SEM photograph by Z. Mach.

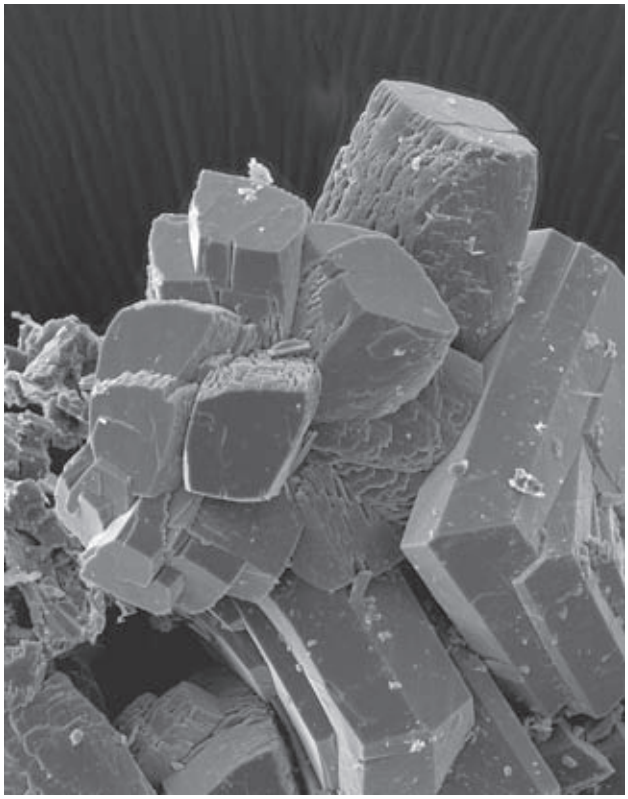

Fig. 14 Crystals of chalcosiderite-turqouise series minerals on tabular crystals of leucophosphite, Huber open pit, Krásno. Width of photo 130 μm. SEM photograph by J. Sejkora and J. Plášil.

Chalcosiderite $CuFe^{3+}_6[PO_4(OH)_2]_4 \cdot 4\ H_2O$
Turquoise $CuAl_6[PO_4(OH)_2]_4 \cdot 4\ H_2O$
(turqouise group)

Chalcosiderite has been described by Mach (1979) and later by Korbel (1991) at the Huber open pit as rare green rosette-shaped agreggates, up to 1.5 mm. It occurs in cavities of quartz gangue with wolframite.

During the present study, members of the turquoise group have been found as relatively widespread minerals at various places of the Huber open pit in phosphate accumulations (or in their proximity) showing a strong supergene alteration. The phosphate accumulations, from mm up to dm in size and located in massive white quartz, consist of fluorapatite, locally with abundant compact isokite and triplite relics. Minor weathered cavities in these accumulations are coated by minute crystalline aggregates of the turquoise group minerals. Macroscopically indistinguishable members of this group are accompanied by fluorapatite of the youngest generation, leucophosphite, pharmacosiderite, rare kolbeckite, whitmoreite and unnamed mineral phases *UNK1*, *UNK3*, *UNK6*, *UNK7*, *UNK8* and *UNK10* (Sejkora *et al*. 2006). Minerals of the turquoise group form crystals (Fig. 14) grouped to irregular spheroidal aggregates deposited individually or grouped in small crystalline coatings (Fig. 15) as the youngest minerals in the phosphate association. Individual aggregates are usually less than 1 mm in size (frequently 0.1–0.3 mm), exceptionally up to 1.8 mm. The colour is usually deep bright green with various shades, lustre is vitreous, only small fragments are partly transparent. The individual aggregates always show compositional zoning (Fig. 16). Zones with predominance of Fe (chalcosiderite) or Al (turquoise) are usually present in a single aggregate.

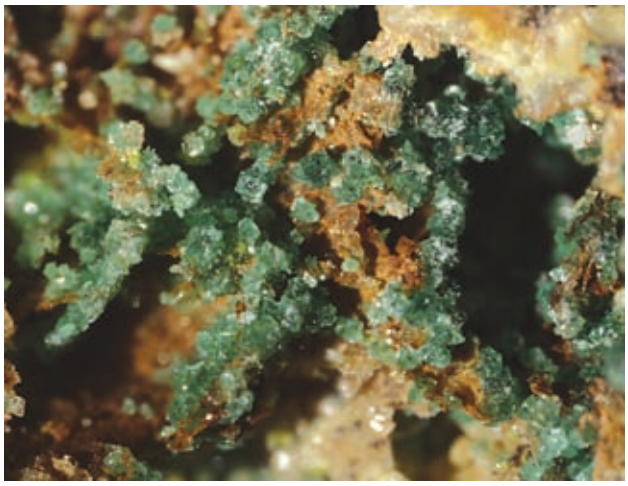

Fig. 15 Semi-spheroidal aggregates of members of the series chalcosiderite – turquoise; Huber open pit, Krásno. Width of photo 4 mm. Microphotography Nicon SMZ1500 by J.&E. Sejkora.

At present, chalcosiderite occurrence has been confirmed at the 5th level of the Huber shaft as green spheres

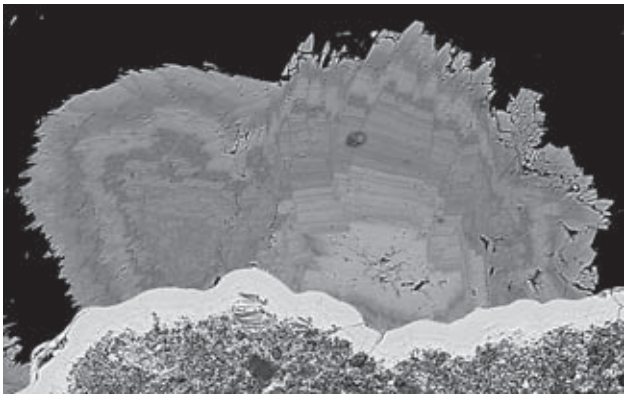

Fig. 16 Complicated zoning in semi-spheroidal aggregates of chalcosiderite (light zones) – turquoise (dark zones) growing on *limonite* crust (light), Huber open pit, Krásno. Width of photo 300 μm. BSE photograph, Cameca SX100, by J. Sejkora and R. Škoda.

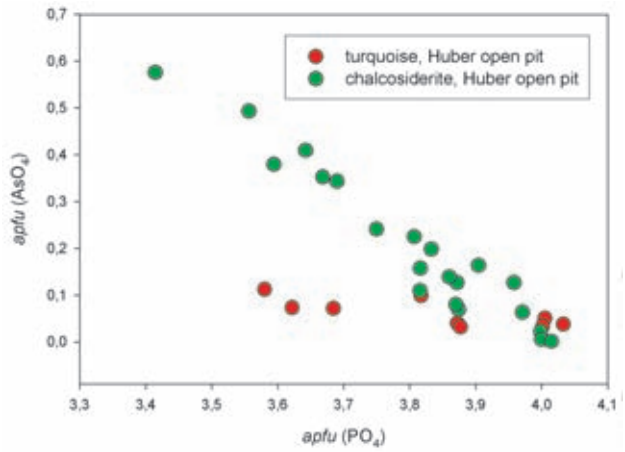

Fig. 18 A plot of (PO_4) *apfu* vs. (AsO_4) *apfu* in the turquoise group minerals. Huber open pit, Krásno.

to 0.5 mm in diameter, associated with crystalline and porous aggregates of isokite. Rare aggregates of chalcopyrite and chalcocite, intergrown in the primary phosphates (triplite), served as the source of copper.

All recorded occurrences of the turquoise group minerals have been verified by X-ray powder diffraction. The present study shows prominent chemical zoning of samples from the Huber open pit. The analyses document the presence of members ranging through nearly the whole isomorphous series chalcosiderite – turquoise (Fig. 17). From the minimal contents of Fe in chalcosiderite at c. 0.88 *apfu* to the minimal contents of Al in turquoise at c. 0.43 *apfu*. The occupancy of the M^{2+} site attains 1.0 to 1.4 *apfu* Cu. This indicates that the studied minerals do not exhibit heterovalent isomorphism of planerite type Cu-□→(PO_4)–(PO_3OH) (Foord – Taggart 1998). The anion group contains regular amounts of As in the range of 0.03–0.11 (turqouise) and up to 0.58 *apfu* (chalcosiderite) (Fig. 18). The first record of elevated Ti content up to 0.12 *apfu* and the presence of fluorine in rare examples up to 0.20 *apfu* in minerals of the turquoise group were given in this study. The representative compositions of members of this group (Table 6), with empirical formulas, document the wide variation. The high totals of some analyses are probably due to sample dehydration by electron beam in vacuum.

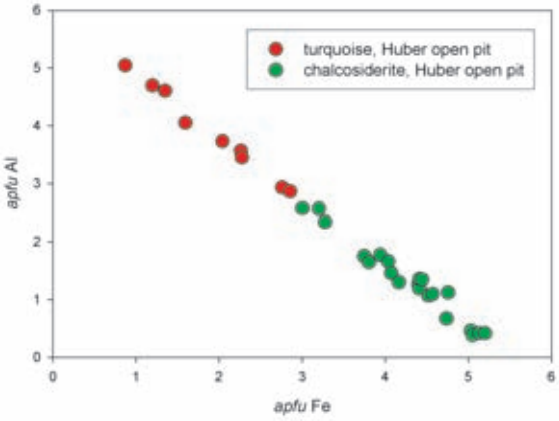

Fig. 17 A plot of Fe *apfu* vs. Al *apfu* in minerals of the turquoise group. Huber open pit, Krásno.

Table 6 Chemical composition of members of the isomorphous series chalcosiderite – turquoise (in wt. %)

	1.	2.	3.	4.	5.	6.	7.	8.
CuO	9.78	10.12	11.85	10.53	9.45	8.94	9.97	8.06
PbO		0.14	0.25	0.25	0.07		0.25	
ZnO		0.23	0.12	0.06	0.43	0.41	0.17	
CaO		0.06	0.02	0.06	0.09	0.03	0.06	
BaO		0.21				0.21		
SrO		0.09					0.02	
Al_2O_3	37.60	33.00	22.30	16.00	13.87	7.30	2.15	
Fe_2O_3		8.95	19.17	25.08	27.14	37.19	41.47	48.56
TiO_2		0.31				0.04		
P_2O_5	34.90	33.51	32.22	31.14	27.56	27.57	25.56	28.77
As_2O_5		1.06	0.54	0.43	4.29	4.16	4.37	
SO_3					0.09	0.12	0.85	
F		0.49	0.04					
-O=F		0.21	0.02					
H_2O*	17.72	17.80	16.50	15.38	15.12	14.52	13.88	14.61
total	100.00	105.77	102.98	98.94	98.10	100.51	99.00	100.00

* H_2O content calculated from the ideal formula $CuM_6[PO_4(OH)_2]_4 \cdot 4\,H_2O$ (M = Fe,Al) and charge balance; empirical formulas were calculated on the basis of 28 (O,OH).

1. theoretical composition of turquoise $CuAl_6[PO_4(OH)_2]_4 \cdot 4\,H_2O$

2. turquoise with the highest Al content analyzed, corresponding to empirical formula: $(Cu_{1.00}Zn_{0.02}Ba_{0.01}Sr_{0.01})_{\Sigma 1.04}(Al_{5.10}Fe_{0.88}Ti_{0.03})_{\Sigma 6.01}[(PO_4)_{3.72}(AsO_4)_{0.07}F_{0.20}]_{\Sigma 3.99}(OH)_{8.47} \cdot 4.00H_2O$.

3. turquoise of an intermediate composition, corresponding to empirical formula: $(Cu_{1.28}Zn_{0.01})_{\Sigma 1.29}(Al_{3.76}Fe_{2.06})_{\Sigma 5.82}[(PO_4)_{3.99}(AsO_4)_{0.04}F_{0.02}]_{\Sigma 4.05}(OH)_{8.21} \cdot 4.00H_2O$.

4. turquoise with composition near the turquoise/chalcosiderite limit, corresponding to empirical formula: $(Cu_{1.22}Ca_{0.01}Pb_{0.01})_{\Sigma 1.24}(Al_{2.90}Fe_{2.90})_{\Sigma 5.80}[(PO_4)_{4.06}(AsO_4)_{0.03}]_{\Sigma 4.09}(OH)_{7.62} \cdot 4.00H_2O$.

5. chalcosiderite with composition near the limit chalcosiderite/turquoise, corresponding to empirical formula: $(Cu_{1.13}Zn_{0.05}Ca_{0.02})_{\Sigma 1.20}(Fe_{3.24}Al_{2.60})_{\Sigma 5.84}[(PO_4)_{3.70}(AsO_4)_{0.36}]_{\Sigma 4.06}(OH)_{7.71} \cdot 4.00H_2O$.

6. chalkosiderite of an intermediate composition, corresponding to empirical formula: $(Cu_{1.08}Zn_{0.05}Ba_{0.01})_{\Sigma 1.14}(Fe_{4.48}Al_{1.38})_{\Sigma 5.86}[(PO_4)_{3.74}(AsO_4)_{0.35}]_{\Sigma 4.09}(OH)_{7.59} \cdot 4.00H_2O$.

7. chalcosiderite with the highest analyzed content, corresponding to empirical formula: $(Cu_{1.27}Zn_{0.02}Pb_{0.01})_{\Sigma 1.30}(Fe_{5.29}Al_{0.43})_{\Sigma 5.72}[(PO_4)_{3.64}(AsO_4)_{0.39}(SO_4)_{0.10}]_{\Sigma 4.13}(OH)_{7.44} \cdot 4.00H_2O$.

8. theoretical composition of chalcosiderite $CuFe_6[PO_4(OH)_2]_4 \cdot 4\,H_2O$

Crandallite $CaAl_3(PO_4)(PO_3OH)(OH)_6$
Goyazite $SrAl_3(PO_4)(PO_3OH)(OH)_6$
Waylandite $BiAl_3(PO_4)_2(OH)_6$
(crandallite group)

Crandallite $CaAl_3(PO_4)(PO_3OH)(OH)_6$

Mrázek (1981) published the first description of crandallite from the Huber open pit as orange semi-spheroidal aggregates to 1 mm. It includes X-ray data, a qualitative chemical analysis and IR spectrum, confirming the presence of the group $(PO_3OH)^{2-}$ in crandallite. Bi-rich crandallite has been described by Novák *et al.* (2001) from greisen dump material deposited behind the former Stannum mine. It forms cryptocrystalline, in part porous, light yellow white or yellow brown aggregates among quartz crystals and earthy crusts, up to 3 mm thick, on cassiterite and quartz. It represents a mixture with unnamed phase *UNK11* (Sejkora *et al.* 2006). Novák *et al.* (2001) presented its unit-cell parameters (Table 7) and chemical analysis, which, based on 2 (P+As+S+Si), gives the empirical formula: $(Ca_{0.50}Sr_{0.34}Bi_{0.17})_{\Sigma 1.01}(Al_{2.66}Fe_{0.25}Cu_{0.02})_{\Sigma 2.93}[(PO_4)_{1.13}(PO_3OH)_{0.68}(AsO_4)_{0.13}(SO_4)_{0.05}]_{\Sigma 1.99}(OH)_{6.00}$.

We have studied samples collected at different places of the Huber open pit. The mineral occurs in minute, less than 1 mm, irregular semi-spheroidal aggregates (Fig. 19) composed of very thin tabular crystals up to 100 μm long (Fig. 20). The mineral is associated with turquoise-group minerals (Fig. 21), young fluorapatite and fluorite in small cavities of coarse-grained quartz gangue. The crandallite aggregates are whitish or light pink to light orange with vitreous lustre and transparent only in thin splinters. Crandallite has also been identified as a component in strongly zoned goyazite and crandallite aggregates (see goayzite for detailed description).

Fig. 19 Irregular semi-spheroidal crandallite aggregates to 1 mm, composed of minute tabular crystals. Huber open pit, Krásno. Width of photo 2.5 mm. Nicon SMZ1500 microphotography by J. & E. Sejkora.

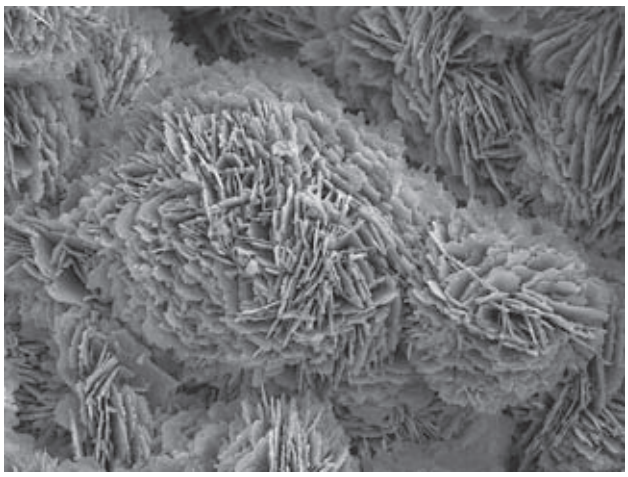

Fig. 20 Thin tabular crandallite crystals composing semi-spheroidal aggregates. Huber open pit, Krásno. Width of photo 130 μm. SEM photograph by J. Sejkora.

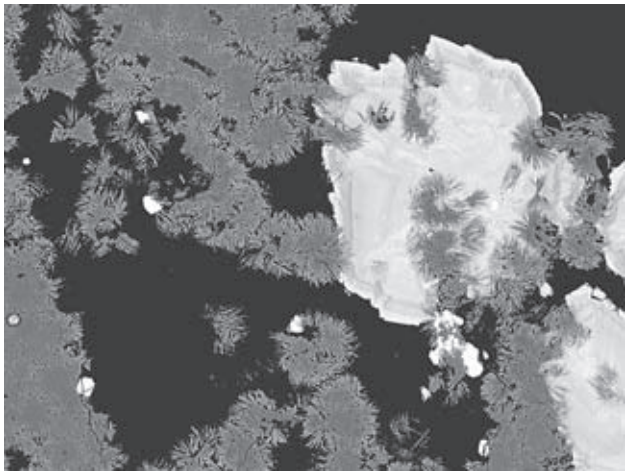

Fig. 21 Semi-spheroidal crandallite aggregates composed of minute tabular crystals (dark) in association with zoned aggregates of the turquoise-group minerals (light). Width of photo 400 μm. Huber open pit, Krásno. BSE photograph, Cameca SX100 by J. Sejkora and R. Škoda.

X-ray powder data as well as refined unit-cell parameters (Table 7) compare well with data for minerals of the crandallite – goyazite series. Comparison of the refined unit-cell parameters, as well as X-ray powder patterns, shows that distinguishing these two mineral species solely by X-ray methods is problematic, owing to wide isomorphism.

The chemical composition of the crandallite-type minerals is characterized by wide isomorphous substitution in all structural sites of the general formula $AB_3(TO_4)(TO_3OH)(OH,F)_6$. Possible substitutions by individual elements in large $^{[12]}A$-, medium $^{[6]}B$- and small $^{[4]}T$-fold positions are shown in Fig. 22. The chemical analyses of crandallite-type minerals from Krásno (Table 8) were recalculated on the basis of (P+As+S+Si) = 2.

Na^+	K^+	H_3O^+	Cs^+	Ag^+	NH_4^+	Rb^+	Tl^+	-	Mg^{2+} Hg^{2+} UO_2^{2+} Pb^{2+} Ba^{2+} Sr^{2+} **$^{[12]}Ca$** Bi^{3+} Y^{3+} REE^{3+} Ac^{3+} Th^{4+}	Zn^{2+} Cu^{2+} Ti^{4+} **$^{[6]}Al_3$** Fe^{3+} Cr^{3+} Ga^{3+} In^{3+} V^{3+} Sc^{3+}	SiO_4^{4-} TiO_43- SbO_4^{3-} VO_4^{3-} AsO_4^{3-} **$^{[4]}PO_4^{3-}$** SO_4^{2-} SeO_4^{2-} CO_3^{2-} CrO_4^{2-}	VO_4^{3-} AsO_4^{3-} PO_4^{3-} **$^{[4]}(PO_3OH)^{2-}$** SO_4^{2-} VO_3OH^{2-} AsO_3OH^{2-} WO_4^{2-} MoO_4^{2-}	Cl **$(OH)_6$** F

Fig. 22 Possible substitutions in crandallite-type minerals (alunite, beudantite and crandallite groups), modified following Schwab *et al*. (2004), with the use of data by Scott (1987), Novák *et al*. (1994), Pe-Piper – Dolansky (2005).

Calcium (0.52–0.85 *apfu*) is the dominant element in *A*-site of crandallite (Fig. 23) and significant quantities of Sr (0.07–0.43 *apfu*) are also present. The contents of other elements, in particular Ba and K, are up to 0.04 *apfu*. Relative to the data published by Novák *et al.* (2001), our samples contained only negligible Bi (below 0.01 *apfu*). The *B*-site in crandallite (Fig. 24) is filled dominantly by Al (2.80–2.91 *apfu*), whereas Fe contents reach only exceptionally 0.02 *apfu*, in difference to analyses presented by Novák *et al.* (2001). There is relatively small deficiency in the *B*-site, with total ranging from 2.82 to 2.95 *apfu*. The tetrahedral *T*-sites (Fig. 25) are dominated by P (1.82–2.00 *apfu*) and there are variable contents of S to 0.18 *apfu* (in difference to data by Novák *et al.* 2001). The (OH) position contains significant fluorine concentrations (Fig. 26), ranging from 0.51 to 1.08 *apfu.* Baldwin *et al.* (2000) reported similar high fluorine contents in crandallites from pegmatites in Namibia. The coefficients in empirical formulas corresponding to selected spot analyses of crandallite from Krásno are given in Table 8.

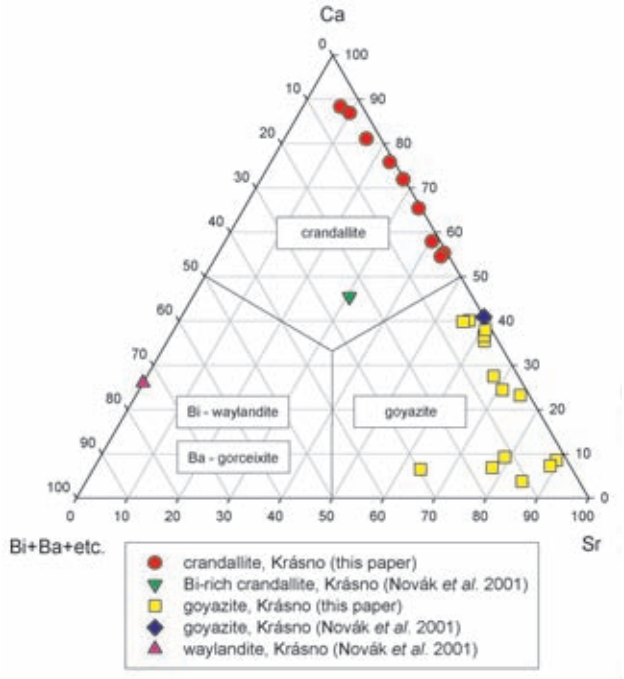

Fig. 23 Ternary plot of *A*-site occupancy (atomic ratio) in crandallite-type minerals from the Huber open pit, Krásno.

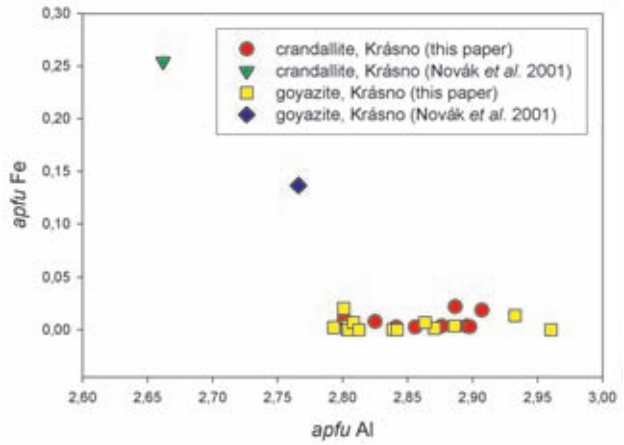

Fig. 24 A plot of *apfu* Al *vs.* Fe in *B*-site of crandallite-type minerals from the Huber open pit, Krásno. The deviation from ideal correlation Al+Fe = 3 is caused by the content of small amounts of Cu and Zn and especially the deficit in *B*-site.

Table 7 Unit-cell parameters for crandallite group minerals (for trigonal space group *R*-3*m*)

		a [Å]	c [Å]	V [Å^3]
crandallite	this paper	7.000(2)	16.226(9)	688.5
crandallite	Mrázek (1981)	7.011(2)	16.56(1)	704.9
crandallite Bi- and Sr-rich	Novák *et al.* (2001)	7.012(2)	16.650(6)	708.9
goayzite	Novák *et al.* (2001)	7.008(2)	16.608(6)	706.4
goayzite	this paper (Schnöd stock)	6.992(2)	16.537(7)	700.1
goyazite	this paper (Huber stock)	7.0214(8)	16.507(3)	704.8

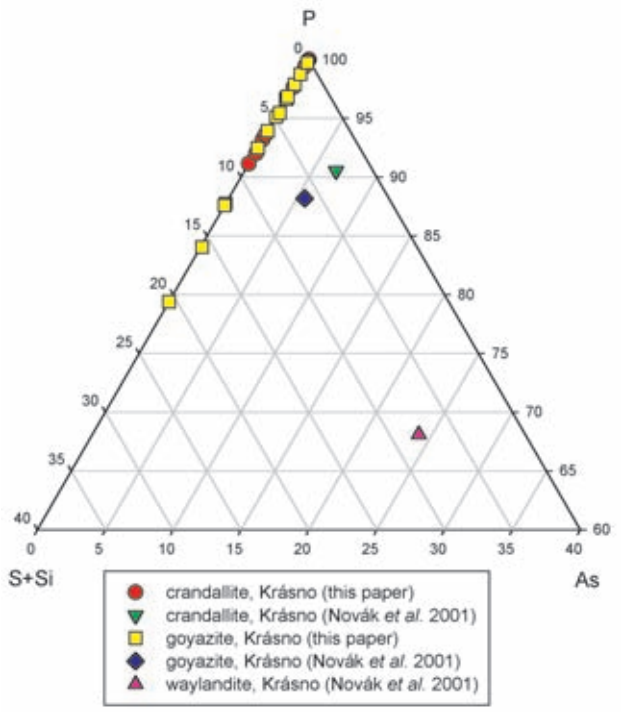

Fig. 25 Part of ternary plot of *T*-sites occupancy (atomic ratio) of crandallite-type minerals from the Huber open pit, Krásno.

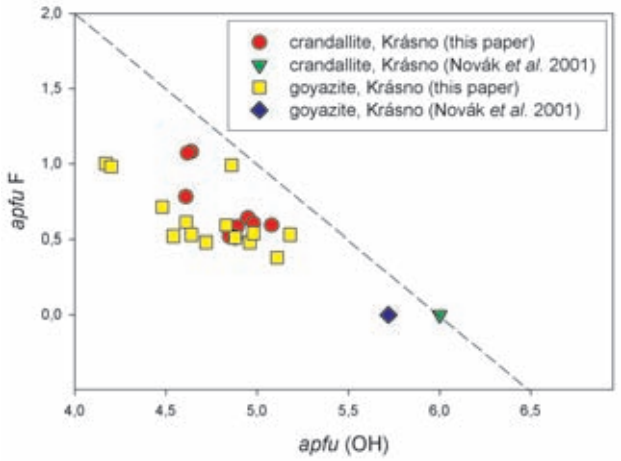

Fig. 26 A plot of *apfu* OH *vs.* F in crandallite-type minerals from the Huber open pit, Krásno. The dashed line corresponds to the theoretical relation (OH)+F = 6.

Goyazite $SrAl_3(PO_4)(PO_3OH)(OH)_6$

Novák *et al.* (2001) published the first description of Bi-rich goyazite on the material from the Huber open pit as light pinkish brown or brownish – greyish white kidney-shaped cryptocrystalline aggregates, up to 1 mm in diameter. They presented its unit-cell parameters (Table 7), and chemical analysis with the following empirical formula based on 2 (P+As+S+Si): $(Sr_{0.55}Ca_{0.38}Bi_{0.26})_{\Sigma 1.19}(Al_{2.76}Fe_{0.14}Cu_{0.07})_{\Sigma 2.97}[(PO_4)_{0.88}(PO_3OH)_{0.88}(AsO_4)_{0.11}(SO_4)_{0.12}]_{\Sigma 1.99}(OH)_{5.72}$.

The present study includes numerous goyazite samples collected at different places of the Huber open pit. Goyazite occurs as equant to spheroidal aggregates (Fig. 27), usually with crystalline surface, up to 2 mm in size (Fig. 28), on quartz crystals in cavities of coarse-grained quartz gangue. Cassiterite, wolframite and clay minerals are associated. The goyazite aggregates are white or whitish-grey, orange colour of some aggregates is probably caused by film of Fe-oxides. Luster is greasy to vitreous, mineral is transparent only in thin splinters. Compact to finely crystalline, light pink goyazite aggre-

Fig. 27 Semi-spheroidal aggregate of crystalline goyazite growing on quartz crystals. Huber open pit, Krásno. Width of photo 3 mm. Nicon SMZ1500 microphotography by J. & E. Sejkora.

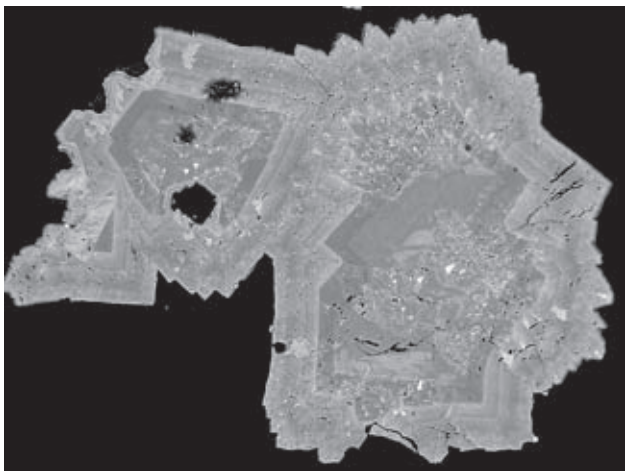

Fig. 28 Strongly zoned aggregate of goyazite crystals (the lighter zones contain higher Ba, darker contain increased Sr and Ca), Huber open pit, Krásno. Width of photo 1500 μm. BSE photo, Cameca SX100 by J. Sejkora and R. Škoda.

gates, up to 2 cm in size, with a weak pearl lustre, are composed of very small (less than 100 μm) trigonal crystals (Fig. 29).

Minerals of crandallite group from the Huber open pit (Fig. 30) include samples with well-formed individual trigonal crystals (Fig. 31), up to 1 mm in size, and their rich aggregates, up to 1–2 cm in size. The aggregates are located in cavities of coarse-grained quartz gangue. They are whitish, buff, light pink to red (due to abundant cassiterite and Fe oxide inclusions) and have a vitreous lustre. The studied crystals show oscillatory zoning (Fig. 32); WD line-scans of Ca and Sr content (Fig. 33) and compositional profiles (Fig. 34) exhibit that numerous zones, less than 2 μm in width, in a single crystal correspond alternatively to goyazite or crandallite.

At the VIIIth level of the Schnöd stock goyazite has been found in unusually large, up to 5 cm long, grape-shaped crystalline aggregates, deposited in cavities in quartz or cavities after leached triplite. The aggregates are light pinkish to buff in colour. Goyazite is associated with chrysocolla, fluorapatite and clay minerals.

X-ray powder data and refined unit-cell parameters (Table 7) correspond to published data for minerals of the goyazite – crandallite series. These data also show that the extensive isomorphism makes X-ray identification of the two mineral species problematic.

With regard to the regular increased contents of F, the chemical analyses of goyazite from Krásno (Table 8) were recalculated on the basis of (P+As+S+Si) = 2. Sr (0.47–0.84 *apfu*) is the dominant element in *A*-site of

Table 8 Chemical composition of crandallite and goayzite (in wt. %)

	1	2	3	4	5	6	7	8	9
K_2O	0.00	0.14	0.23	0.31	0.00	0.05	0.03	0.00	0.33
CaO	6.91	10.08	10.82	10.97	4.17	0.77	0.78	0.87	2.60
BaO	0.49	0.25	0.32	0.25	0.55	9.14	4.38	1.27	0.00
SrO	10.27	3.70	2.27	1.70	13.45	14.10	16.30	19.60	0.00
MgO	0.00	0.05	0.00	0.00	0.06	0.05	0.00	0.00	0.00
PbO	0.00	0.00	0.02	0.06	0.12	0.14	0.42	0.00	0.00
CuO	0.06	0.00	0.00	0.00	0.00	0.00	0.00	0.00	0.00
MnO	0.03	0.03	0.00	0.00	0.00	0.00	0.00	0.00	0.00
ZnO	0.00	0.11	0.59	0.55	0.03	0.00	0.00	0.00	0.00
Al_2O_3	33.13	33.88	33.98	34.31	33.23	32.48	32.04	32.61	17.88
Fe_2O_3	0.20	0.15	0.40	0.35	0.00	0.00	0.04	0.00	12.19
Bi_2O_3	0.00	0.00	0.03	0.23	0.02	0.09	0.02	0.00	29.13
SiO_2	0.00	0.00	0.00	0.00	0.00	0.00	0.00	0.00	1.66
As_2O_5	0.02	0.00	0.00	0.00	0.00	0.00	0.06	0.00	9.71
P_2O_5	32.16	33.20	32.73	32.86	32.58	29.52	30.49	27.98	17.00
SO_3	0.85	0.22	0.05	0.00	0.47	1.16	1.59	4.47	0.00
F	2.25	3.47	4.71	4.74	2.68	4.06	4.19	2.52	0.00
H_2O*	12.19	11.86	11.68	11.76	11.70	11.23	10.36	11.31	9.04
O=F	-0.95	-1.46	-1.98	-2.00	-1.13	-1.71	-1.77	-1.06	0.00
total	97.61	95.67	95.86	96.09	97.92	101.09	98.93	99.58	99.54
K^+	0.000	0.013	0.021	0.029	0.000	0.005	0.003	0.000	0.040
Ca^{2+}	0.531	0.764	0.836	0.845	0.320	0.064	0.062	0.069	0.264
Ba^{2+}	0.014	0.007	0.009	0.007	0.015	0.277	0.127	0.037	0.000
Sr^{2+}	0.427	0.152	0.095	0.071	0.558	0.632	0.699	0.841	0.000
Mg^{2+}	0.000	0.006	0.000	0.000	0.006	0.006	0.000	0.000	0.000
Pb^{2+}	0.000	0.000	0.000	0.001	0.002	0.003	0.008	0.000	0.000
Cu^{2+}	0.003	0.000	0.000	0.000	0.000	0.000	0.000	0.000	0.000
Mn^{2+}	0.002	0.002	0.000	0.000	0.000	0.000	0.000	0.000	0.000
Zn^{2+}	0.000	0.006	0.032	0.029	0.002	0.000	0.000	0.000	0.000
Bi^{3+}	0.000	0.000	0.001	0.004	0.000	0.002	0.000	0.000	0.711
A-site	0.977	0.948	0.994	0.986	0.904	0.988	0.899	0.946	1.015
Al^{3+}	2.801	2.825	2.887	2.907	2.804	2.960	2.793	2.842	1.995
Fe^{3+}	0.011	0.008	0.022	0.019	0.000	0.000	0.002	0.000	0.868
B-site	2.812	2.833	2.909	2.926	2.804	2.960	2.795	2.842	2.863
Si^{4+}	0.000	0.000	0.000	0.000	0.000	0.000	0.000	0.000	0.157
As^{5+}	0.001	0.000	0.000	0.000	0.000	0.000	0.002	0.000	0.481
P^{5+} (PO_4)	0.999	1.000	1.001	1.004	1.000	1.002	0.998	1.000	1.073
P^{5+} (PO_3OH)	0.954	0.989	0.997	0.996	0.975	0.931	0.911	0.752	0.289
S^{6+}	0.046	0.011	0.003	0.000	0.025	0.067	0.088	0.248	0.000
T-site	2.000	2.000	2.000	2.000	2.000	2.000	2.000	2.000	2.000
F	0.511	0.777	1.074	1.079	0.606	0.992	0.981	0.590	0.000
OH	4.879	4.606	4.618	4.643	4.614	4.861	4.201	4.828	5.422
OH+F site	5.391	5.383	5.692	5.722	5.220	5.853	5.182	5.418	5.422

1–4 – representative spot analyses of crandallite, Krásno (this paper)
5–8 – representative spot analyses of goyazite, Krásno (this paper)
9 – waylandite, Krásno (Novák *et al.* 2001)
Empirical formulas were calculated on the basis of (P+As+Si+S) = 2.00;
H_2O* – content is calculated from the ideal formula and charge balance.

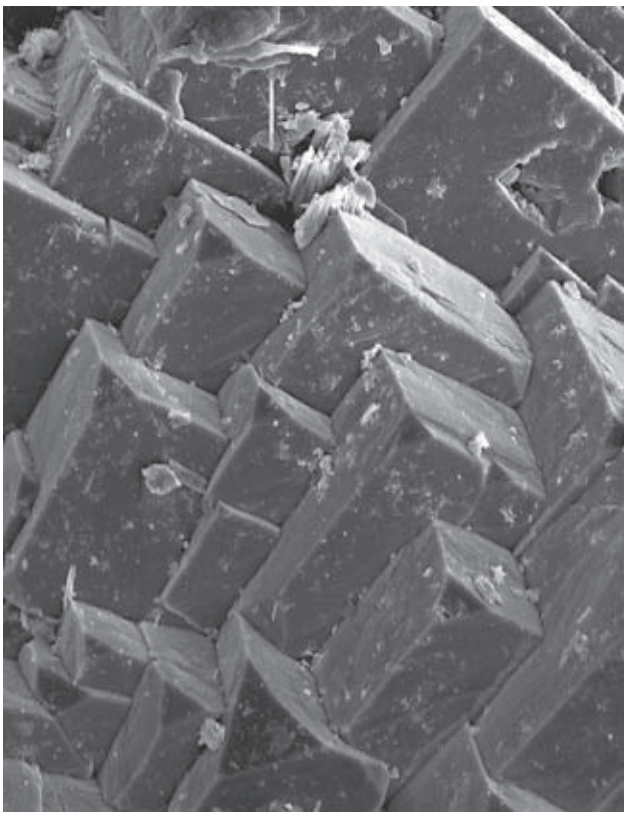

Fig. 29 Trigonal goyazite crystals, Huber open pit, Krásno. Width of photo 60 μm. SEM photograph by J. Sejkora and J. Plášil.

Fig. 30 Rich aggregates of trigonal crystals of crandallite-group minerals, Huber open pit, Krásno. Width of photo 4.5 mm. Nicon SMZ1500 microphotography by J. & E. Sejkora.

Fig. 31 Strongly zoned crystals of crandallite-goyazite, Huber open pit, Krásno. Width of photo 7 mm. Nicon SMZ1500 microphotography by J. & E. Sejkora.

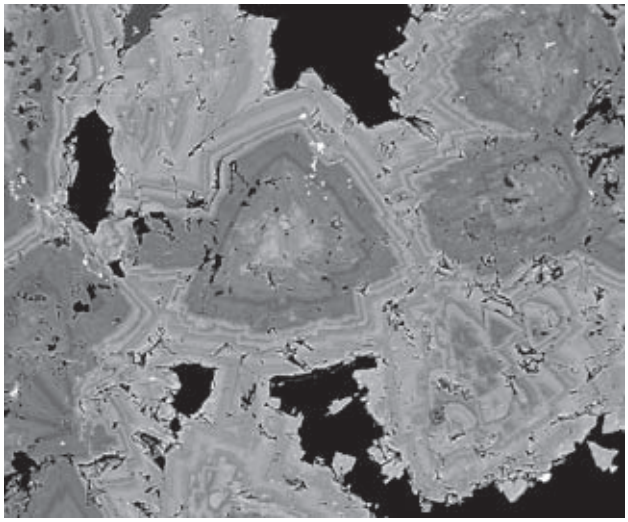

Fig. 32 Group of strongly zoned "crystals" of crandallite-group minerals. The light zones are rich in Sr (goayzite), dark in Ca (crandallite); the light minute inclusions belong to cassiterite. Huber open pit, Krásno. Width of photo 600 μm. BSE photo, Cameca SX100, by J. Sejkora and R. Škoda.

goyazite (Fig. 23), but the contents of the crandallite component (Ca 0.03–0.35 *apfu*) and gorceixite component (Ba 0.01 to 0.27 *apfu*) are also significant. The *B*-site in goyazite (Fig. 24), is dominated by Al (2.79–2.96 *apfu*). In difference to data reported by Novák *et al.* (2001), the Fe contents rarely attain 0.02 *apfu*; the total for atoms in the *B*-site (2.80–2.96 *apfu*) shows a small deficit compared to the theoretical value. The As-content reported by Novák *et al*. (2001) has not been found in the present study. Fluorine contents (Fig. 26), ranging from 0.38 to 1.00 *apfu*, substitute for (OH). Similar contents of F were reported in goyazite from pegmatites in Namibia (Baldwin *et al*. 2000) and from carbonatites in Tanzania (McKie 1962). The coefficients in empirical formulas corresponding to selected spot analyses of goyazite from Krásno are given in Table 8.

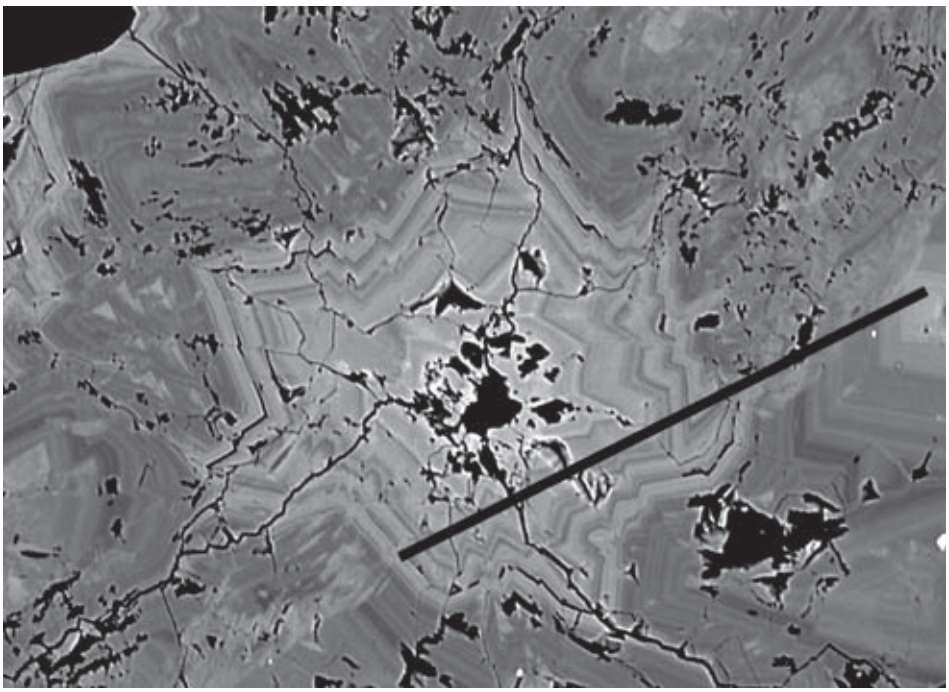

Fig. 33 WD scan of Sr and Ca contents in strongly zoned aggregate composed of goyazite (lighter) and crandallite (darker zones), Huber open pit, Krásno. Width of photo 220 μm. BSE photo, Cameca SX100, by J. Sejkora and R. Škoda.

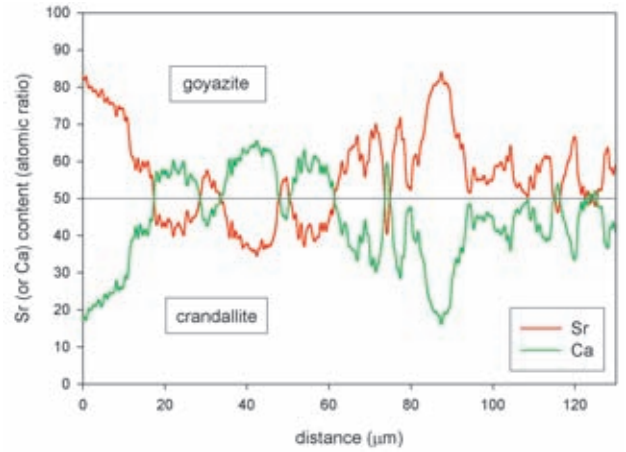

Fig. 34 Profile of Ca *vs.* Sr contents (Ca+Sr atoms = 100, WD analysis) in strongly zoned "crystal" of crandallite-group minerals. Huber open pit, Krásno.

Waylandite $BiAl_3(PO_4)_2(OH)_6$

Novák *et al*. (2001) have described waylandite in a sample from the Huber open pit. It forms light yellow brown, mat and partly porous cryptocrystalline aggregates of earthy appearance on cassiterite and quartz. The association includes *"varlamoffite"* with ca 8 wt. % Fe, dickite with muscovite admixture and coatings of rusty brown Fe oxides-hydroxides *("limonite")*.

Novák *et al.* (2001) gave for waylandite X-ray powder diffraction data and refined unit-cell parameters (Table 9), which fall between the published data for waylandite and zairite (Bi-Fe-P-dominant member of the crandallite group), closer to waylandite. It is in agreement with the chemical composition of waylandite from Krásno. The chemical analysis of waylandite (Table 8, Novák *et al.* 2001) yielded on the basis of 2 (P+As+Si) the following crystallochemical formula: $(Bi_{0.71}Ca_{0.26}K_{0.04})_{\Sigma 1.01}(Al_{1.99}Fe_{0.87})_{\Sigma 2.86}[(PO_4)_{1.07}(AsO_4)_{0.48}(PO_3OH)_{0.29}(SiO_4)_{0.16}]_{\Sigma 2.00}(OH)_{5.42}$. A similar content of crandallite component (0.26 *apfu* Ca in *A*-site in sample from Krásno) in waylandite was reported in samples from Uganda (Knorring – Mrose 1963) and Namibia (Blass – Wittern 1994). The *B*-site contains notable Fe (0.87 *apfu*), which has not been reported yet for waylandite.

Table 9 Unit-cell parameters of waylandite (for trigonal space group *R*-3*m*)

			a [Å]	c [Å]	V [Å^3]
waylandite	Krásno	Novák *et al.* (2001)	6.984(2)	16.304(6)	688.7
waylandite	Cornwall	Clark *et al.* (1986)	6.9834(3)	16.175(1)	684.1
waylandite	Uganda	Bayliss (1986)	6.974(1)	16.293(4)	686.3
zairite	Zaire (Congo)	Wambeke (1975)	7.015(5)	16.37(1)	697.6

Earlshannonite $Mn^{2+}Fe^{3+}_2(PO_4)_2(OH)_2 \cdot 4H_2O$ Whitmoreite $Fe^{2+}Fe^{3+}_2(PO_4)_2(OH)_2 \cdot 4H_2O$ (arthurite group)

Minerals of the arthurite group occur in samples of phosphate accumulations from the Huber open pit in two different mineral associations. The first one consists of irregular whitmoreite aggregates, up to 100 μm in size (Fig. 35), which are replaced by younger phases *UNK1* and *UNK3* (Sejkora *et al.* 2006), and themself replace aggregates of older isokite and fluorapatite.

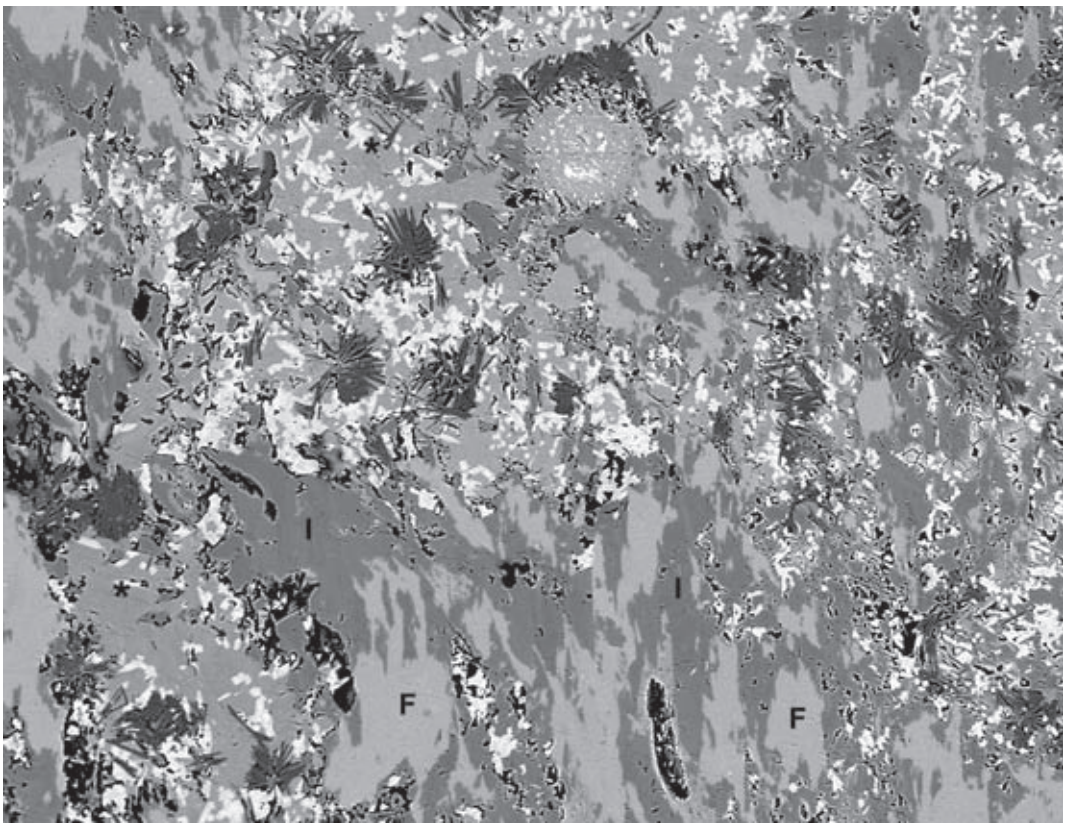

Fig. 35 Complicated aggregate of phosphates from the Huber open pit, Krásno. The oldest mineral fluorapatite (F) is replaced by isokite (I), aggregate of these two minerals is in turn replaced by whitmoreite (*), which contains abundant grains of *UNK3* (very light) and it is itself replaced by the youngest phase *UNK1* (aggregates of dark tabular crystals). Width of photo 600 μm. Cameca SX100, BSE photograph by J. Sejkora and R. Škoda.

The second mineral association occurs in cavities, 2 up to 3 cm in diameter, in triplite accumulations, almost completely altered to compact pink brown fluorapatite. Minerals of the arthurite group are accompanied by abundant, well-formed translucent leucophosphite crystals, younger fluorapatite crystals or aggregates, less common minerals of the chalkosiderite – turquoise group, and rare white skeletal aggregates of *UNK1*. Whitmoreite forms rare translucent, colourless to very light yellow-green tabular to lath-shaped crystals, up to 0.1 mm long. It is intergrown with yellow-green phase *UNK6* showing the same morphology, and darker green *UNK7* grouped to small radiating aggregates or random crystal clusters. Crystals show distinct colour zoning, with lighter green zones (whitmoreite, earlshannonite, *UNK8*) and darker green zones (*UNK7*). Material with chemical composition corresponding to Zn- and Mg-rich earlshannonite has been found in this association only as very tiny and irregular (to 10 μm) zone in aggregate of whitmoreite and *UNK7* (Sejkora *et al*. 2006).

Due to small dimensions of earlshannonite and whitmoreite, it was not possible to examine these phases by X-ray powder diffraction. Their classification with the arthurite group is based mainly on stoichiometry and their intergrowths with, and even distinct zones within, crystals of other members of the arthurite group (*UNK6*, *UNK7*, *UNK8* – Sejkora *et al*. 2006).

The chemical composition of the arthurite group minerals can be expressed by a general formula $AB_2(TO_4)_2(OH,O)_2 \cdot 4H_2O$. A detailed characteristics of occupancy of individual sites is given in description of the new mineral species *UNK6* (Sejkora *et al*. 2006). Two chemically distinct verieties of whitmoreite from Krásno have been found (Table 10). The *A*-site in Cu-rich whitmoreite (Fig. 36) contains dominant Fe^{2+} (0.84–0.88 *apfu*)

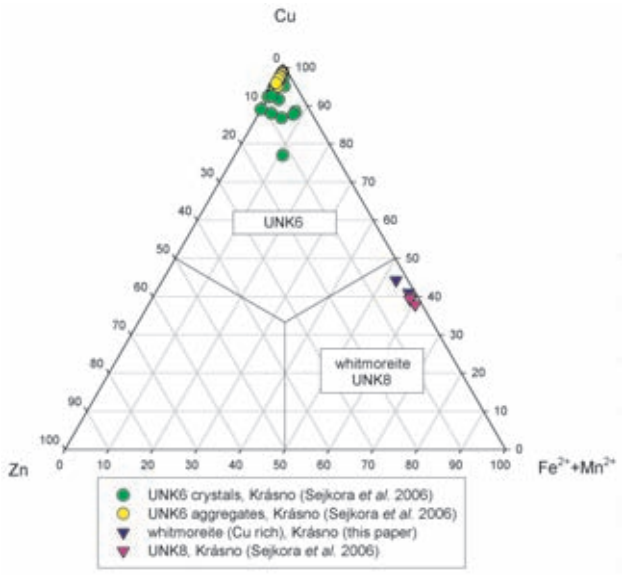

Fig. 36 Ternary plot of *A*-site occupancy by Cu-Zn-(Fe^{2+}+Mn^{2+}) (atomic ratio) for arthurite group mineral phases (Cu-rich whitmoreite, *UNK6*, *UNK8*) from Krásno.

and significant Cu ranging from 0.63 to 0.71 *apfu*. The *B*-site contains Fe^{3+} (1.32–1.49 *apfu*), Al (0.44–0.55 *apfu*) and Ti (0.06–0.13 *apfu*). Phosphorus in tetrahedral *T*-site (1.94 *apfu*) strongly predominates over As (0.06 *apfu*). The chemical composition of Cu-rich whitmoreite can be expressed by the empirical formula $(Fe^{2+}_{0.87}Cu_{0.67}Zn_{0.03})_{\Sigma 1.57}(Fe^{3+}_{1.41}Al_{0.50}Ti_{0.10})_{\Sigma 2.01}[(PO_4)_{1.94}(AsO_4)_{0.06}]_{\Sigma 2.00}(OH)_{3.27} \cdot 4.00H_2O$.

Cu-poor whitmoreite contains in *A*-site (Fig. 37) only a minor amounts of Cu (up to 0.02 *apfu*) and increased Zn (0.15–0.41 *apfu*), besides the dominant Fe^{2+} (0.40–0.69 *apfu*). This probably suggests only a limited isomorphous substitution of Fe^{2+} by Cu and Zn in arthurite group minerals. Fe^{3+} (1.40–1.95 *apfu*) is the dominant element in the *B*-site (Fig. 38). The tetrahedral *T*-site is commonly dominated by P (1.96–1.98 *apfu*) but As-rich members (As 0.56–0.79 *apfu*) containing P in the range 1.20–1.43 *apfu* also occur (Fig. 39). The empirical formula of As-rich members is on the basis of (P+As+S+Si) = 2 $(Fe^{2+}_{0.49}Zn_{0.37}Na_{0.03}Mn_{0.02}Mg_{0.01}Cu_{0.01})_{\Sigma 0.93}(Fe^{3+}_{1.91}Al_{0.07}Ti_{0.01})_{\Sigma 1.99}[(PO_4)_{1.28}(AsO_4)_{0.72}]_{\Sigma 2.00}(OH)_{1.86} \cdot 4.00H_2O$.

The *A*-site in Zn- and Mg-rich earlshannonite (Table 10) is dominated by Mn^{2+} (0.37 *apfu*) and contains significant Zn (0.33 *apfu*), Mg (0.22 *apfu*) and Fe^{2+} (0.12 *apfu*). The *B*-site is occupied mainly by Fe^{3+} (1.94 *apfu*) and the tetrahedral *T*-site contains P (1.80 *apfu*) predominating over As (0.19 *apfu*). The empirical formula on the basis of (P+As+S+Si) = 2 is $(Mn_{0.37}Zn_{0.33}Mg_{0.22}Fe^{2+}_{0.13}Cu_{0.03}Na_{0.02})_{\Sigma 1.10}(Fe_{1.94}Al_{0.03}Ti_{0.03})_{\Sigma 2.00}[(PO_4)_{1.80}(AsO_4)_{1.20}]_{\Sigma 2.00}(OH)_{2.29} \cdot 4.00H_2O$.

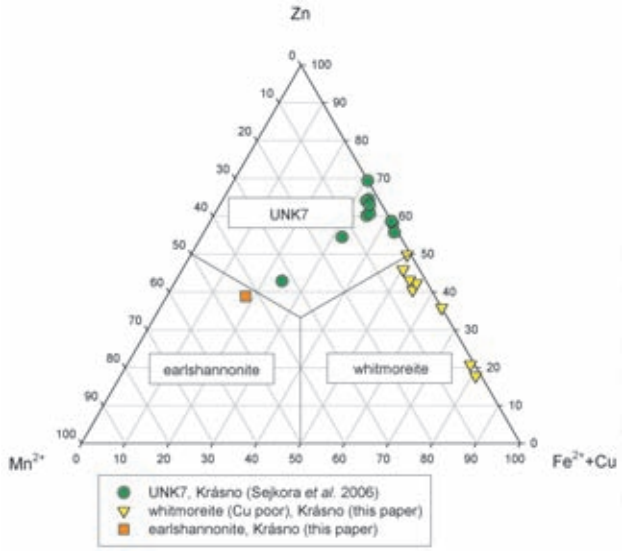

Fig. 37 Ternary plot of *A*-site occupancy by Zn-Mn^{2+}-(Fe^{2+}+Cu) (atomic ratio) for arthurite group mineral phases (Cu-poor whitmoreite, earlshannonite, *UNK7*) from Krásno.

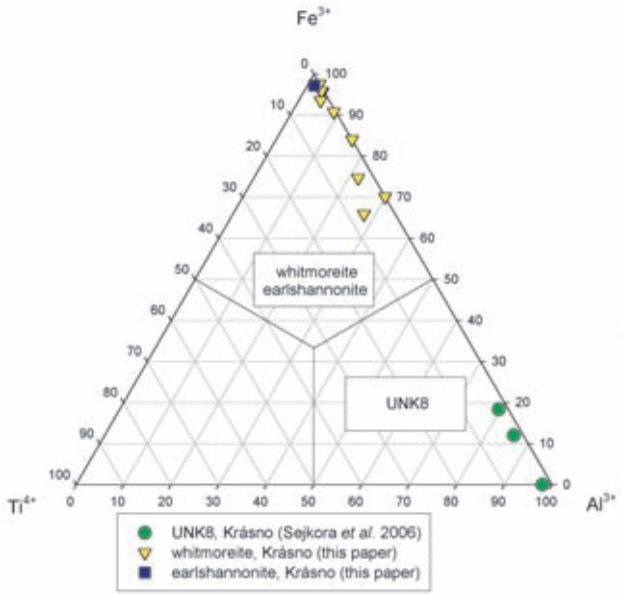

Fig. 38 Ternary plot of *B*-site occupancy by Fe^{3+}-Ti-Al (atomic ratio) for arthurite-group mineral phases (whitmoreite, earlshannonite, *UNK8*) from Krásno.

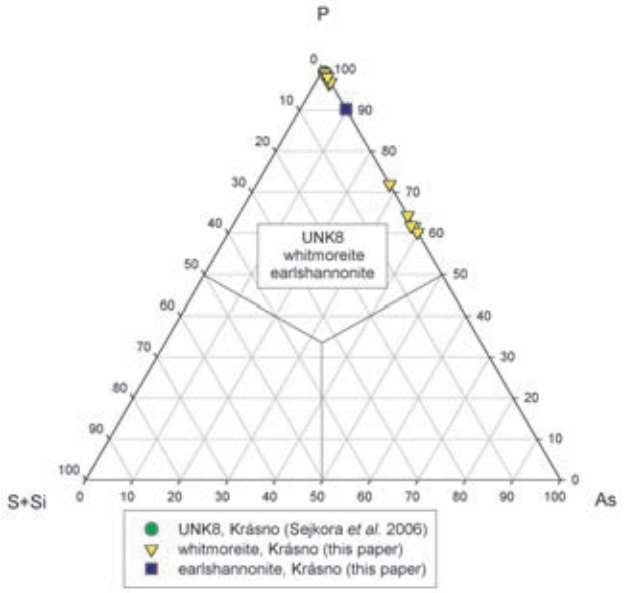

Fig. 39 Ternary plot of *T*-site occupancy by P-(S+Si)-As (atomic ratio) for arthurite group mineral phases (whitmoreite, earlshannonite, *UNK8*) from Krásno.

Fluellite $Al_2(PO_4)F_2(OH) \cdot 7H_2O$

Fluellite has been rarely found in cavities, 1 to 5 cm across, in coarse-grained quartz at several places of the Huber open pit. It usually forms inconspicuous perfect

Table 10 Chemical composition of whitmoreite and earlshannonite (in wt. %)

	1	2	3	4	5	6	7	8
Na_2O	0.16	0.01	0.00	0.02	0.20	0.21	0.14	0.33
K_2O	0.06	0.06	0.05	0.07	0.03	0.01	0.05	0.07
CuO	0.48	10.72	10.13	11.32	0.18	0.09	0.38	0.00
MnO	5.51	0.02	0.00	0.03	0.34	0.52	0.31	0.45
ZnO	5.68	0.55	0.38	0.71	5.95	5.61	5.88	6.35
BaO	0.09	0.06	0.00	0.13	0.04	0.09	0.00	0.00
SrO	0.01	0.05	0.11	0.00	0.02	0.00	0.02	0.02
CaO	0.45	0.04	0.06	0.02	0.07	0.06	0.10	0.03
PbO	0.00	0.12	0.11	0.13	0.01	0.00	0.00	0.04
MgO	1.90	0.00	0.00	0.00	0.11	0.02	0.00	0.14
FeO*	1.89	12.49	12.81	12.18	6.97	6.69	6.43	6.14
Fe_2O_3*	32.72	22.55	23.92	21.17	30.53	30.62	31.15	30.66
Al_2O_3	0.32	5.08	4.49	5.66	0.76	0.79	0.81	0.97
SiO_2	0.05	0.02	0.02	0.02	0.04	0.05	0.05	0.02
TiO_2	0.48	1.60	1.09	2.11	0.22	0.18	0.16	0.61
As_2O_5	4.70	1.40	1.35	1.45	16.47	16.42	17.97	13.24
P_2O_5	26.98	27.60	27.54	27.66	18.16	18.28	17.81	20.94
SO_3	0.02	0.05	0.11	0.00	0.00	0.00	0.00	0.00
H_2O**	19.92	20.31	20.24	20.38	18.57	18.56	18.50	18.90
total	101.40	102.73	102.40	103.06	98.63	98.19	99.75	98.90
Na	0.024	0.002	0.000	0.004	0.032	0.033	0.022	0.052
K	0.006	0.006	0.005	0.008	0.003	0.001	0.005	0.007
Ca	0.038	0.003	0.005	0.002	0.006	0.006	0.009	0.003
Fe^{2+}	0.125	0.865	0.888	0.842	0.485	0.464	0.439	0.417
Ba	0.003	0.002	0.000	0.004	0.001	0.003	0.000	0.000
Sr	0.000	0.003	0.005	0.000	0.001	0.000	0.001	0.001
Mg	0.223	0.000	0.000	0.000	0.013	0.002	0.000	0.017
Pb	0.000	0.003	0.003	0.003	0.000	0.000	0.000	0.001
Cu	0.028	0.671	0.634	0.707	0.011	0.005	0.023	0.000
Mn	0.368	0.001	0.000	0.002	0.024	0.036	0.021	0.031
Zn	0.331	0.033	0.023	0.043	0.365	0.344	0.354	0.380
A total	1.146	1.589	1.564	1.614	0.941	0.895	0.874	0.908
Al^{3+}	0.030	0.495	0.439	0.552	0.074	0.077	0.078	0.093
Fe^{3+}	1.942	1.405	1.493	1.317	1.912	1.911	1.912	1.870
Ti^{4+}	0.028	0.100	0.068	0.131	0.014	0.011	0.010	0.037
B total	2.000	2.000	2.000	2.000	2.000	2.000	2.000	2.000
Si	0.004	0.001	0.002	0.001	0.003	0.004	0.004	0.002
As	0.194	0.061	0.058	0.063	0.717	0.712	0.766	0.561
P	1.801	1.935	1.933	1.936	1.280	1.284	1.230	1.437
S	0.001	0.003	0.007	0.000	0.000	0.000	0.000	0.000
T total	2.000	2.000	2.000	2.000	2.000	2.000	2.000	2.000
H	10.282	11.271	11.197	11.345	9.854	9.769	9.726	9.795
OH	2.287	3.272	3.196	3.348	1.859	1.762	1.727	1.792
H_2O	3.997	3.999	4.000	3.998	3.998	4.003	4.000	4.001

Empirical formulas were calculated on the basis of (P+As+Si+S) = 2.00;
* – calculation of Fe_{tot} to Fe^{2+} and Fe^{3+} is based on the assumption that Fe^{3+} (together with Al^{3+} and Ti^{4+}) completely fills the B^{3+} position and only the surplus Fe (above 2 *pfu*) enters the site A^{2+} as Fe^{2+};
** – H_2O content is calculated from the ideal formula (H_2O = 4.00) and charge balance.
1 – earlshannonite (spot analysis); 2 – Cu-rich whitmoreite (mean of two spot analyses); 5 – Cu-poor whitmoreite (mean of nine spot analyses); 3, 4, 6, 7, 8 – selected spot analyses of whitmoreite.

dipyramidal crystals, up to 1 cm in size (Fig. 40). They are very brittle, water-clear and translucent or slightly turbid to white and transparent, with an intense vitreous lustre. Fluellite is associated with quartz, white and violet fluorite, colourless to light yellowish topaz crystals, cassiterite, wavellite and dickite.

X-ray powder data of fluellite from Krásno (Table 11) and its refined unit-cell parameters (Table 12) are in good agreement with published data. The quantitative chemical analyses yielded Al_2O_3, P_2O_5 and F only (Table 13). Calculation of the theoretical content of H_2O corresponding to ideal formula provided the total near 120 wt. %. It indicates a strong dehydration, corresponding to loss of two H_2O molecules during sample coating in vacuum and analysis. This loss is indicated by irregular fracturing of the analyzed samples. The empirical formula of fluellite calculated on the basis of 14 (O,OH,F) is $Al_{1.98}(PO_4)_{1.07}F_{1.99}(OH)_{0.75}$. $7H_2O$, close to the ideal formula.

Fluorapatite $Ca_5(PO_4)_3(F,Cl,OH)$

Fluorapatite is the most widespread phosphate in the Krásno ore district. It occurs in a variety of morphological forms and is abundant in all its parts (Beran 1999; Beran – Sejkora 2006). In the course of the present study fluorapatite occurrences in phosphate accumulations and their surrounding have been examined in detail. Four types of fluorapatite were recognized with regard to morphological character and position in mineral association:

a) Fluorapatite I forms dark green, exceptionally yellow, grey to black coarse-grained aggregates with grains up to 5 cm, intergrown in white quartz in proximity of phosphate accumulations. In contrast to phosphate accumulation located only 5–20 mm aside, this fluorapatite is not altered by hydrothermal or supergene processes.

b) Fluorapatite II is represented by compact to very fine-grained aggregates of red-brown to brown colour, from several mm to over 1 m in size. Light pink, pink-brown and light brown colour of the aggregates is less common. This fluorapatite is intergrown with white compact or coarse-grained quartz. Aggregates often contain relics and nests of triplite (or zwieselite) of variable colour. Detailed study indicates that fluorapatite II intensively replaced triplite (or zwieselite) and it is in turn extensively replaced by isokite. This process results in aggregates composed of predominant isokite and showing variable textures. Compact fluorapatite aggregates of white, grey or light green colour, replaced in some instances by minerals of the rockbridgeite – frondelite series, morinite, phosphosiderite, and *UNK3* are less common. The compact type of fluorapatite II shows tendency to late hydrothermal or supergene alterations, resulting in cavities more than 10 cm across.

c) Fluorapatite III was found in leached cavities in phosphate accumulations. It forms abundant corroded relics, aggregates and particularly white powdery coatings or filling. Fluorapatite III here also forms colourless, grey, or light pink fine acicular crystals with a silky lustre and colourless, white beige, grey, light pink or greenish tabular to columnar crystals to 1 mm in size, grouped in small aggregates. Leucophosphite, pharmaco-

Fig. 40 Translucent fluellite crystals near 1 cm in size in cavity of coarse-grained quartz, Huber open pit, Krásno. Nicon SMZ1500 microphotography by J.&E. Sejkora.

siderite, kolbeckite, minerals of the turquoise group, and *UNK1, UNK3, UNK4, UNK6, UNK7, UNK8* (Sejkora *et al.* 2006) occur in close association with fluorapatite III.

d) Fluorapatite IV occurs in cavities of quartz gangue, without apparent relation to phosphate accumulations. It forms irregular crystalline aggregates or minute acicular to columnar crystals, sometimes grouped in radiating aggregates. It is colourless, white, grey, yellowish, pink or light violet and is associated with goyazite, crandallite, pharmacosiderite, cassiterite, wolframite, fluorite and clay minerals. Old historical finds of well-crystallized fluorapatite specimens showing variety of colours and crystal morphology (Beran 1999), probably belong to this type of occurrence.

All the described fluorapatite types were confirmed by X-ray powder diffraction, in more than 70 individual samples. Minor deviations from ideal fluorapatite diffraction patterns are probably caused by elevated contents of Mn a Fe in the particular samples.

The general formula of fluorapatite can be presented as $A_5(TO_4)_3Z$, with *A*-site dominanted by Ca, and variable quantities of Mn, Fe, Sr, REE, Pb, Na etc. (Leroy – Bres 2001; Chen *et al.* 2002; Hughes *et al.* 2004). The tetrahedral *T*-site contains P as strongly dominating elements besides As, V, C, Si, S, Mn^{5+} and Cr^{5+} (Hughes *et al.* 2004). In the *Z*-site, the fluorine content must be higher than (OH) or Cl (hydroxylapatite and chlorapatite).

Fluorapatites of all the morphological (or genetic) types from the Huber open pit, from the 5th level of the Huber shaft and from samples probably coming from the Gellnauer vein system have been studied by electron microprobe (Table 14). It is interesting that chemical composition in all studied samples shows small variation, irrespective of their morphological or genetic type or actual

Table 11 X-ray powder diffraction data of fluellite

I_{rel}	*d*	*h*	*k*	*l*	I_{rel}	*d*	*h*	*k*	*l*	I_{rel}	*d*	*h*	*k*	*l*
100	6.491	1	1	1	5	2.3162	3	1	5	7	1.6985	2	6	2
3	5.290	0	0	4	5	2.2978	2	4	2	3	1.6863	5	1	1
9	4.982	0	2	2	12	2.2590	3	3	1	7	1.6820	4	4	2
1	4.910	1	1	3	26	2.1637	3	3	3	5	1.6585	0	6	6
8	3.964	2	0	2	7	2.1505	2	4	4	7	1.6327	3	5	5
6	3.409	2	2	0	13	2.1403	4	0	0	6	1.5715	5	1	5
43	3.244	2	2	2	6	2.0414	3	1	7	4	1.5673	2	2	12
18	3.094	1	3	3	5	1.9833	0	2	10	5	1.5462	2	6	6
8	2.991	0	2	6	7	1.9579	2	4	6	7	1.5271	3	5	7
11	2.867	2	2	4	2	1.9437	1	3	9	5	1.4964	0	4	12
11	2.766	1	1	7	7	1.9391	1	5	5	5	1.4724	1	3	13
17	2.743	3	1	1	6	1.8167	3	3	7	6	1.4331	4	4	8
3	2.728	2	0	6	8	1.7987	2	2	10	6	1.3847	5	3	7
15	2.670	1	3	5	7	1.7636	0	0	12	6	1.3720	6	2	2
2	2.648	0	0	8	4	1.7611	3	5	1	9	1.3608	4	0	12
6	2.489	0	4	4	5	1.7407	4	2	6					
10	2.452	2	2	6	11	1.7040	4	4	0					

Table 12 Unit-cell parameters of fluellite (for orthorhombic space group *Fddd*)

	Krásno this paper	Cornwall Guy – Jeffrey (1966)	Cornwall ICDD 19-0038	Australia ICDD 37-0450
a [Å]	8.558(1)	8.546(8)	8.546	8.5726(8)
b [Å]	11.274(1)	11.222(5)	11.259	11.255(1)
c [Å]	21.179(2)	21.158(5)	21.151	21.186(2)
V [Å^3]	2043.5(3)	2029.12	2035.1	2044.1

Table 13 Chemical composition of fluellite (in wt. %)

	mean	range (4 analyses)	ideal
Al_2O_3	36.40	36.06–36.98	30.89
P_2O_5	27.29	26.93–27.74	21.51
F	13.65	13.37–13.96	11.51
H_2O	47.95		40.95
-F=O	5.75		4.86
total	119.54		100.00

Additional elements were analyzed, including Na, K, Mn, Sr, Ca, Ba, Cu, Zn, Fe, Bi, Si, As, S a Cl; the analysis confirmed their absence or abundances below detection limit of c. 0.01–0.05 wt. %.

Table 14 Chemical composition of fluorapatite (in wt. %)

	M	M	M	M	M	O	O	O	O	O	G	G
Na_2O	0.05	0.34	0.18	0.23	0.06	0.27	0.23	0.00	0.21	0.29	0.34	0.08
K_2O	0.00	0.00	0.00	0.00	0.00	0.00	0.00	0.00	0.03	0.03	0.00	0.00
PbO	0.00	0.00	0.00	0.00	0.05	0.00	0.02	0.00	0.00	0.00	0.10	0.00
CuO	0.00	0.00	0.00	0.00	0.00	0.00	0.00	0.00	0.00	0.24	0.22	0.00
ZnO	0.00	0.00	0.10	0.00	0.00	0.00	0.14	0.00	0.03	0.08	0.13	0.00
FeO	1.49	0.06	1.02	2.13	0.57	2.49	1.34	0.11	1.77	4.09	2.52	0.67
MnO	4.06	0.20	2.93	4.76	2.56	3.90	2.55	0.51	3.72	3.15	3.59	2.12
BaO	0.00	0.00	0.00	0.01	0.26	0.00	0.04	0.00	0.06	0.13	0.19	0.00
SrO	0.00	0.09	0.22	0.63	0.07	0.50	0.16	0.02	0.59	0.29	0.45	0.00
CaO	51.40	55.87	51.84	49.42	51.99	48.36	49.81	55.00	49.52	46.26	49.02	52.84
MgO	0.00	0.00	0.05	0.04	0.01	0.09	0.30	0.02	0.05	0.05	0.02	0.00
Al_2O_3	0.25	0.00	0.01	0.00	0.00	0.00	0.97	0.00	0.01	0.04	0.01	0.00
TiO_2	0.00	0.00	0.01	0.01	0.00	0.00	0.18	0.04	0.00	0.02	0.28	0.00
SiO_2	0.00	0.00	0.00	0.00	0.00	0.00	0.03	0.00	0.01	0.08	0.02	0.00
P_2O_5	41.51	41.54	41.79	40.82	42.93	40.49	40.63	43.12	41.32	37.48	39.50	42.00
As_2O_5	0.00	0.00	0.00	0.00	0.00	0.00	0.00	0.00	0.00	0.00	0.00	0.00
SO_3	0.03	1.01	0.16	0.26	0.00	0.45	0.05	0.04	0.36	0.53	0.15	0.04
Cl	0.00	0.03	0.51	1.11	0.01	1.22	0.00	0.08	0.88	0.89	0.68	0.00
F	3.71	3.05	3.65	2.51	3.44	2.62	3.26	3.68	3.13	3.09	3.29	3.37
-O=Cl	0.00	-0.01	-0.12	-0.25	0.00	-0.28	-0.15	-0.02	-0.20	-0.20	-0.15	0.00
-O=F	-1.56	-1.28	-1.54	-1.06	-1.45	-1.10	-1.37	-1.55	-1.32	-1.30	-1.39	-1.42
*H_2O	0.99	1.27	0.00	1.50	0.00	0.57	0.29	0.00	0.00	1.85	1.77	0.22
total	101.93	102.17	100.81	102.13	100.49	99.58	98.48	101.05	100.16	97.09	100.74	99.92
S^{6+}	0.002	0.064	0.010	0.017	0.000	0.029	0.020	0.002	0.023	0.037	0.010	0.002
P^{5+}	2.998	2.936	2.990	2.983	3.000	2.971	2.980	2.998	2.976	2.956	2.988	2.998
As^{5+}	0.000	0.000	0.000	0.000	0.000	0.000	0.000	0.000	0.000	0.000	0.000	0.000
Si^{4+}	0.000	0.000	0.000	0.000	0.000	0.000	0.000	0.000	0.001	0.007	0.002	0.000
subtot	3.000	3.000	3.000	3.000	3.000	3.000	3.000	3.000	3.000	3.000	3.000	3.000
Ti^{4+}	0.000	0.000	0.001	0.001	0.000	0.000	0.000	0.002	0.000	0.001	0.018	0.000
Al^{3+}	0.025	0.000	0.001	0.000	0.000	0.000	0.002	0.000	0.001	0.004	0.001	0.000
Pb^{2+}	0.000	0.000	0.000	0.000	0.001	0.000	0.000	0.000	0.000	0.000	0.002	0.000
Cu^{2+}	0.000	0.000	0.000	0.000	0.000	0.000	0.000	0.000	0.000	0.017	0.015	0.000
Zn^{2+}	0.000	0.000	0.006	0.000	0.000	0.000	0.001	0.000	0.002	0.005	0.009	0.000
Fe^{2+}	0.106	0.004	0.072	0.154	0.039	0.181	0.096	0.008	0.126	0.319	0.189	0.047
Mn^{2+}	0.294	0.014	0.209	0.348	0.179	0.286	0.232	0.035	0.268	0.248	0.271	0.151
Ba^{2+}	0.000	0.000	0.000	0.000	0.008	0.000	0.003	0.000	0.002	0.005	0.007	0.000
Sr^{2+}	0.000	0.004	0.011	0.031	0.003	0.025	0.020	0.001	0.029	0.016	0.023	0.000
Ca^{2+}	4.698	4.999	4.695	4.571	4.599	4.490	4.643	4.840	4.513	4.618	4.692	4.773
Mg^{2+}	0.000	0.000	0.006	0.005	0.002	0.011	0.006	0.002	0.006	0.007	0.003	0.000
Na^{+}	0.008	0.056	0.029	0.038	0.009	0.045	0.038	0.000	0.034	0.053	0.059	0.013
K^{+}	0.000	0.000	0.000	0.000	0.000	0.000	0.001	0.000	0.003	0.004	0.000	0.000
subtot	5.131	5.077	5.031	5.148	4.841	5.039	5.043	4.888	4.984	5.297	5.290	4.985
Cl^{-}	0.001	0.004	0.073	0.163	0.001	0.179	0.100	0.011	0.126	0.141	0.104	0.001
F^{-}	1.002	0.805	0.975	0.686	0.897	0.718	0.889	0.956	0.842	0.911	0.930	0.897
*OH^{-}	0.278	0.353	0.000	0.429	0.000	0.163	0.084	0.000	0.000	0.523	0.534	0.061
subtot	1.281	1.162	1.049	1.278	0.898	1.061	1.073	0.967	0.968	1.574	1.567	0.958

O – Huber open pit; M – 5th level of the Huber shaft; G – Gellnauer vein system.
Empirical formulas were calculated on the basis of (P+As+S+Si) = 3 and charge balance; water content is calculated from charge balance.

location. On the other hand, compositional variation in one type of fluorapatite from a single location may exceed differences among fluorapatite samples from other localities.

The *A*-site in fluorapatite from Krásno contains, in addition to dominating Ca, only Mn and Fe as important elements entering via homeovalent substitution $(Mn,Fe)Ca_{-1}$. Manganese shows the range of 0–0.39 *apfu.* The iron content is almost always lower than Mn content (Fig. 41), but it is rather high (up to 0.32 *apfu*) in comparison with fluorapatites from pegmatites and granitic rocks (Moore 1982). Similar Fe contents in apatite were observed from beryl-columbite-phosphate pegmatite in Olary Block, Australia (up to 0.33 *apfu*), where apatite is associated with triplite (Lottermoser – Lu 1997). Sr contents do not exceed 0.05 *apfu*. The total of Mn+Fe+Sr in part of specimens correlates with Cl content (Fig. 42). The *T*-site contains only minor As and Si, the content of S is in the range of 0 to 0.03 (a singular case with 0.07) *apfu* in addition to dominating P. Regarding the *Z*-site occupancy, all studied samples belong to fluorapatite (Fig. 43); F always dominates over Cl and the content of (OH) was calculated by stoichiometry. Empirical formulas calculated on the basis of (P+As+S+Si) = 3, corresponding to selected spot analyses of fluorapatite from Krásno, are given in Table 14.

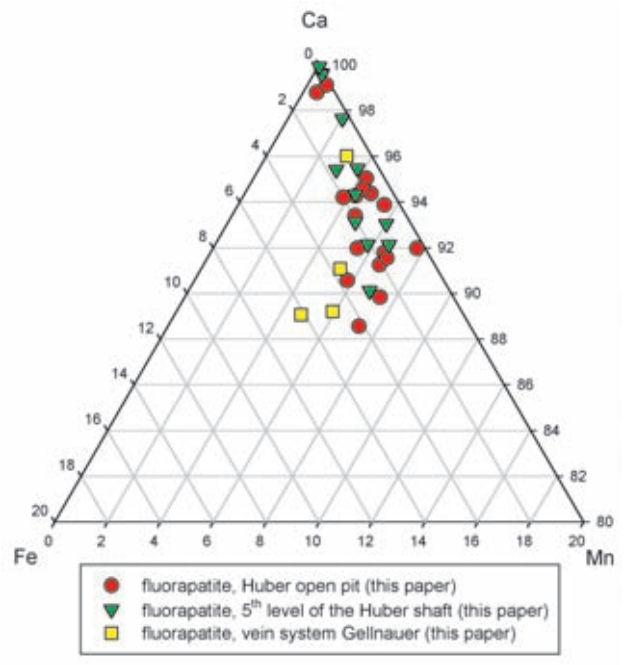

Fig. 41 Part of ternary plot of *A*-site occupancy (atomic ratio) in fluorapatite from Krásno.

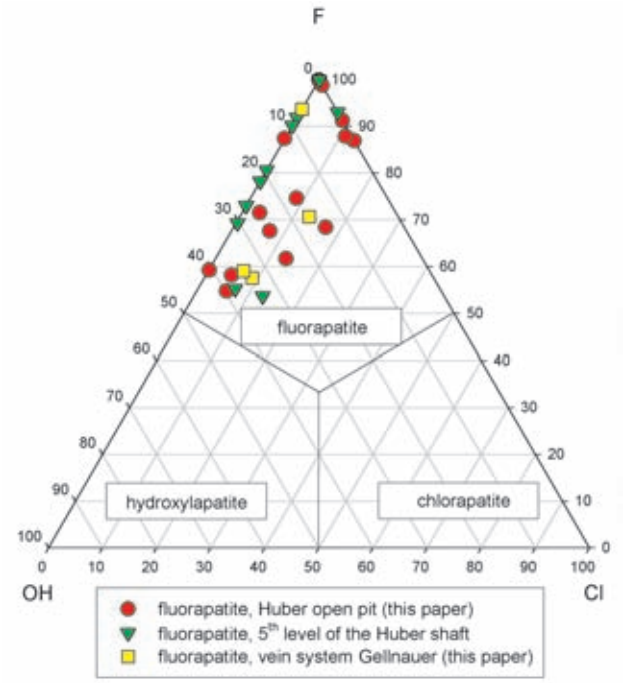

Fig. 43 Ternary plot of *Z*-site occupancy (F-Cl-OH by difference) in fluorapatite from Krásno.

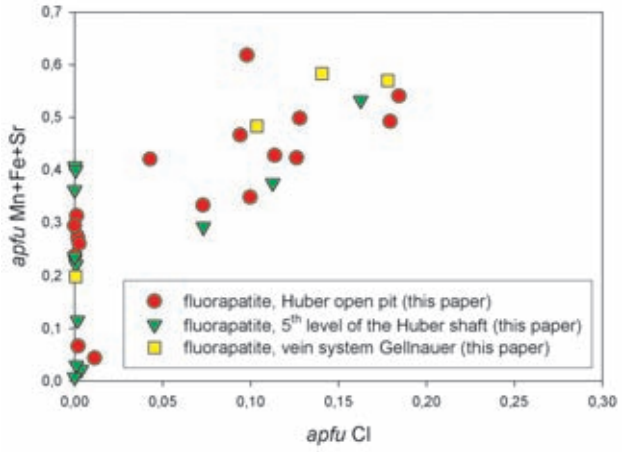

Fig. 42 A plot of *apfu* Cl *vs.* (Mn+Fe+Sr) in fluorapatite from Krásno.

Minerals of the frondelite – rockbridgeite series $Mn^{2+}Fe^{3+}_4(PO_4)_3(OH)_5 – Fe^{2+}Fe^{3+}_4(PO_4)_3(OH)_5$

Minerals of the frondelite – rockbridgeite series were encountered during the present study only in samples from phosphate accumulation at the 5th level of the Huber shaft. Identification of rare rockbridgeite from more abundant frondelite is possible only by quantitative study of chemical composition.

Rockbridgeite occurs as fine-grained to compact aggregates, up to several cm across, composed of tiny equant grains less than 0.1 mm. The aggregates have dark black-green or black colour with a dark green streak. This mineral replaced older reddish brown fluorapatite and probably also triplite (however, their contacts were rarely observed) and it is intensively replaced by younger beraunite, *UNK9* and partly by the youngest light blue phosphosiderite and Mn oxides. In triplite and rockbridgeite aggregates, younger phosphosiderite preferentially replaced triplite (Fig. 44). Also observed was white, fine-grained to compact fluorapatite IV, as one of the youngest minerals in this association.

Frondelite forms up to 15 cm long aggregates replacing older triplite and reddish-brown fluorapatite (partly replaced by younger isokite). Frondelite occurs in two distinct varieties showing differences in morfology and colour. The older frondelite I forms crystalline aggregates of dark black-green or black colour and dark green streak,

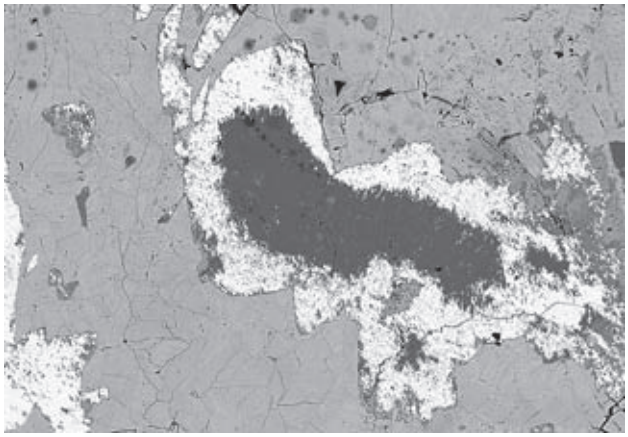

Fig. 44 Rockbridgeite (grey groundmass) with triplite relics (light) intensively replaced by phosphosiderite (dark). 5th level of the Huber shaft, Krásno. Width of photo 1200 μm. Cameca SX100, BSE photograph by J. Sejkora and R. Škoda.

with grain-size less than 0.1 mm (Fig. 45). Small cavities, 2–3 mm in size, rarely contain black minute, highly lustrous prismatic crystals 0.1 mm in size (Fig. 46). The younger type of frondelite II has been found as fine-grained radiating aggregates, up to 1 cm in diameter, red-brown to brown in colour (Fig. 47). Some of the aggregates show colour zoning in various shades of brown. The younger frondelite II is usually deposited directly on the older green type I; in some cases, there are aggregates of *UNK9* at the boundary of the two types. Both types of frondelite were replaced by beraunite and later on, all these minerals by the youngest phosphosiderite (Fig. 48). Morinite and purple-coloured strengite are closely associated.

Fig. 45 Black frondelite I aggregates in compact mass of fluorapatite partly replaced by isokite. 5th level of the Huber shaft, Krásno. Width of 31 mm. Nicon SMZ1500 microphotography by J. & E. Sejkora.

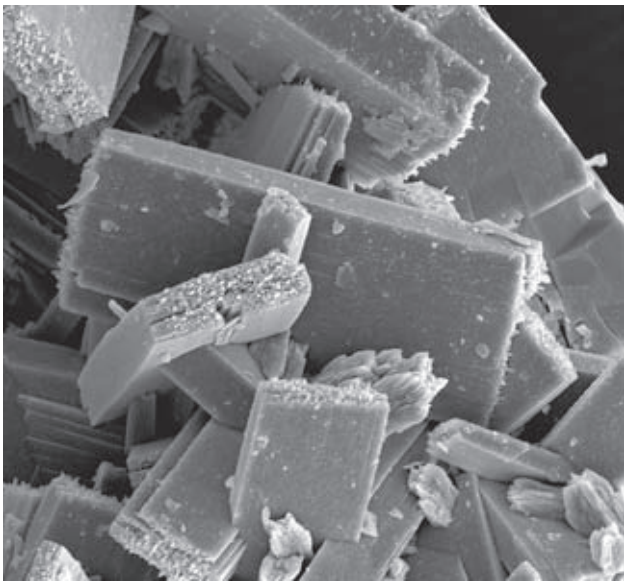

Fig. 46 Prismatic crystals of frondelite I. 5th level of the Huber shaft, Krásno. Width of 60 µm. SEM photograph by J. Sejkora and J. Plášil.

Fig. 47 Radiating aggregates of younger frondelite II. 5th level of the Huber shaft, Krásno. Width of 6 mm. Nicon SMZ1500 microphotography by J. & E. Sejkora.

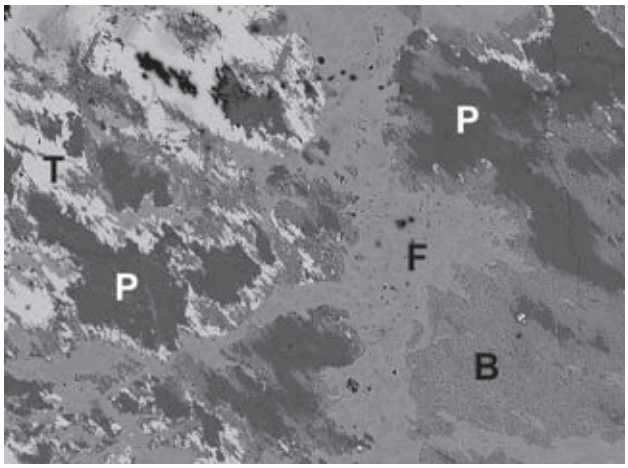

Fig. 48 Agregates of frondelite (F) and triplite (T); beraunite (B) replaces frondelite; in the same sample beraunite and triplite are replaced by younger phosphosiderite (P). 5th level of the Huber shaft, Krásno. Width of photo 1000 µm. Cameca SX100, BSE photograph by J. Sejkora and R. Škoda.

It is not possible to identify rockbridgeite from frondelite on the basis of X-ray diffraction data, as can be seen from diffraction patterns of over 15 samples of chemically defined material. The variation observed in one species exceeds differences between the two species (Table 15). The refined unit-cell parameters (Table 16) correspond to the published data for minerals of rockbridgeite – frondelite series.

The chemical composition of minerals of the rockbridgeite – frondelite series can be expressed by the general formula $AB_4(TO_4)_3(OH)_5$. In order to simplify calculation, it is assumed that the *A*-site is filled by Mn (exclusively as Mn^{2+}), Zn^{2+} and other M^{+} and M^{2+} cations. The Fe^{2+} content is derived from filling the *A*-site to ideal A = 1. The remaining Fe (as Fe^{3+}), Al^{3+} and Ti^{4+} fill the *B*-site. It should be noted that Lindberg (1949) and

Moore (1970) include in *A*-site also Fe^{3+} and in *B*-site also Mn^{3+}; Lindberg – Frondel (1950) considered entry of Zn^{2+} exclusively in *B*-site in Zn-rich rockbridgeite, without any supporting evidence.

The *A*-site occupancy indicates that majority of studied samples from Krásno (Fig. 49) corresponds to fron-

Table 15 X-ray powder diffraction data of minerals in the series rockbridgeite – frondelite.

sample A		sample B		sample C				
I_{rel}	d	I_{rel}	d	I_{rel}	d	h	k	l
64	6.913	61	6.967	63	6.929	0	2	0
17	4.840	15	4.846	27	4.842	1	1	0
18	4.623	12	4.658	25	4.652	1	1	1
21	4.367	11	4.366	30	4.366	0	2	3
31	4.208	15	4.209	41	4.221	0	0	4
33	3.665	21	3.673	37	3.665	1	1	3
53	3.595	41	3.602	71	3.605	0	2	4
51	3.447	49	3.456	50	3.444	1	3	0
83	3.386	100	3.413	87	3.392	0	4	1
	3.386	23	3.389	29	3.377	1	3	1
100	3.184	88	3.198	100	3.189	1	3	2
34	3.027	33	3.030	51	3.037	0	2	5
26	2.957	22	2.964	31	2.960	0	4	3
38	2.798	23	2.805	35	2.817	0	0	6
41	2.763	31	2.763	42	2.770	1	1	5
	—	22	2.683	34	2.677	0	4	4
29	2.588	19	2.589	33	2.583	2	0	0
37	2.4269	47	2.4259	54	2.4319	1	1	6
	2.4269		2.4259	33	2.4178	1	5	1
29	2.4083	31	2.4101	61	2.4117	1	3	5
23	2.2720	17	2.2671	38	2.2781	0	2	7
21	2.1759	17	2.1783	29	2.1804	1	3	6
20	2.1537	20	2.1529	37	2.1601	1	1	7
	—	19	2.1180	38	2.1127	1	5	4
23	2.0601	17	2.0662	36	2.0575	2	4	1
21	2.0227	20	2.0340	35	2.0257	0	6	4
31	1.9647	21	1.9681	33	1.9678	2	2	5
16	1.8487	17	1.8599	36	1.8491	1	7	0
15	1.8308	16	1.8347	34	1.8317	2	2	6
13	1.7312	9	1.7420	33	1.7329	0	8	0
19	1.7136	11	1.7143	32	1.7174	1	5	7
14	1.6933	9	1.6903	19	1.6892	2	6	2
13	1.6813	7	1.6804	18	1.6866	0	0	10
21	1.6425	16	1.6464	31	1.6496	0	4	9
17	1.6055	19	1.6092	33	1.6035	0	8	4
15	1.5938	17	1.5947	29	1.5976	2	6	4
13	1.5876	11	1.5889	19	1.5912	3	3	2
	1.5876		1.5889		1.5912	2	2	8

A – Mn-rich rockbridgeite (*A*-site: $Fe_{0.56}Mn_{0.38}Zn_{0.04}Ca_{0.02}$)
B – black-green granular frondelite I (*A*-site: $Mn_{0.82}Fe_{0.07}Zn_{0.07}Ca_{0.02}Na_{0.01}$)
C – brown-black frondelite II from radiating aggregate (*A*-site: $Mn_{0.90}Zn_{0.07}Ca_{0.02}Na_{0.01}$)

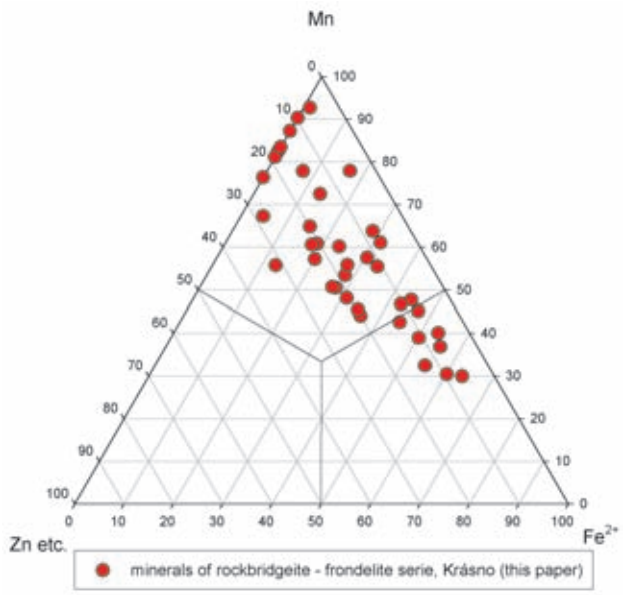

Fig. 49 Ternary plot of *A*-site occupancy (atomic ratio) in minerals of the rockbridgeite – frondelite series from Krásno. Zn etc. = Zn+Na+K+Ca+Ba+Sr+Mg+Pb+Cu.

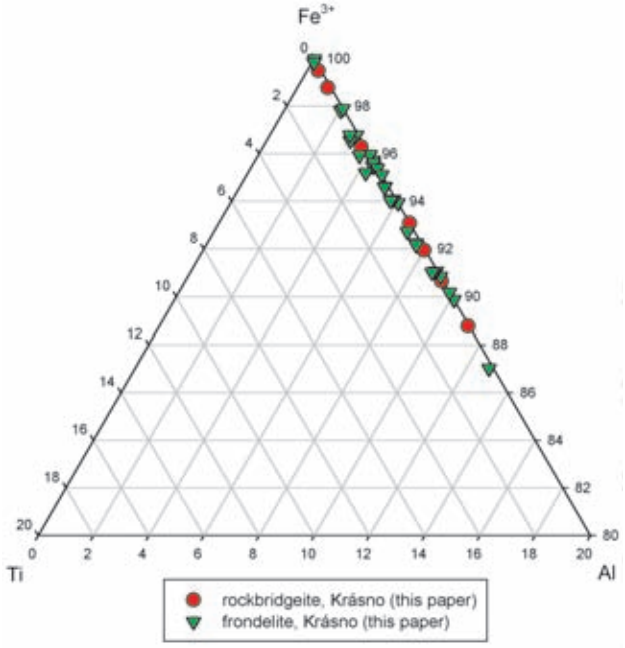

Fig. 50 Part of ternary plot of *B*-site occupancy (atomic ratio) in minerals of the rockbridgeite – frondelite series from Krásno.

Table 16 Unit-cell parameters of minerals of the rockbridgeite – frondelite series (for orthorhombic space group *Cmcm*)

	Krásno A this paper	Krásno B this paper	Krásno C this paper	rockbridgeite ICDD 34-150	rockbridgeite Moore (1970)	frondelite ICDD 35-625	frondelite ICDD 8-83
a [Å]	5.176(3)	5.176(2)	5.177(2)	5.185(1)	5.172(4)	5.182(1)	5.21
b [Å]	13.873(7)	13.932(5)	13.864(5)	13.846(2)	13.78(1)	13.810(1)	13.89
c [Å]	16.810(8)	16.811(6)	16.878(5)	16.782(2)	16.805(9)	16.968(3)	17.01
V [Å^3]	1207.1(8)	1212.4(6)	1211.4(5)	1204.8	1198.0	1214.3	1231.0

A – Mn-rich rockbridgeite (*A*-site: $Fe_{0.56}Mn_{0.38}Zn_{0.04}Ca_{0.02}$)
B – black-green granular frondelite I (*A*-site: $Mn_{0.82}Fe_{0.07}Zn_{0.07}Ca_{0.02}Na_{0.01}$)
C – brown-black frondelite II from radiating aggregate (*A*-site: $Mn_{0.90}Zn_{0.07}Ca_{0.02}Na_{0.01}$)

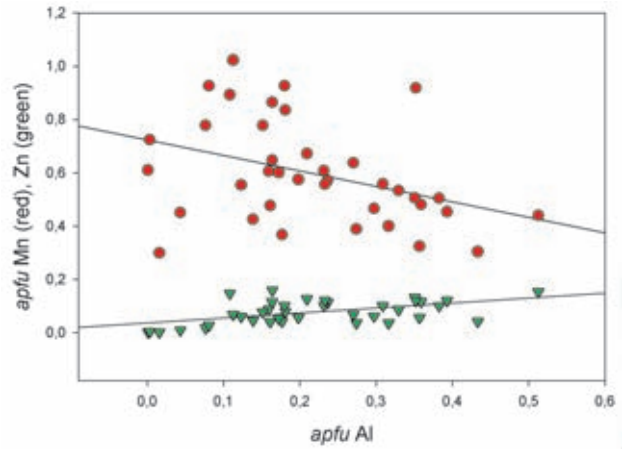

Fig. 51 Correlation of Al vs. Mn and Zn in minerals of the rockbridgeite – frondelite series from Krásno, expressed by regression curves.

delite with Mn content 0.44–1.02 *apfu* Mn, Fe^{2+} (up to 0.44), Zn (up to 0.16), Na, Ca and Mg (max. 0.08 *apfu*). Only several samples correspond to Mn-rich rockbridgeite with Fe^{2+} (0.45–0.63 *apfu*) predominating above Mn (0.30–0.45 *apfu*) and only minor Zn (up to 0.06 *apfu*). The *B*-site in frondelite and rockbridgeite (Fig. 50) contains in addition to Fe^{3+} also Al (up to 0.51 *apfu*) and minor Ti to 0.02 *apfu*. It is interesting that increasing Al in *B*-site correlates with decrease in Mn and increase in Zn in *A*-site (Fig. 51). The tetrahedral *T*-site contains besides predominating P only minor contents of As, Si and S (max. 0.01–0.02 *apfu*). None of the studied samples shows substitution of (OH) by Cl or F. The empirical formulas calculated on the basis of (P+As+S+Si) = 3, corresponding to representative spot analyses of minerals of the rockbridgeite – frondelite series from Krásno, are presented in Table 17.

Table 17 Chemical composition of minerals of rockbridgeite – frondelite series (in wt. %).

	1	2	3	4	5	6	7	8	9	10
Na_2O	0.01	0.02	0.00	0.03	0.07	0.00	0.00	0.07	0.12	0.16
K_2O	0.00	0.00	0.01	0.00	0.00	0.00	0.00	0.01	0.01	0.00
CaO	0.24	0.15	0.12	0.00	0.08	0.07	0.07	0.37	0.02	0.31
FeO*	6.79	6.16	5.97	5.13	4.00	3.75	3.14	0.78	0.00	0.00
BaO	0.15	0.07	0.13	0.04	0.00	0.28	0.03	0.00	0.11	0.00
SrO	0.00	0.00	0.01	0.01	0.03	0.00	0.00	0.02	0.00	0.10
MgO	0.03	0.03	0.03	0.11	0.11	0.07	0.00	0.04	0.03	0.05
PbO	0.15	0.06	0.01	0.00	0.11	0.01	0.00	0.00	0.04	0.00
CuO	0.09	0.02	0.00	0.51	0.00	0.21	0.00	0.00	0.00	0.00
MnO	3.39	4.03	4.40	4.86	4.85	6.11	6.95	8.16	11.22	8.86
ZnO	0.55	0.54	0.47	0.13	1.96	0.78	0.86	0.95	0.87	0.97
Al_2O_3	3.47	1.39	2.50	0.34	4.05	0.98	2.12	1.14	0.89	1.38
Fe_2O_3*	43.11	46.24	44.93	47.31	43.10	47.03	43.88	46.69	44.33	44.81
TiO_2	0.02	0.03	0.02	0.06	0.08	0.04	0.13	0.20	0.19	0.01
SiO_2	0.03	0.07	0.02	0.07	0.02	0.00	0.05	0.05	0.00	0.11
As_2O_5	0.07	0.00	0.01	0.00	0.26	0.23	0.09	0.01	0.00	0.00
P_2O_5	33.29	32.80	32.93	32.34	32.71	32.77	32.48	31.45	32.90	31.82
SO_3	0.06	0.00	0.04	0.00	0.00	0.04	0.11	0.00	0.00	0.00
H_2O*	6.54	6.63	6.77	6.58	7.02	6.72	6.35	7.12	6.15	6.37
total	97.98	98.23	98.35	97.50	98.43	99.08	96.24	97.05	96.89	94.95
Na^+	0.001	0.004	0.000	0.006	0.014	0.000	0.000	0.014	0.025	0.035
K^+	0.000	0.000	0.001	0.000	0.000	0.000	0.000	0.002	0.002	0.000
Ca^{2+}	0.028	0.017	0.014	0.000	0.009	0.008	0.008	0.045	0.003	0.037
Fe^{2+}	0.602	0.556	0.537	0.470	0.359	0.336	0.285	0.074	0.000	0.000
Ba^{2+}	0.006	0.003	0.005	0.002	0.000	0.012	0.001	0.000	0.004	0.000
Sr^{2+}	0.000	0.000	0.001	0.001	0.002	0.000	0.000	0.001	0.000	0.006
Mg^{2+}	0.004	0.005	0.004	0.018	0.018	0.011	0.000	0.007	0.005	0.008
Pb^{2+}	0.004	0.002	0.000	0.000	0.003	0.000	0.000	0.000	0.001	0.000
Cu^{2+}	0.007	0.001	0.000	0.042	0.000	0.017	0.000	0.000	0.000	0.000
Mn^{2+}	0.304	0.369	0.400	0.451	0.440	0.555	0.638	0.778	1.024	0.836
Zn^{2+}	0.043	0.043	0.037	0.010	0.155	0.061	0.069	0.079	0.069	0.080
subtotal	1.000	1.000	1.000	1.000	1.000	1.000	1.000	1.000	1.133	1.001
Al^{3+}	0.433	0.177	0.316	0.043	0.513	0.123	0.270	0.151	0.113	0.181
Fe^{3+}	3.438	3.760	3.634	3.901	3.480	3.791	3.579	3.957	3.592	3.755
Ti^{4+}	0.002	0.002	0.002	0.005	0.006	0.003	0.010	0.017	0.015	0.001
subtotal	3.874	3.938	3.952	3.949	3.999	3.917	3.860	4.125	3.721	3.937
Si^{4+}	0.003	0.008	0.002	0.008	0.002	0.000	0.005	0.006	0.000	0.012
As^{5+}	0.004	0.000	0.000	0.000	0.014	0.013	0.005	0.001	0.000	0.000
P^{5+}	2.988	2.992	2.994	2.992	2.983	2.984	2.981	2.993	3.000	2.987
S^{6+}	0.005	0.000	0.003	0.000	0.000	0.003	0.009	0.000	0.000	0.000
subtotal	3.000	3.000	3.000	3.000	3.000	3.000	3.000	3.000	3.000	3.000
OH	4.624	4.778	4.854	4.810	5.025	4.801	4.591	5.349	4.418	4.732

1–4 rockbridgeite, Krásno; 5–10 frondelite, Krásno
FeO* and Fe_2O_3* – calculated on the basis of assumed occupancy of *A*- and *B*- sites,
H_2O* – calculated on the basis of charge balance.

Goyazite

see minerals of the crandallite group

Isokite $CaMg(PO_4)F$

Fischer (1957) described isokite in samples collected by J. Kutina on dumps in the Horní Slavkov ore district (mining area at the Schnöd stock) as fine-grained compact aggregates in association with triplite and (fluor)apatite. Fisher (1957) in his somewhat tentative interpretation assumed that isokite was formed by a late hydrothermal alteration of dark ("light brown") type of triplite and mentioned its formation in the sequence triplite – isokite – apatite. Information obtained in the present study indicates that some data presented by Fisher (1957) are somewhat problematic, in particular the position of apatite, which he considered as younger than isokite, and particularly the suggestion concerning quartz: ("… quartz formed post-isokite.").

During our research, isokite has been identified as one of the most widespread phosphates in the Krásno ore district. It is probable that in the past, isokite was considered compact fluorapatite, due to its inconspicuous appearance. Newly studied isokite samples come from numerous places in the Huber open pit, from phosphate accumulations at the 5th level of Huber shaft and it was identified in historical museum specimens from the Gellnauer vein system. No differences have been noted in macroscopic and microscopic properties among isokite samples collected at various partial localities.

The most common and inconspicuous form of isokite is as rather hard and compact fine-grained aggregates of light pink, pink-brown to light brown colour with a weak greasy lustre, up to 10 cm across (Fig. 52). Isokite is intergrown with variable quantity of older fluorapatite in these aggregates, which are macroscopically indistinquishable from aggregates of fluorapatite around older triplite (with various colour), always intergrown in massive and coarse-grained quartz. The microscopic observations show that isokite always replaced only fluorapatite and not directly triplite (Fig. 53). The observed interfaces triplite – isokite are free of indications of alteration, but isokite aggregates often contain fluorapatite relics (Fig. 54). Hochleitner – Fehr (2005) described a similar occurrence of compact isokite formed in the sequnce triplite – Mn-rich fluorapatite – isokite from pegmatite at Senhora de Assunção (Portugal).

Fig. 52 Aggregates of compact isokite (intergrown with fluorapatite) around aggregates of older triplite with white quartz. 5th level of the Huber shaft, Krásno. Width of photo 20 mm. Nicon SMZ1500 microphotography by J. & E. Sejkora.

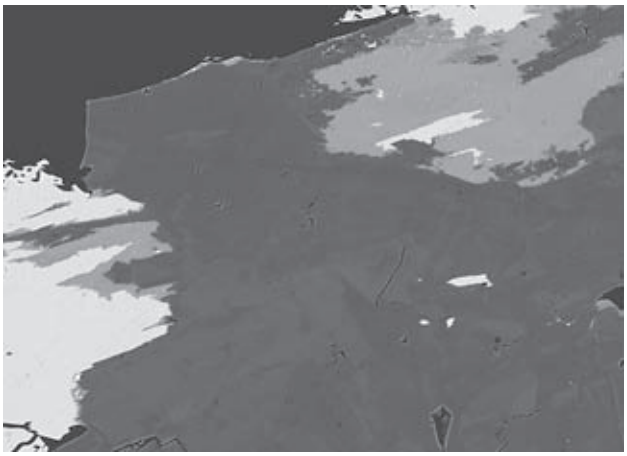

Fig. 53 Irregular zoned aggregate of isokite (dark) replacing fluorapatite (grey), which replaced the oldest mineral triplite (white), Huber open pit, Krásno. Width of photo 500 μm. BSE photograph Cameca SX100 by J. Sejkora and R. Škoda.

A second type of isokite forms soft, incoherent to earthy aggregates, up to 5 cm in size, of whitish, yellowish, light pink to yellow-brown colour. It is macroscopically more conspicuous than isokite of the first type. It is associated with compact isokite aggregates of the first type, fluorapatite and triplite. The soft isokite II aggregates are composed of fine, equant and usually corroded grains less than 0.1 mm in size (Fig. 55). Analyses of both types of isokite from various places show chemical and X-ray diffraction identity. In the preferred interpretation, soft isokite II was produced by weathering of less stable fluorapatite in compact isokite+fluorapatite aggregates, not formed as a younger (second) generation of isokite. Isokite I and II are associated with fluorapatite, triplite (zwieselite), minerals of the rockbridgeite – frondelite series, rare whitmoreite, turquoise group minerals, strengite, *UNK3*, zircon, Nb-rich rutile and sulfides (arsenopyrite, chalcopyrite etc.). Small parallel aggregates of acicular isokite III crystals of mm scale have been observed in cavities of phosphate accumulations (Fig. 56). This very rare type of isokite III probably rep-

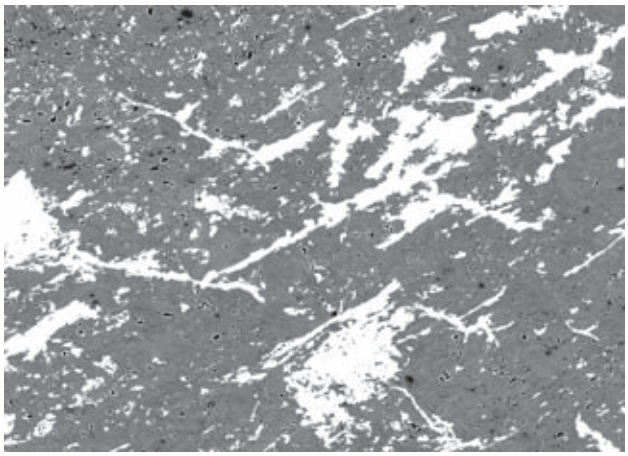

Fig. 54 Isokite aggregate (darker groundmass) with numerous replacement relics of fluorapatite (light). Huber open pit, Krásno. Width of photo 800 μm. BSE photograph Cameca SX100 by J. Sejkora and R. Škoda.

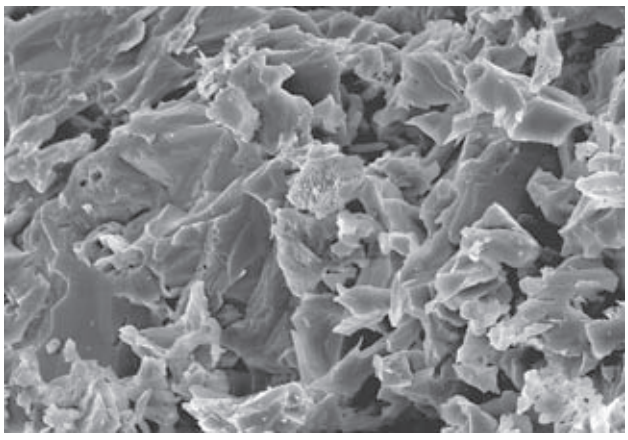

Fig. 55 Irregular isokite grains. 5th level of the Huber shaft, Krásno. Width of photo 60 μm. SEM photograph by J. Sejkora.

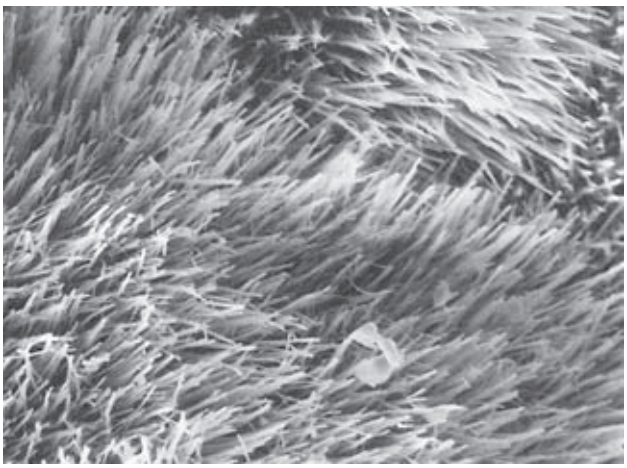

Fig. 56 Aggregate of isokite acicular crystals in parallel growth. Huber open pit, Krásno. Width of photo 130 μm. SEM photograph by M. Fikar.

Ca, *B*-site by Mg, tetrahedral *T*-site by P and *Z*-site by F (isokite) or OH (panasqueiraite, Isaacs – Peacor 1981). The isokite chemical composition in all analyzed samples is rather similar and is very close to the end member composition (Table 20). Fluorine content shows a higher variability (Fig. 57), from the Huber open pit (0.68–0.84) to the 5th level of the Huber shaft (0.78–0.91 *apfu* F). Ca and Mg contents (*A*- and *B*- site) are near the theoretical ratio 1:1 (0.95–1.01 *apfu* Ca; 0.86–1.01 *apfu* Mg). The minor contents of Fe (0.01–0.08 *apfu*, in samples from the Gellnauer vein system 0.10–0.12 *apfu*) and Mn (0.01–0.02 *apfu*) enter the isokite structure by substitutions $(Fe,Mn)Ca_{-1}$ and $(Fe,Mn)Mg_{-1}$, without showing a preference for one of the alternatives (Fig. 58). Analyzed samples from the 5th level of the Huber shaft show slightly increased contents of Na (Fig. 59) and S (Fig. 60) in comparison with other samples. The Na concentration

Table 18 X-ray powder diffraction pattern of isokite

I_{rel}	*d*	*h*	*k*	*l*	I_{rel}	*d*	*h*	*k*	*l*	I_{rel}	*d*	*h*	*k*	*l*
17	4.377	0	2	0	26	2.0690	0	4	1	13	1.5368	1	3	-4
13	3.614	0	2	1	25	2.0393	3	1	-1	13	1.5199	4	2	-2
39	3.198	0	0	2	14	1.9598	3	1	-3	9	1.5073	4	0	-4
100	3.177	1	1	1	19	1.8829	1	3	-3	10	1.4949	3	3	-4
68	3.016	2	0	-2	16	1.8709	2	0	-4	22	1.4795	1	3	3
31	2.7833	2	0	0	24	1.8052	0	4	2	5	1.4505	3	1	-5
86	2.6253	1	3	-1	12	1.7710	1	1	-4	11	1.4269	1	5	-3
49	2.5829	0	2	2	11	1.7387	3	3	-2	9	1.4214	2	4	-4
49	2.5829	1	3	0	63	1.7192	2	2	-4	15	1.3917	4	0	0
7	2.4845	2	2	-2	27	1.7052	2	0	2	11	1.3863	3	3	1
2	2.3782	1	1	-3	7	1.6850	1	1	3	14	1.3435	3	5	-1
44	2.2987	1	3	-2	9	1.6693	1	5	0	17	1.3127	2	6	-2
33	2.2287	1	1	2	28	1.6552	3	3	-3	12	1.3026	4	4	-2
35	2.2155	1	3	1	12	1.6020	0	0	4	13	1.2769	1	3	-5
29	2.1035	3	1	-2	25	1.5564	1	5	1	15	1.2343	2	0	-6

Table 19 Unit-cell parameters of isokite (for monoclinic space group *C*2/*c*)

	Krásno this paper	Senhora de Assunção Hochleitner – Fehr (2005)	Isoka Deans – McConnell (1955)
a [Å]	6.517(1)	6.527(5)	6.52(5)
b [Å]	8.746(1)	8.744(5)	8.75(5)
c [Å]	7.499(1)	7.501(6)	7.51(5)
β [°]	121.35(1)	121.34(1)	121.5(2)
V [Å^3]	365.0(1)	365.68	365.3

resents a true younger, remobilized generation of this mineral.

X-ray powder diffraction data for isokite from Krásno (Table 18) correspond to published data. The unit-cell parameters were refined in the space group *C*2/*c* (Table 19). The alternative of non-standard space group *A*2/*a*, proposed by Jaffe *et al.* (1992) with regard to probable isostructural relation of isokite to titanite (Povarennykh 1972), yields on theoretical calculation of diffraction maxima intensity values which do not correspond to experimentally obtained patterns.

The general chemical formula for isokite-related minerals is $AB(TO_4)Z$. The *A*-site is occupied dominantly by

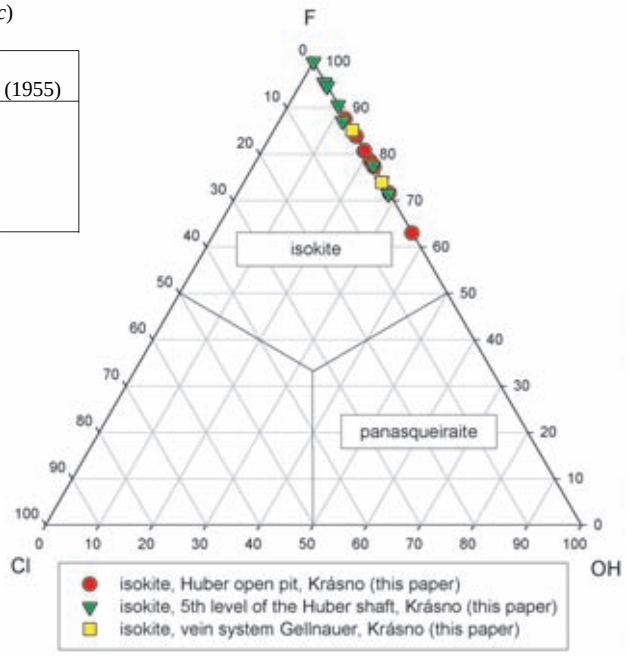

Fig. 57 Ternary plot of F-Cl-OH occupancy in *Z*-site (atomic ratio) for isokite from Krásno.

Table 20 Chemical composition of isokite (in wt. %)

	M	O	M	M	G	G	M	M
Na_2O	0.34	0.04	0.18	0.08	0.11	0.15	0.07	0.06
K_2O	0.02	0.01	0.01	0.01	0.00	0.00	0.02	0.02
CaO	30.75	31.05	30.33	30.84	29.19	29.97	31.53	32.11
SrO	0.01	0.07	0.12	0.00	0.06	0.04	0.02	0.06
BaO	0.00	0.13	0.00	0.00	0.00	0.04	0.13	0.00
MgO	21.32	21.68	20.83	19.74	20.68	18.97	20.91	21.24
MnO	0.73	0.52	0.44	0.70	0.32	0.50	0.27	0.38
FeO	1.73	1.44	1.32	2.31	4.86	4.17	1.48	1.01
CuO	0.00	0.00	0.24	0.01	0.23	0.07	0.00	0.10
ZnO	0.06	0.08	0.00	0.00	0.00	0.09	0.04	0.11
PbO	0.04	0.02	0.00	0.07	0.00	0.03	0.14	0.00
Al_2O_3	0.00	0.00	0.00	0.03	0.07	0.00	0.05	0.03
TiO_2	0.13	0.01	0.25	0.04	0.08	0.14	0.01	0.07
SiO_2	0.00	0.00	0.04	0.04	0.06	0.00	0.05	0.10
P_2O_5	39.36	40.27	39.38	38.68	38.10	37.96	40.19	40.13
As_2O_5	0.02	0.08	0.00	0.00	0.02	0.13	0.00	0.00
SO_3	0.51	0.14	0.34	0.25	0.25	0.13	0.00	0.00
Cl	0.19	0.02	0.04	0.02	0.06	0.03	0.02	0.01
F	9.36	8.02	9.36	9.45	8.56	8.89	9.40	9.48
-O=F.Cl	-3.98	-3.38	-3.95	-3.98	-3.62	-3.75	-3.96	-3.99
*H_2O	0.57	1.02	0.20	0.24	1.32	0.66	0.23	0.42
total	101.14	101.22	99.11	98.52	100.35	98.23	100.61	101.32
Na^+	0.020	0.002	0.010	0.005	0.006	0.009	0.004	0.003
K^+	0.001	0.000	0.000	0.001	0.000	0.000	0.001	0.001
Ca^{2+}	0.974	0.969	0.964	0.999	0.959	0.991	0.989	1.007
Sr^{2+}	0.000	0.001	0.002	0.000	0.001	0.001	0.000	0.001
Ba^{2+}	0.000	0.001	0.000	0.000	0.000	0.000	0.002	0.000
Mg^{2+}	0.940	0.941	0.921	0.890	0.945	0.873	0.912	0.926
Mn^{2+}	0.018	0.013	0.011	0.018	0.008	0.013	0.007	0.009
Fe^{2+}	0.043	0.035	0.033	0.058	0.125	0.108	0.036	0.025
Cu^{2+}	0.000	0.000	0.005	0.000	0.005	0.002	0.000	0.002
Zn^{2+}	0.001	0.002	0.000	0.000	0.000	0.002	0.001	0.002
Pb^{2+}	0.000	0.000	0.000	0.001	0.000	0.000	0.001	0.000
Al^{3+}	0.000	0.000	0.000	0.001	0.002	0.000	0.002	0.001
Ti^{4+}	0.003	0.000	0.006	0.001	0.002	0.003	0.000	0.002
subtotal	1.998	1.965	1.946	1.973	2.052	1.999	1.954	1.977
Si^{4+}	0.000	0.000	0.001	0.001	0.002	0.000	0.002	0.003
P^{5+}	0.988	0.996	0.991	0.993	0.992	0.995	0.998	0.997
As^{5+}	0.000	0.001	0.000	0.000	0.000	0.002	0.000	0.000
S^{6+}	0.011	0.003	0.007	0.006	0.006	0.003	0.000	0.000
subtotal	1.000	1.000	1.000	1.000	1.000	1.000	1.000	1.000
F^-	0.875	0.738	0.878	0.903	0.830	0.867	0.870	0.877
Cl^-	0.009	0.001	0.002	0.001	0.003	0.002	0.001	0.001
*OH^-	0.113	0.199	0.040	0.050	0.266	0.136	0.045	0.083
subtotal	0.998	0.939	0.920	0.954	1.100	1.005	0.915	0.960

M – 5th level, Huber shaft; O – Huber open pit; G – Gellnauer vein system. Empirical formulas were calculated on the basis of (P+As+S+Si) = 1 and charge balance; H_2O content is calculated from charge balance.

tent is probably not controlled by the substitution NaAl-$Ca_{-1}Mg_{-1}$, as could be suggested by structural relationship with lacroixite $NaAlPO_4(F,OH)$), but probably by substitution of the type $NaSR^{2+}_{-1}P_{-1}$ (Fig. 59), which is related to a hypothetic end-member composition $NaR^{2+}SO_4(F,OH)$. The empirical formulas of isokite from Krásno calculated on the basis of (P+As+S+Si) = 1 are given in Table 20.

Kolbeckite $ScPO_4 . 2H_2O$

The uncommon occurences of kolbeckite are tied to irregular cavities (up to 6 cm) in strongly altered phosphate accumulations (fluorapatite and isokite; rarely with triplite relics) in the Huber open pit. The mineral forms

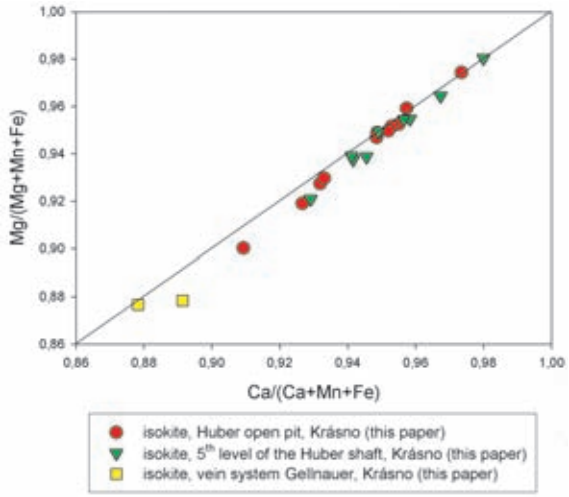

Fig. 58 Correlation of Ca/(Ca+Mn+Fe) and Mg/(Mg+Mn+Fe) for isokite from Krásno close to 1:1 (indicated by line) shows no preference in entry of Mn and Fe in the Ca-site or the Mg-site, respectively. Concentrations of elements are in apfu.

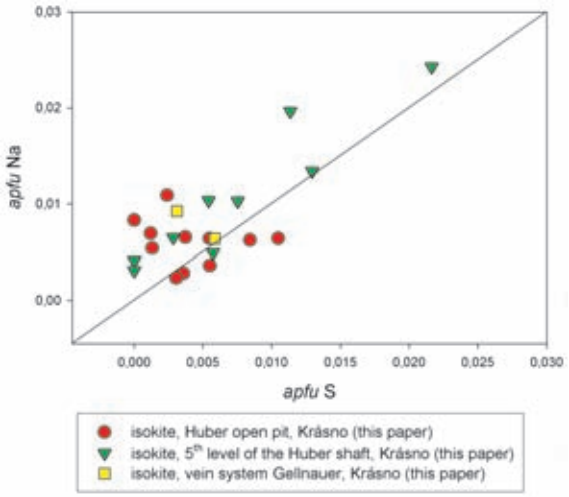

Fig. 59 A plot of apfu S vs. Na in isokite from Krásno. Positive corelation of Na and S close to 1:1 (indicated by line) suggests substitution $NaSR^{2+}_{-1}P_{-1}$.

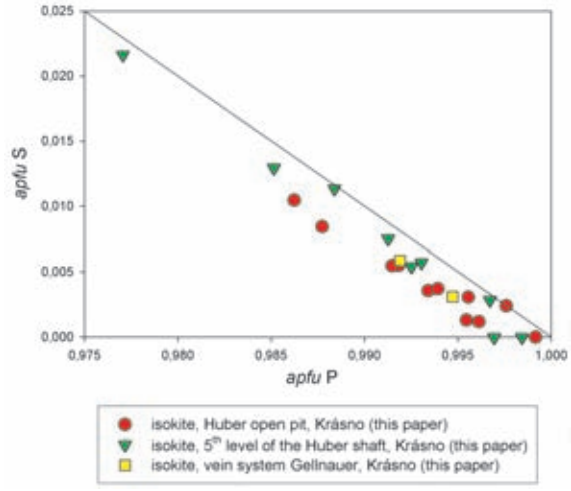

Fig. 60 A plot of apfu P vs. apfu S for isokite from Krásno. The line corresponds to an ideal correlation P+S = 1.

minute crystalline aggregates of whitish colour, up to 200 μm large. The white colour of kolbeckite, relative to distinctly blue kolbeckite crystals from the nearby locality Vysoký kámen (Sejkora *et al.* 2006), makes the mineral inconspicuous and similar, both macroscopically and microscopically, to aggregates of late fluorapatite or leucophosphite. Kolbeckite aggregates (Fig. 61) are usually intergrown with minerals of the turquoise group, *UNK3*, pharmacosiderite, *UNK1* and closely associated with fluorapatite, leucophosphite and rutile.

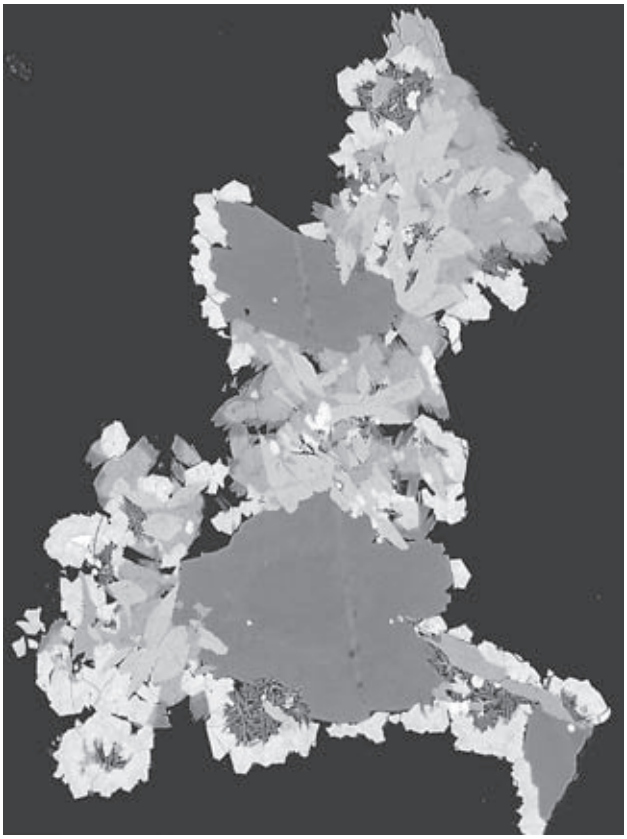

Fig. 61 Kolbeckite aggregates (dark grey) overgrown by elongated crystals of *UNK3* (in places with rhombic shapes), zoned aggregates of mineral of the turquoise group (darker) and pharmacosiderite crystals (light); also present are distinctly tabular aggregates of *UNK1*. Huber open pit, Krásno. Width of photo 400 μm. Cameca SX100, BSE photograph by J. Sejkora and R. Škoda.

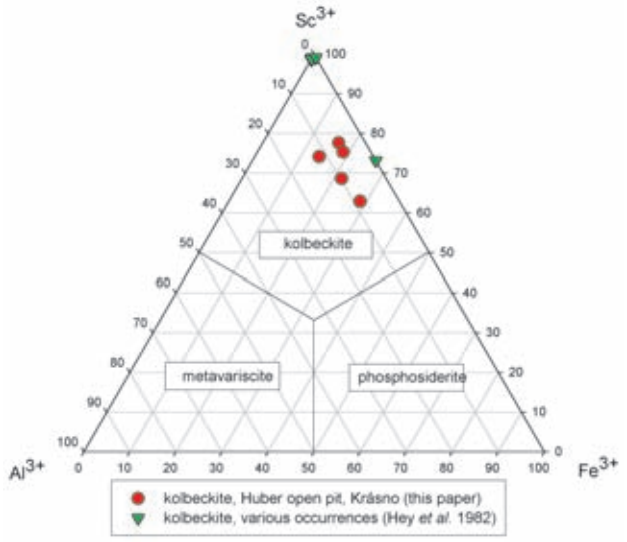

Fig. 62 Ternary plot of Sc-Fe-Al occupancy of cation site (atomic ratio) for kolbeckite.

Due to the small size of the aggregates, kolbeckite samples were examined only by electron microprobe (Table 21). The cation-group in kolbeckite (Fig. 62) contains besides the dominant Sc (0.63–0.75 *apfu*) significant Al (0.06–0.11 *apfu*) and especially Fe^{3+} (0.14–0.28 *apfu*). Up to present, significant Fe^{3+} (0.28 *apfu*) contents were reported only in kolbeckite from Potash Sulfur Springs, Arkansas (Hey *et al.* 1982). In the anion group, dominant P is accompanied by low As (up to c. 0.02 *apfu*) and traces of S and Si (max. 0.002 *apfu*). The empirical formula of kolbeckite from the Huber open pit is $(Sc_{0.70}Fe_{0.19}Al_{0.08})_{\Sigma 0.97}(PO_4)_{1.00} \cdot 2.00H_2O$.

Table 21 Chemical composition of kolbeckite (in wt. %)

	mean	1	2	3	4	5	*1
ZnO	0.34	0.64	0.54	0.42	0.00	0.12	
MnO	0.06	0.00	0.00	0.03	0.09	0.17	
CaO	0.06	0.00	0.12	0.08	0.05	0.07	
PbO	0.05				0.13	0.11	
BaO	0.04	0.00	0.00	0.06	0.00	0.15	
Sc_2O_3	26.53	25.83	28.65	27.38	23.49	27.32	39.19
Al_2O_3	2.29	2.70	1.58	1.61	2.36	3.21	
Fe_2O_3	8.55	9.45	7.07	7.88	12.35	6.01	
SiO_2	0.03	0.00	0.03	0.03	0.03	0.05	
As_2O_5	0.60	0.75	0.54	0.92	0.69	0.11	
P_2O_5	39.03	39.37	39.29	38.30	38.25	39.94	40.33
SO_3	0.04	0.03	0.08	0.00	0.00	0.09	
H_2O*	20.28	20.31	20.30	20.15	20.12	20.44	20.48
total	97.91	99.06	98.21	96.86	97.54	97.78	100.00
Ca	0.002	0.000	0.004	0.003	0.002	0.002	0.000
Ba	0.000	0.000	0.000	0.001	0.000	0.002	0.000
Pb	0.000	0.000	0.000	0.000	0.001	0.001	0.000
Mn	0.002	0.000	0.000	0.001	0.002	0.004	0.000
Zn	0.008	0.014	0.012	0.009	0.000	0.003	0.000
Al	0.082	0.095	0.056	0.058	0.085	0.113	0.000
Fe^{3+}	0.194	0.212	0.160	0.182	0.284	0.135	0.000
Sc^{3+}	0.699	0.671	0.751	0.733	0.625	0.714	1.000
Si	0.001	0.000	0.001	0.001	0.001	0.002	0.000
As^{5+}	0.009	0.012	0.009	0.015	0.011	0.002	0.000
P^{5+}	0.999	0.994	1.001	0.996	0.990	1.013	1.000
S^{6+}	0.001	0.001	0.002	0.000	0.000	0.002	0.000
H	4.002	4.004	4.002	3.998	4.001	3.996	4.001
H_2O	2.001	2.002	2.001	1.999	2.000	1.998	2.000

mean and five (1–5) spot analyses; *1 – theoretical composition of kolbeckite $ScPO_4 \cdot 2H_2O$
Empirical formulas were calculated on the basis of 6 O *apfu*; H_2O* – water content calculated from the ideal formula (H_2O = 2.00).

Leucophosphite $KFe_2(PO_4)_2(OH) \cdot 2H_2O$

Common leucophosphite as one of the latest minerals in corroded cavities in phosphate accumulations has been found in samples from the Huber open pit. It typically

forms rich crystalline aggregates or crusts up to 0.5 cm in size, composed of well-formed tabular crystals (Figs 63, 64) only 0.1–1 mm, exceptionally 3 mm long. Leucophosphite is colourless and translucent, light yellowish, grey or grey green and has a strong vitreous lustre. Fluorapatite, minerals of the turquoise group, pharmacosiderite, kolbeckite, whitmoreite and probable new species *UNK1, UNK3, UNK6, UNK7, UNK8, UNK10* (Sejkora *et al.* 2006) are associated. One cavity contained K-deficient leucophosphite (designated as type b below) in yellowish crystalline aggregates (Figs 65, 66) several mm in size, intergrown in and overgrown on fibrous beraunite aggregates in association with *UNK3* (Fig. 67). The individual tabular crystals are well-formed and similar to those of the first type decribed.

The X-ray powder data and refined unit-cell parameters (Table 22) for the two types of leucophosphite are closely similar and correspond to published data for this species and also to the theoretical pattern calculated from structural data (Dick – Zeiske 1997). For K-deficient leu-

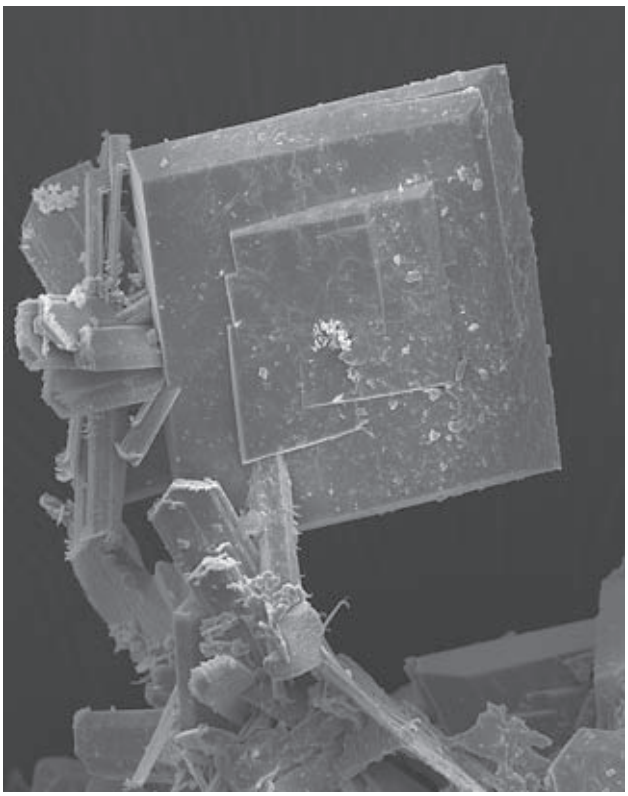

Fig. 64 Tabular leucophosphite (a) crystals; Huber open pit, Krásno. Width of photo 110 μm. SEM photograph by J. Sejkora.

Fig. 63 Leucophosphite (a) crystal in a cavity in phoshate aggregate; Huber open pit, Krásno. Width of photo 2 mm. Microphotography Nicon SMZ1500 by J. & E. Sejkora.

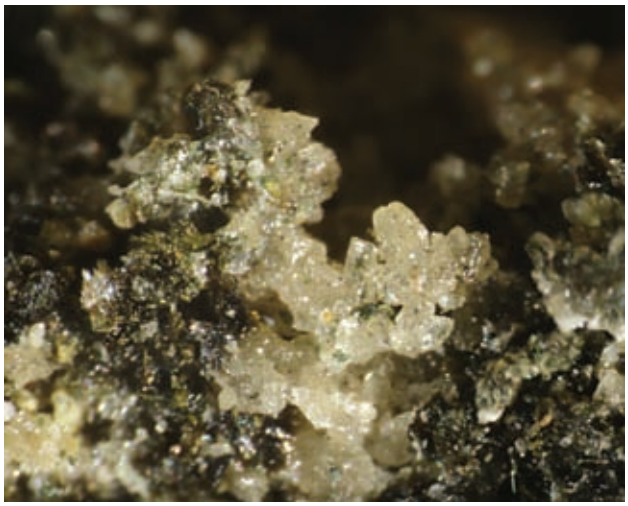

Fig. 65 Crystals of K-deficient leucosphosphite (b) on beraunite; Huber open pit, Krásno. Width of photo 2 mm. Nicon SMZ1500 microphotography by J. & E. Sejkora.

Table 22 Unit-cell parameters of leucophosphite (for monoclinic space group $P2_1/n$)

	Krásno (a) this paper	Krásno (b) this paper	Sapucaia Lindberg (1957)	Tip Top Moore (1972)	Těškov Dick – Zeiske (1997)
a [Å]	9.770(8)	9.807(5)	9.73(4)	9.782(9)	9.758(4)
b [Å]	9.649(4)	9.677(3)	9.60(4)	9.658(9)	9.647(4)
c [Å]	9.683(7)	9.684(4)	9.69(4)	9.751(9)	9.736(4)
β [°]	102.47(1)	102.36(1)	102.3(3)	102.24(1)	102.50(3)
V [Å^3]	891.4(5)	897.7(4)	884.4	900.2	894.8

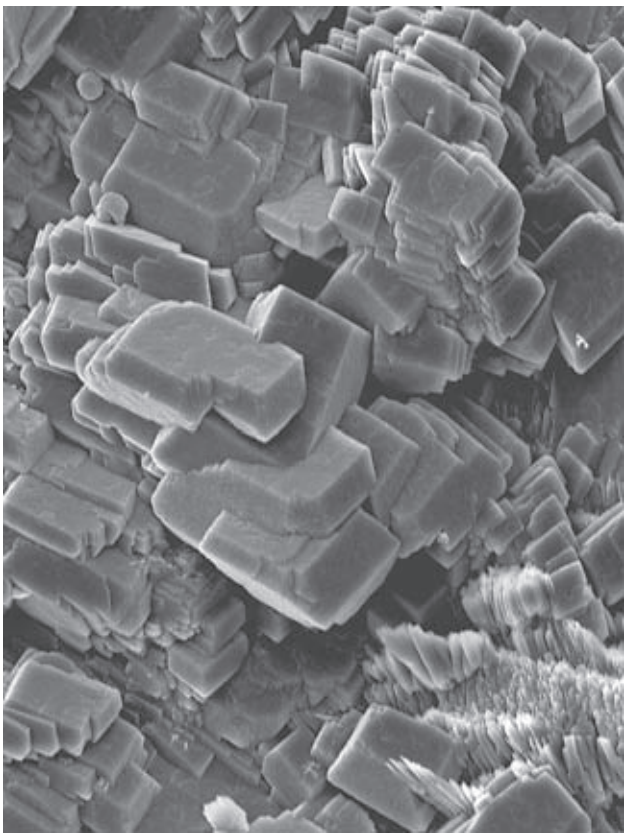

Fig. 66 Crystals of K-deficient leucophosphite (b) on fibrous beraunite; Huber open pit, Krásno. Width of photo 40 μm. SEM photograph by J. Sejkora.

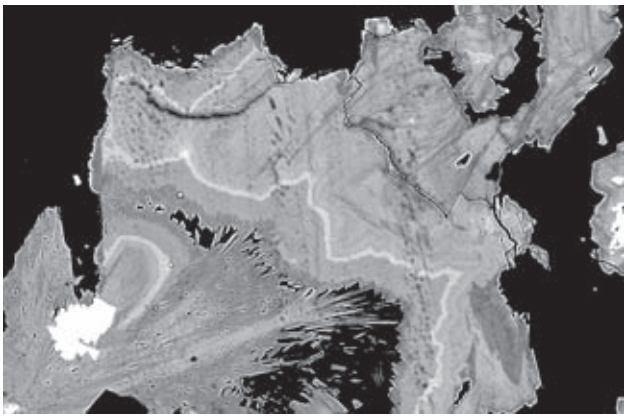

Fig. 67 Zoned crystalline aggregates of K-deficient leucophosphite (b) intergrown with aggregates of fibrous beraunite; (zoning is caused by Fe/Al and P/As variation, K content is constant). The white grains correspond to *UNK3*. Huber open pit, Krásno. Width of photo 300 μm. Cameca SX100, BSE photograph by J. Sejkora and R. Škoda.

cophosphite (b) the parameter a (9.807 Å) is higher than the published data (9.73–9.78 Å). This increase in a value does not correspond to the trends of known substitution (K-NH_4, Fe-Al) in leucophosphite-group minerals (Marincea *et al.* 2002).

The ideal formula for leucophosphite-related minerals (Dick – Zeiske 1997) can be expressed as $M^{1+}M^{3+}_2(PO_4)_2(OH) \cdot 2H_2O$. The M^{1+} site is filled by K (leucophosphite, tinsleyite), (NH_4) group (spheniscidite) and a smaller quantity of Na. The M^{3+} site is dominated by Fe^{3+} (leucophosphite, spheniscidite) or Al^{3+} (tinsleyite). Quantitative chemical analyses of leucophosphite (Table 23) show that there are two varieties with different occupancy of the M^{1+} site in the general formula (Fig. 68). In the predominating variety (a) the site M^{1+} is almost completely filled by K (0.84 to 0.98 *apfu*), accompanied by minor Na (max. 0.02 *apfu*) and deficit in M^{1+} site is in the range of 0.02–0.15 *pfu*. The less common variety (b) contains in the M^{1+} site only 0.48 to 0.67 *apfu* K, accompanied by Na max. 0.01 *apfu* and a significant deficit in the range of 0.33–0.52 *pfu*. This deficit could be explained by the presence of $(NH_4)^+$ ion in place of K, i.e., by substitution toward sphenicsidite. However, this mineral has been described only from guano beds (Wilson – Bain 1976, 1986), from phosphate concretions hosted in Miocene diatomites and diatomaceous shales (Medrano – Piper 1997), and from highly fertilized soils (Dick – Zeiske 1997). The possible presence of the $(NH_4)^+$ group in the two types of leucophosphite from Krásno was examined by infrared absorption spektroskopy (FTIR spectrophotometr Nicolet 740, KBr disk, analyst M. Novotná). However, both samples gave practically identical infrared spectra and there were no absorption bands in regions charakteristic for bond vibrations of $(NH_4)^+$ groups (Farmer *et al.* 1974). Therefore, presence of vacancies is a probable explanation for deficiency of cations in the M^{1+} site. The structure of leucophosphite is characterized by position of weakly bonded K atoms in channels running parallel to the *b*-axis (Dick – Zeiske 1997). Some of the published analyses of leucophosphite-related minerals also show deficit in M^{1+} site [leucoph-

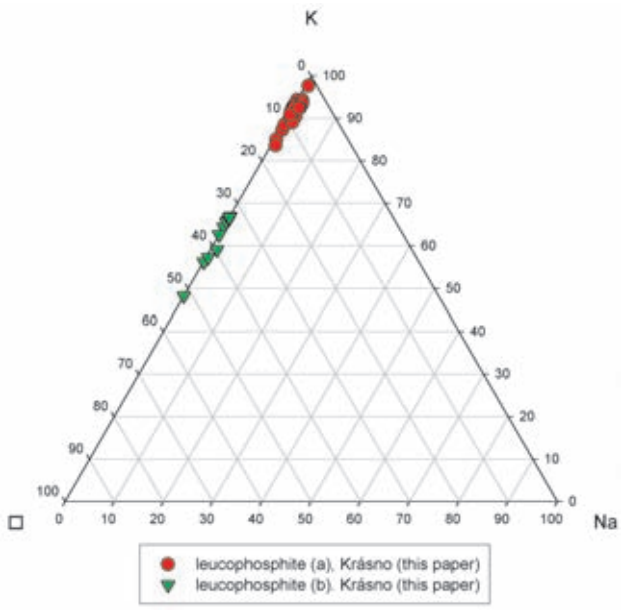

Fig. 68 Ternary plot of occupation of M^{1+} site (atomic ratio) in leucophosphite, Huber open pit, Krásno. □ – vacancy in M^{1+} site.

Table 23 Chemical composition of leucophosphite (wt. %).

	leucophosphite (b) – K-deficient					leucophosphite (a)				
	mean	1	2	3	4	mean	5	6	7	8
Na_2O	0.02	0.00	0.01	0.01	0.01	0.05	0.04	0.09	0.01	0.11
K_2O	7.75	5.95	7.19	8.37	8.37	10.87	10.46	11.49	11.09	10.91
CaO	0.12	0.31	0.09	0.12	0.09	0.15	0.64	0.05	0.10	0.00
BaO	0.03	0.00	0.00	0.00	0.00	0.07	0.00	0.00	0.32	0.00
SrO	0.00	0.00	0.00	0.00	0.00	0.03	0.11	0.00	0.00	0.00
MnO	0.07	0.17	0.00	0.10	0.03	0.03	0.02	0.02	0.10	0.00
PbO	0.02	0.12	0.00	0.04	0.00	0.03	0.00	0.06	0.19	0.07
CuO	0.00					0.35	0.46	0.00	0.04	0.46
ZnO	0.56	0.82	0.34	0.68	0.32	0.37	0.24	0.13	0.30	0.12
Al_2O_3	3.82	1.35	5.56	3.31	6.31	3.43	3.56	5.88	4.50	1.95
Fe_2O_3	37.23	39.18	34.35	38.11	33.97	33.21	32.16	30.93	32.14	36.32
SiO_2	0.02	0.03	0.00	0.00	0.00	0.01	0.00	0.02	0.02	0.03
TiO_2	0.22	0.03	0.51	0.20	0.34	0.25	0.11	0.17	0.21	0.42
As_2O_5	1.17	1.80	0.42	1.00	0.29	0.76	2.94	0.10	0.34	0.76
P_2O_5	37.05	35.95	38.30	37.04	37.59	35.36	35.13	36.55	36.10	35.06
SO_3	0.02	0.08	0.00	0.03	0.04	0.06	0.15	0.09	0.16	0.00
H_2O*	12.02	11.50	11.95	12.12	12.36	11.74	11.20	11.98	11.75	11.92
total	100.11	97.29	98.72	101.13	99.70	96.79	97.20	97.55	97.36	98.12
Na	0.002	0.000	0.001	0.001	0.001	0.007	0.004	0.011	0.001	0.014
K	0.618	0.483	0.562	0.670	0.667	0.913	0.850	0.943	0.917	0.924
□	0.380	0.517	0.437	0.329	0.333	0.081	0.146	0.046	0.082	0.063
total M^{1+} site	1.000	1.000	1.000	1.000	1.000	1.000	1.000	1.000	1.000	1.000
Ca	0.008	0.021	0.006	0.008	0.006	0.010	0.044	0.003	0.007	0.000
Ba	0.001	0.000	0.000	0.000	0.000	0.002	0.000	0.000	0.008	0.000
Sr	0.000	0.000	0.000	0.000	0.000	0.001	0.004	0.000	0.000	0.000
Pb	0.000	0.002	0.000	0.001	0.000	0.001	0.000	0.001	0.003	0.001
Cu	0.000	0.000	0.000	0.000	0.000	0.018	0.022	0.000	0.002	0.023
Mn	0.004	0.009	0.000	0.005	0.001	0.002	0.001	0.001	0.005	0.000
Zn	0.026	0.038	0.015	0.031	0.015	0.018	0.011	0.006	0.015	0.006
Al	0.281	0.101	0.401	0.245	0.464	0.266	0.267	0.446	0.344	0.153
Fe^{3+}	1.750	1.874	1.583	1.798	1.597	1.645	1.542	1.498	1.567	1.815
Ti^{4+}	0.010	0.002	0.024	0.009	0.016	0.012	0.005	0.008	0.010	0.021
total M^{3+} sites	2.080	2.048	2.030	2.098	2.099	1.976	1.896	1.963	1.961	2.019
Si^{4+}	0.001	0.002	0.000	0.000	0.000	0.001	0.000	0.001	0.001	0.002
As^{5+}	0.038	0.060	0.013	0.033	0.010	0.026	0.098	0.003	0.011	0.026
P^{5+}	1.959	1.935	1.987	1.966	1.989	1.970	1.895	1.991	1.980	1.971
S^{6+}	0.001	0.004	0.000	0.001	0.002	0.003	0.007	0.004	0.008	0.000
total anion sites	2.000	2.000	2.000	2.000	2.000	2.000	2.000	2.000	2.000	2.000
H	4.827	4.553	4.653	4.933	4.961	4.818	4.474	4.849	4.780	4.989
OH	0.832	0.559	0.655	0.931	0.961	0.809	0.474	0.844	0.777	0.983
H_2O	1.998	1.997	1.999	2.001	2.000	2.004	2.000	2.003	2.001	2.003

1–4 – representative spot analyses of K-deficient leucophosphite (b); 5–8 – representative spot analyses of leucophosphite (a). H_2O* calculated from the theoretical content of H_2O = 2.00 and charge balance; empirical formulas were calculated on the basis of (P+As+S+Si) = 2.

osphite: 0.27 *pfu* – Lottermoser – Lu (1997); tinsleyite: 0.11 *pfu* – Dunn *et al.* (1984) and 0.06–0.14 *pfu* – Marincea *et al.* (2002)].

Because contents of other elements do not correlate with the magnitude of deficit (vacancy) in the M^{1+} site, it is possible to discuss occupancy of other structure sites for both varieties of leucophosphite. The M^{3+} site is always dominated by Fe^{3+} (1.49–1.98 *apfu*) over Al (0.05–0.46 *apfu*); the Al content corresponding to tinsleyite component varies in the range c. 3–23 mol. % (Fig. 69). The contents of Ca, Ba, Sr, Pb, Mn and Zn are irregular and relatively small (max. 0.04 *apfu*). The total for this position is 1.90 to 2.13 *apfu*. The tetrahedral sites of the anion group (Fig. 70) contain predominating P (1.85–1.99 *apfu*), with As contents 0–0.14 *apfu* and minor S and Si (max. 0.01 *apfu*).

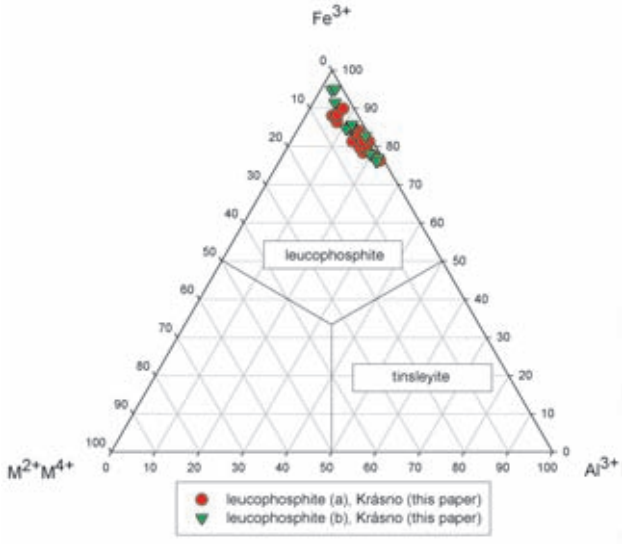

Fig. 69 Ternary plot of occupation of the M^{3+} sites (atomic ratio) in leucophosphite, Huber open pit, Krásno.

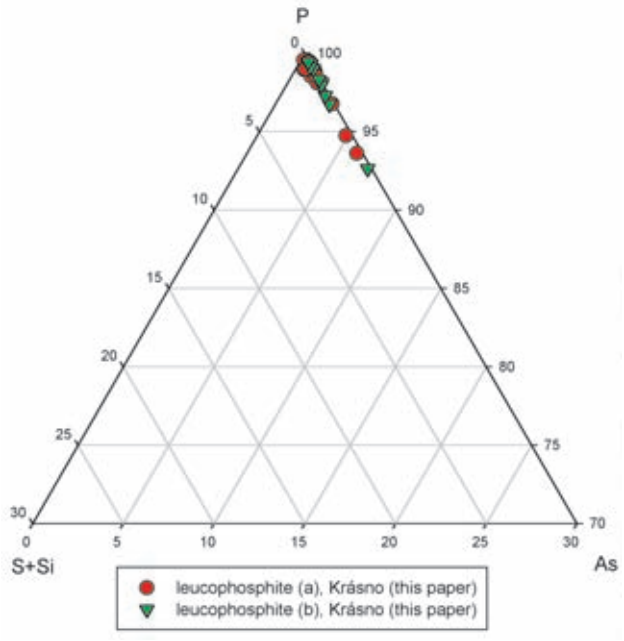

Fig. 70 Part of ternary plot of occupation of the anion sites (in molar unit) in leucophosphite. Huber open pit, Krásno.

The empirical formula for the predominating type (a) of leucophosphite (average of 23 spot analyses) on the basis of (P+As+S+Si) = 2 is $(K_{0.91}Na_{0.01})_{\Sigma 0.92}(Fe_{1.65}Al_{0.27}Cu_{0.02}Zn_{0.02}Ti_{0.01})_{\Sigma 1.97}[(PO_4)_{1.97}(AsO_4)_{0.03}]_{\Sigma 2.00}(OH)_{0.81} . 2.00H_2O$, for the rare K-deficient leukophosphite (b) (average of 11 spot analyses) the formula is $K_{0.62}(Fe_{1.75}Al_{0.28}Zn_{0.03}Ca_{0.01}Ti_{0.01})_{\Sigma 2.08}[(PO_4)_{1.96}(AsO_4)_{0.04}]_{\Sigma 2.00}(OH)_{0.83} . 2.00H_2O$.

Morinite $NaCa_2Al_2(PO_4)_2F_4(OH) . 2H_2O$

Morinite has been found in several samples of phosphate accumulations collected at the 5th level of the Huber shaft. It forms whitish and light pink irregular granular aggregates up to 5 mm across, with a weak pearly to vitreous lustre (Fig. 71). Closely associated minerals include frondelite, *UNK9*, beraunite, fluorapatite, bluish phosphosiderite (Fig. 72) and rare purple red strengite. Morinite belongs to the youngest minerals in this association.

Morinite was identified by X-ray powder diffraction data as a phase predominating in a mixture with small quantities of strengite and fluorapatite. The refined unit-cell parameters of morinite (Table 24) closely correspond to data published for this mineral. The general chemical formula of morinite can be presented as $A^+B^{2+}{}_2C^{3+}{}_2(TO_4)_2F_4(OH) . 2H_2O$, where A = Na, B = Ca, C = Al and T = P (Hawthorne 1979). The chemical composition of morinite from Krásno (Table 25) corresponds to the above formula; minor differences are noted in the content of F and partly in presence of Fe and Mn. In the *A*-site, Na strongly predominates above K content. The

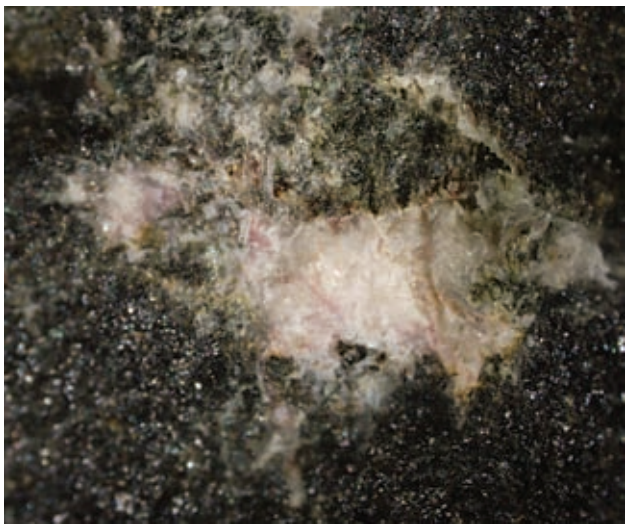

Fig. 71 Light pink morinite aggregates intergrown with dark frondelite. 5th level of the Huber shaft, Krásno. Width of photo 5 mm. Nicon SMZ1500 microphotography by J.&E. Sejkora.

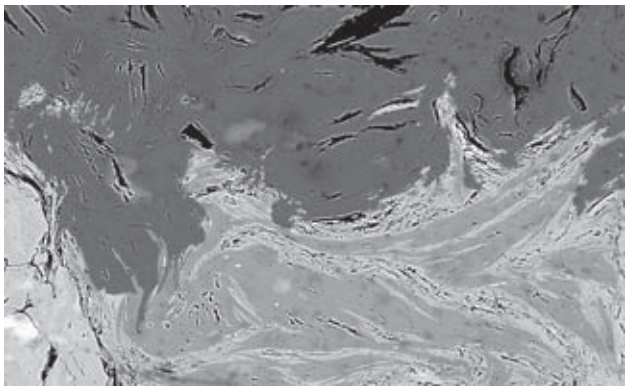

Fig. 72 Morinite (dark) intergrown with fluorapatite (light fibrous and compact) and phosphosiderite (medium grey). 5th level of the Huber shaft, Krásno. Width of photo 400 μm. Cameca SX100, BSE photograph by J. Sejkora and R. Škoda.

Table 24 Unit-cell parameters of morinite (for monoclinic space group $P2_1/m$)

	this paper	Hawthorne (1979)
a [Å]	9.465(4)	9.454(3)
b [Å]	10.691(5)	10.692(4)
c [Å]	5.459(2)	5.444(2)
β [°]	105.58(3)	105.46(2)
V [Å^3]	532.1(4)	530.4

observed deficit in this site (0.02–0.20 *pfu*) may correspond to vacancy. In the *B*-site (Fig. 73), dominating Ca is accompanied by Fe (up to 0.16) and Mg (to 0.16 *apfu*), which positively correlate with F content (Fig. 74). A presence of Fe in the *C*-site, seemingly indicated by lower

totals in this position (1.83–2.01 *apfu*), is not probable with regard to the absence of Fe/Al correlation. Phosphorus predominates in the tetrahedral sites, minor and irregular contents of Si, S and As attain only 0.01–0.02 *apfu*. Fluorine contents (Fig. 75) correspond to entry of this element (up to 0.44 *apfu*) in the *(OH)*-site. The published chemical analyses of morinite from various localities (Palache *et al.* 1951; Ficher – Runner 1958; Fischer 1960) do not show such high F contents. The empirical formulas for representative spot analyses of morinte from Krásno, based on (P+As+S+Si) = 2, are given in Table 25.

Table 25 Chemical composition of morinite (in wt. %)

	1	2	3	4	5	6	7
Na_2O	5.40	6.01	5.02	5.75	6.27	6.28	5.12
K_2O	0.02	0.01	0.01	0.08	0.01	0.02	0.01
CaO	21.82	21.70	21.83	22.84	22.84	23.29	23.02
SrO	0.00	0.11	0.02	0.00	0.00	0.00	0.00
BaO	0.17	0.06	0.00	0.00	0.02	0.00	0.07
MgO	1.35	0.80	0.27	0.15	0.09	0.15	0.21
MnO	0.78	0.65	0.34	0.26	0.10	0.18	0.20
FeO	0.99	1.32	2.35	0.57	0.35	0.32	0.32
ZnO	na	0.12	0.16	0.03	0.06	0.00	0.19
PbO	0.02	0.08	0.02	0.01	0.00	0.00	0.08
Al_2O_3	19.14	20.30	20.26	20.22	20.60	20.40	21.27
TiO_2	0.00	0.03	0.09	0.05	0.01	0.03	0.01
SiO_2	0.00	0.00	0.00	0.26	0.03	0.04	0.04
P_2O_5	28.97	29.10	28.85	28.81	29.28	29.50	29.41
As_2O_5	0.01	0.21	0.00	0.00	0.00	0.00	0.00
SO_3	0.14	0.21	0.01	0.16	0.01	0.24	0.06
Cl	0.01	0.01	0.00	0.02	0.00	0.01	0.00
F	17.30	16.42	15.87	15.29	14.89	14.97	15.17
O=F, Cl	-7.28	-6.92	-6.68	-6.44	-6.27	-6.30	-6.39
*H_2O (OH)	0.91	1.52	1.62	1.93	2.19	2.25	2.13
*H_2O	7.29	7.44	7.31	7.34	7.40	7.47	7.46
total	97.02	99.17	97.31	97.31	97.88	98.93	98.37
Na^+	0.850	0.935	0.796	0.900	0.980	0.966	0.795
K^+	0.002	0.001	0.001	0.008	0.001	0.002	0.001
subtotal	0.852	0.937	0.797	0.908	0.981	0.969	0.796
Ca^{2+}	1.898	1.867	1.914	1.976	1.972	1.982	1.974
Sr^{2+}	0.000	0.005	0.001	0.000	0.000	0.000	0.000
Ba^{2+}	0.005	0.002	0.000	0.000	0.001	0.000	0.002
Mg^{2+}	0.164	0.096	0.033	0.018	0.011	0.018	0.025
Mn^{2+}	0.053	0.044	0.024	0.018	0.007	0.012	0.013
Fe^{2+}	0.067	0.089	0.161	0.038	0.024	0.021	0.021
Zn^{2+}	0.000	0.007	0.010	0.002	0.003	0.000	0.011
Pb^{2+}	0.001	0.002	0.000	0.000	0.000	0.000	0.002
Al^{3+}	1.832	1.922	1.954	1.924	1.957	1.910	2.006
Ti^{4+}	0.000	0.002	0.005	0.003	0.000	0.002	0.000
subtotal	4.019	4.035	4.102	3.979	3.975	3.945	4.056
Si^{4+}	0.000	0.000	0.000	0.021	0.002	0.003	0.003
P^{5+}	1.991	1.979	1.999	1.969	1.998	1.983	1.993
As^{5+}	0.001	0.009	0.000	0.000	0.000	0.000	0.000
S^{6+}	0.008	0.012	0.001	0.009	0.000	0.014	0.004
subtotal	2.000	2.000	2.000	2.000	2.000	2.000	2.000
F^-	4.441	4.171	4.107	3.905	3.796	3.759	3.840
Cl^-	0.001	0.001	0.000	0.003	0.000	0.001	0.000
*OH^-	0.287	0.771	0.859	0.875	1.091	1.023	1.075
subtotal	4.730	4.944	4.966	4.784	4.887	4.783	4.915
*H_2O	2	2	2	2	2	2	2

1–7 – spot analyses of morinite from Krásno; H_2O* and (OH)* calculated from the theoretical content of H_2O = 2.00 and charge balance; empirical formulas were calculated on the basis of (P+As+S+Si) = 2.

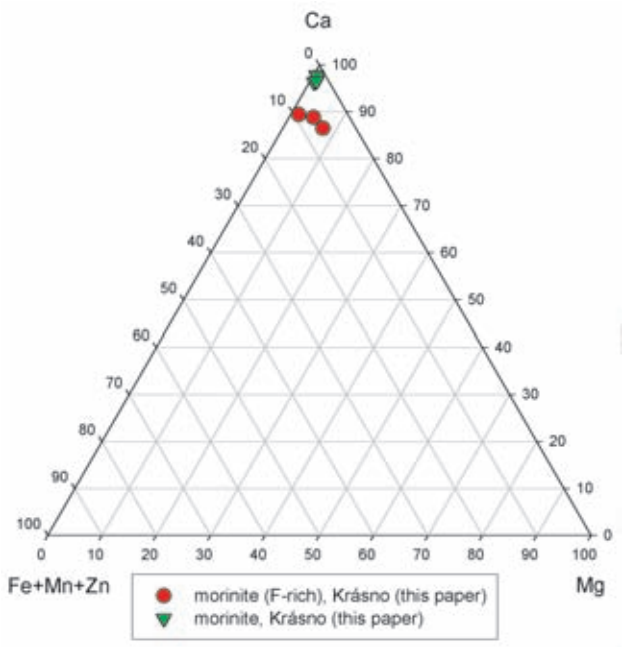

Fig. 73 Ternary plot of the B^{2+}-sites occupancy (atomic ratio) in morinite. 5th level of the Huber shaft, Krásno.

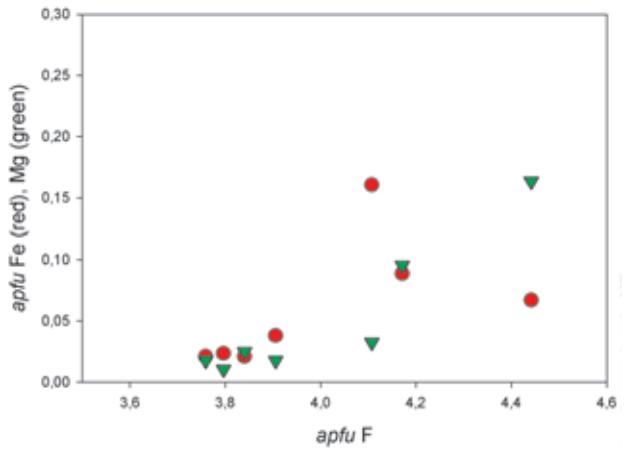

Fig. 74 A plot of *apfu* F *vs. apfu* Fe and Mg for morinite from the 5th level of the Huber shaft, Krásno.

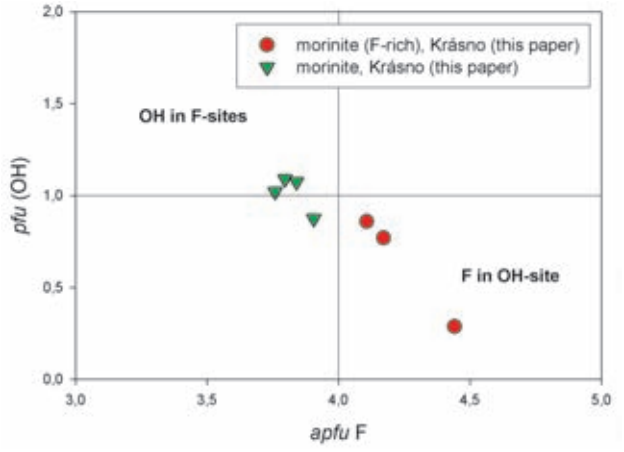

Fig. 75 A plot of *apfu* F *vs. pfu* (OH) in *F,OH-sites* for morinite from the 5th level of the Huber shaft, Krásno.

Natrodufrénite $NaFe^{2+}Fe^{3+}_5(PO_4)_4(OH)_6 \cdot 2H_2O$
Mn-rich dufrénite $(o,Na,Ca)Mn^{2+}Fe^{3+}_5(PO_4)_4(OH)_6 \cdot 2H_2O$

Dufrénite-related minerals of microscopic size have been found only in several specimens of strongly altered phosphate accumulation collected at the 5th level of the Huber shaft. Relatively more abundant natrodufrénite forms irregular aggregates, up to 100 μm long, intergrown typically with frondelite and *UNK9*, in close association with fluorapatite, Mn-rich dufrénite, fluorite and K-Mn oxides. The rare Mn-rich dufrénite forms fibrous to radiating aggregates (Fig. 76), up to 200 μm across, in close association with fluorite, natrodufrénite, *UNK9*, phosphosiderite and beraunite.

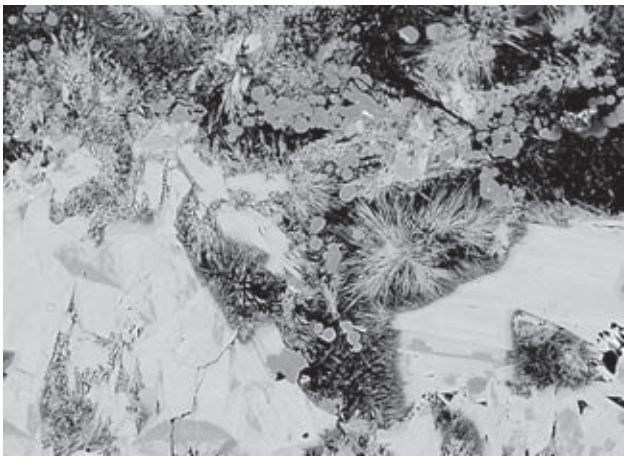

Fig. 76 Compact aggregate composed of natrodufrénite (darker) and *UNK9* (lighter parts); the rich acicular aggregates are Mn-rich dufrénite, grey spheroidal aggregates are fluorite. 5th level of the Huber shaft, Krásno. Width of photo 400 μm. Cameca SX100, BSE photograph by J. Sejkora and R. Škoda.

Because of the small size of natrodufrénite and Mn-rich dufrénite aggregates the minerals were confirmed only by electron microprobe (Table 26). The relatively low totals of Mn-rich dufrénite analyses are probably due to the very finely fibrous character of the analyzed samples. The general formula of dufrénite-related minerals can be presented as $ABC_5(PO_4)_4(OH)_6 \cdot 2H_2O$, with Na, K, Ca and vacancies in the *A*-site; *B*-site is occupied by M^{2+} elements such as Fe, Mn, Mg, Mn and Zn and C-site is filled dominantly by Fe^{3+} or Al^{3+} (Fontan *et al.* 1982; Selway *et al.* 1997; Anthony *et al.* 2000). At present, natrodufrénite (A=Na, B=Fe^{2+}, C=Fe^{3+}), dufrénite (A=vacancy and Ca, B=Fe^{2+}, C=Fe^{3+}) and burangaite (A=Na, B=Fe^{2+}, C=Al^{3+}) are the valid mineral species in this group.

In the studied natrodufrénite from Krásno, Na (0.65–0.98 *apfu*) predominates over Ca (0.12–0.23 *apfu)* in the *A*-site. This composition corresponds to the data published for natrodufrénite and burangaite (Fig. 77). In the studied Mn-rich dufrénite, Ca (0.07–0.10 *apfu*) and Na contents (0.04–0.32 *apfu*) are low and the site is dominantly vacant (0.57–0.88 *pfu*). The *B*-site in samples from Krásno is characterized by unusually high Mn content (Fig. 78), 0.27–0.41 *apfu* in natrodufrénite (accompanied by 0.36–0.56 *apfu* Fe and 0.17–0.23 *apfu* Mg), and 0.78–0.95 *apfu* Mn in Mn-rich dufrénite (with up to 0.17 *apfu* Fe and up to 0.07 *apfu* Zn). Formally, the studied material could be considered as new mineral species – Mn analogue of dufrénite and natrodufrénite. However, on the basis of obtained analyses and published data it is not possible to exclude the possibility that Mn enters the *C*-site of crystal structure. In the *C*-site of both phases from Krásno (Fig. 79) Fe^{3+} (4.43–5.28 *apfu*) strongly pre-

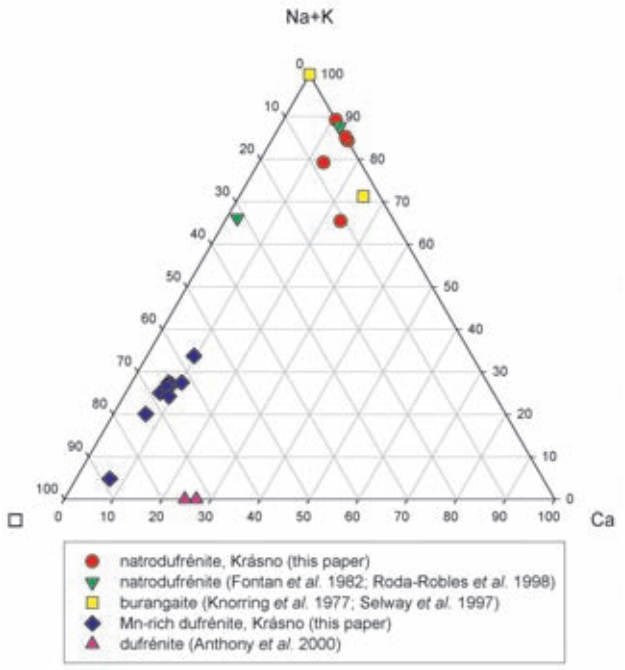

Fig. 77 Ternary plot of *A*-site occupancy (atomic ratio) in dufrénite-related minerals. □ – vacancy in *A*-site.

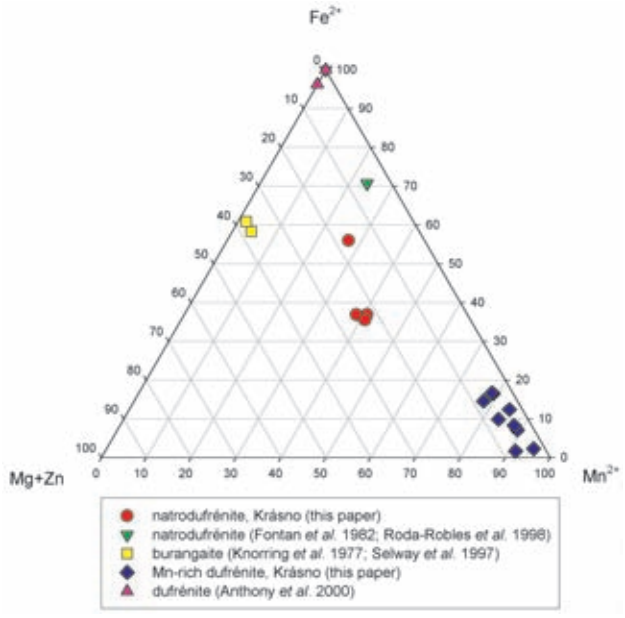

Fig. 78 Ternary plot of occupation of *B*-site (in molar unit) in dufrénite-related minerals.

Table 26 Chemical composition of natrodufrénite and Mn-rich dufrénite (in wt. %)

	natrodufrénite				Mn-rich dufrénite			
	1	2	3	4	5	6	7	8
Na_2O	2.98	2.33	3.08	3.52	0.78	0.66	0.16	0.76
K_2O	0.01	0.00	0.00	0.00	0.05	0.05	0.02	0.07
CaO	1.03	1.52	1.03	0.77	0.49	0.41	0.44	0.55
FeO*	3.36	4.62	3.06	2.95	0.79	1.33	1.18	0.13
BaO	0.00	0.00	0.00	0.00	0.06	0.13	0.17	0.04
MgO	0.98	0.78	1.09	1.02	0.03	0.01	0.01	0.06
CuO	0.00	0.00	0.00	0.00	0.09	0.00	0.00	0.06
MnO	3.05	2.20	3.16	3.36	6.57	6.19	6.26	6.97
ZnO	0.12	0.00	0.13	0.16	0.37	0.39	0.67	0.47
Al_2O_3	1.19	0.10	1.29	1.78	0.45	0.16	1.25	0.44
Fe_2O_3*	43.18	44.44	43.57	42.61	43.70	44.52	46.00	44.21
SiO_2	0.00	0.00	0.00	0.00	0.09	0.03	0.03	0.05
TiO_2	0.09	0.00	0.10	0.03	0.15	0.17	0.05	0.19
As_2O_5	0.03	0.00	0.09	0.06	0.10	0.14	0.16	0.17
P_2O_5	32.81	32.57	32.76	32.80	30.67	31.19	31.97	30.25
SO_3	0.00	0.00	0.00	0.00	0.06	0.18	0.05	0.10
H_2O*	10.23	10.05	10.46	10.40	9.63	9.59	10.35	9.92
total	99.06	98.60	99.81	99.46	94.06	95.13	98.76	94.44
Na^+	0.832	0.654	0.859	0.981	0.230	0.191	0.044	0.229
K^+	0.001	0.001	0.000	0.000	0.009	0.010	0.004	0.014
Ca^{2+}	0.160	0.236	0.160	0.119	0.081	0.066	0.069	0.092
□	0.007	0.109	0.000	0.000	0.680	0.733	0.883	0.665
A-site	1.000	1.000	1.019	1.099	1.000	1.000	1.000	1.000
Fe^{2+}	0.404	0.560	0.368	0.355	0.100	0.167	0.146	0.017
Ba^{2+}	0.000	0.000	0.000	0.000	0.004	0.007	0.010	0.002
Mg^{2+}	0.211	0.169	0.234	0.218	0.006	0.003	0.003	0.015
Cu^{2+}	0.000	0.000	0.000	0.000	0.010	0.000	0.000	0.007
Mn^{2+}	0.372	0.271	0.385	0.410	0.852	0.787	0.779	0.914
Zn^{2+}	0.013	0.000	0.014	0.017	0.042	0.043	0.073	0.054
B-site	1.000	1.000	1.000	1.000	1.014	1.007	1.010	1.009
Al^{3+}	0.203	0.017	0.219	0.301	0.081	0.028	0.216	0.081
Fe^{3+}	4.676	4.851	4.721	4.613	5.030	5.031	5.088	5.154
Ti^{4+}	0.010	0.000	0.011	0.004	0.017	0.019	0.005	0.022
C-site	4.889	4.868	4.950	4.918	5.128	5.077	5.310	5.257
Si^{4+}	0.000	0.000	0.000	0.000	0.013	0.005	0.004	0.008
As^{5+}	0.002	0.000	0.007	0.005	0.008	0.011	0.012	0.013
P^{5+}	3.998	4.000	3.993	3.995	3.971	3.965	3.978	3.967
S^{6+}	0.000	0.000	0.000	0.000	0.007	0.020	0.005	0.012
T-*site*	*4.000*	*4.000*	*4.000*	*4.000*	*3.987*	*3.995*	*3.996*	*3.992*
H^+	9.822	9.725	10.045	9.981	9.826	9.605	10.148	10.252
OH*	5.828	5.731	6.039	5.975	5.822	5.612	6.141	6.243
H_2O*	1.997	1.997	2.003	2.003	2.002	1.996	2.004	2.004

natrodufrénite, Krásno: 1 – mean of 5 spot analyses, 2–4 – representative spot analyses; Mn-rich dufrénite, Krásno: 5 – mean of 9 spot analyses, 6–8 – representative spot analyses. FeO* a Fe_2O_3* calculated from the proposed general formula; H_2O* and (OH)* calculated from the theoretical content of H_2O = 2.00 and charge balance; empirical formulas were calculated on the basis of (P+As+S+Si) = 4.

dominates over Al content with the maximum value of 0.30 *apfu*. Phosphorus is the major element in tetrahedral sites of both phases, As, S and Si contents reach 0.01–0.02 *apfu*. The empirical formula of natrodufrénite from Krásno calculated on the basis of (P+As+S+Si) = 4 is presented as $(Na_{0.83}Ca_{0.16}□_{0.01})_{\Sigma 1.00}(Fe_{0.40}Mn_{0.37}Mg_{0.21}Zn_{0.01})_{\Sigma 0.99}(Fe_{4.68}Al_{0.20}Ti_{0.01})_{\Sigma 4.89}(PO_4)_{4.00}(OH)_{5.82} . 2H_2O$. For Mn-rich dufrénite the empirical formula calculated on the same basis is $(□_{0.68}Na_{0.23}Ca_{0.08})_{\Sigma 1.00}(Mn_{0.85}Fe_{0.10}Zn_{0.04}Cu_{0.01})_{\Sigma 1.00}(Fe_{5.03}Al_{0.08}Ti_{0.02})_{\Sigma 5.13}[(PO_4)_{3.97}(AsO_4)_{0.01}(SO_4)_{0.01}(SiO_4)_{0.01}]_{\Sigma 4.00}(OH)_{5.82} . 2.00H_2O$.

Phosphosiderite $Fe^{3+}PO_4 . 2H_2O$

Phosphosiderite is a relatively common mineral in phosphate accumulations from the 5th level of the Huber shaft. It forms irregular aggregates, up to 2 mm across, and veinlets to 5 mm thick (Fig. 80). Phosphosiderite has characteristic bluish grey colour and a weak lustre. It is intergrown with frondelite (Fig. 81), rockbridgeite, *UNK9,* beraunite, morinite, fluorapatite, and Mn-rich dufrenite. Beran (1999) reported from the same locality phosphosiderite as brown to black compact aggregates up to 10 cm long. The latter type of material was not available in the present study.

Phosphosiderite was identified by X-ray powder diffraction; refined unit-cell parameters (Table 27) are in good agreement with data published for this species. The chemical composition of phosphosiderite (Table 28) is close to the ideal formula – Fe (0.91–0.98 *apfu*), with limited substitution by Al (up to 0.04) and Mn (up to 0.02 *apfu*). Phosphorus dominates in the anion group, S and As are very low (0.004 *apfu*). The empirical formula of phosphosiderite can be presented on the basis of (P+As+S) = 1 as $(Fe_{0.95}Mn_{0.01}Al_{0.02})_{\Sigma 0.98}(PO_4)_{1.00} . 2H_2O$.

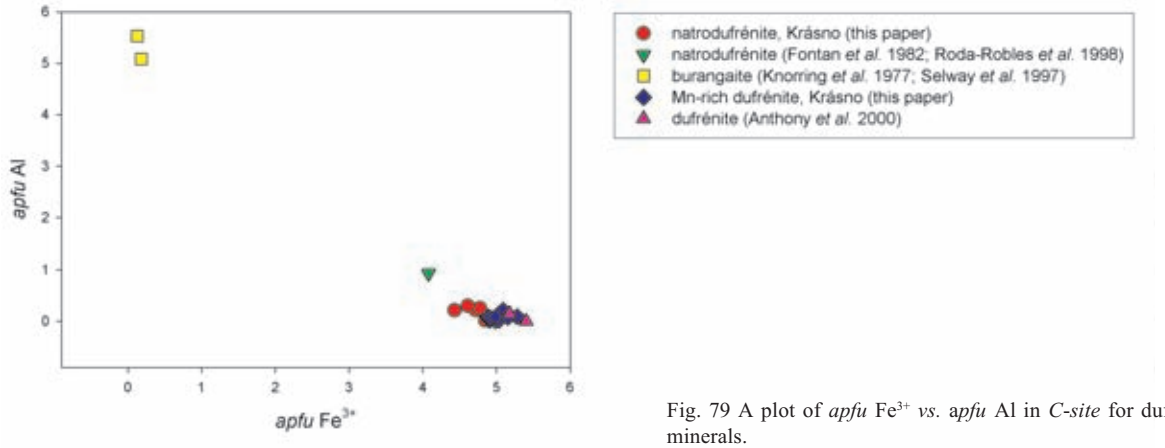

Fig. 79 A plot of *apfu* Fe^{3+} *vs.* a*pfu* Al in *C-site* for dufrénite-related minerals.

Fig. 80 Bluish grey phosphosiderite aggregates intergrown with dark aggregates of frondelite. 5th level of the Huber shaft, Krásno. Width of photo 3.5 mm. Nicon SMZ1500 microphotography by J. & E. Sejkora.

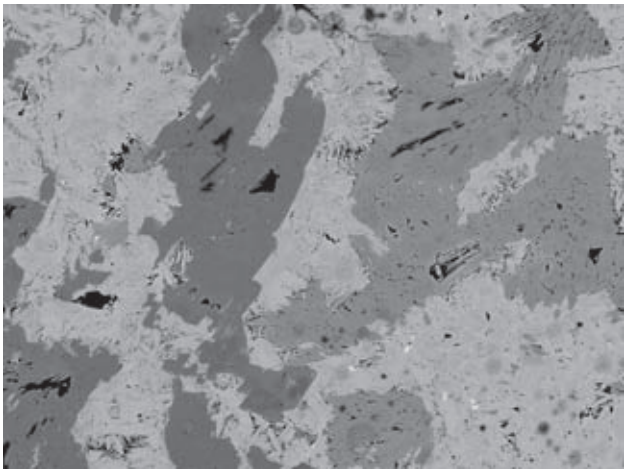

Fig. 81 Frondelite aggregates (light) replaced by beraunite (grey) and phosphosiderite (dark); 5th level of the Huber shaft, Krásno. Width of photo 1 mm. Cameca SX100, BSE photograph by J. Sejkora and R. Škoda.

Table 27 Unit-cell parameters of phosphosiderite (for monoclinic space group $P2_1/n$)

	this paper	Fanfani – Zanazzi (1966)	Borensztajn (1966)
a [Å]	5.317(8)	5.330(3)	5.32(5)
b [Å]	9.84(9)	9.809(4)	9.75(5)
c [Å]	8.673(4)	8.714(5)	8.65(5)
β [°]	90.1	90.6(1)	90.6
V [Å^3]	453.8	455.6	448.7

Table 28 Chemical composition of phosphosiderite (in wt. %)

	1	2	3	4	5	6
CaO	0.09	0.17	0.11	0.03	0.08	0.05
BaO	0.04	0.00	0.18	0.01	0.07	0.00
MgO	0.02	0.02	0.00	0.03	0.03	0.04
PbO	0.06	0.19	0.00	0.00	0.00	0.00
MnO	0.52	0.15	0.47	0.58	0.56	0.80
ZnO	0.05	0.09	0.11	0.00	0.02	0.05
Al_2O_3	0.42	0.53	0.16	0.55	0.46	0.61
Fe_2O_3	39.97	39.99	40.34	41.07	40.70	40.60
As_2O_5	0.06	0.00	0.11	0.06	0.05	0.08
P_2O_5	37.51	38.50	37.55	38.12	37.84	37.55
SO_3	0.04	0.06	0.06	0.02	0.00	0.00
TiO_2	0.07	0.00	0.00	0.03	0.16	0.00
H_2O*	19.08	19.57	19.12	19.38	19.23	19.09
total	97.94	99.26	98.20	99.87	99.20	98.86
Ca^{2+}	0.003	0.005	0.004	0.001	0.003	0.002
Ba^{2+}	0.001	0.000	0.002	0.000	0.001	0.000
Mg^{2+}	0.001	0.001	0.000	0.001	0.001	0.002
Pb^{2+}	0.000	0.002	0.000	0.000	0.000	0.000
Mn^{2+}	0.014	0.004	0.012	0.015	0.015	0.021
Zn^{2+}	0.001	0.002	0.003	0.000	0.000	0.001
Al^{3+}	0.016	0.019	0.006	0.020	0.017	0.023
Fe^{3+}	0.945	0.922	0.952	0.957	0.955	0.960
Ti^{4+}	0.002	0.000	0.000	0.001	0.004	0.000
subtotal	0.983	0.955	0.979	0.995	0.996	1.008
As^{5+}	0.001	0.000	0.002	0.001	0.001	0.001
P^{5+}	0.998	0.999	0.997	0.999	0.999	0.999
S^{6+}	0.001	0.001	0.001	0.000	0.000	0.000
subtotal	1.000	1.000	1.000	1.000	1.000	1.000
H_2O	4.000	4.000	3.999	4.001	4.001	4.000

1 – mean of 18 spot analyses; 2–6 – representative spot analyses. H_2O* calculated on the basis of theoretical content H_2O = 2.00, empirical formulas were calculated on the basis of (P+As+S) = 1.

Rockbridgeite

see minerals of the frondelite – rockbridgeite series

Strengite $Fe^{3+}PO_4 . 2H_2O$

Very rare strengite occurs in cavities of phosphate accumulations at the 5th level of the Huber shaft on minute crystals of rockbridgeite – frondelite or fluorapatite as perfect elongated crystals up to 4 mm long (Fig. 82), with a striking purple red colour and an intense vitreous lustre. Strengite of the same colour in 1 mm long grains intergrown with morinite aggregates and fluorapatite was very rare. It has been identified by X-ray powder diffraction; its refined unit-cell parameters correspond closely the published data (Table 29). A semiquantitative study of chemical composition of strengite confirmed major contents of Fe and P, contents of other elements (Al, Mn, As, etc.) were below detection limit of the used method (c. 0.2–0.5 wt. %).

Minerals of the triplite – zwieselite series $Mn^{2+}_2(PO_4)(F,OH) – Fe^{2+}_2(PO_4)(F,OH)$

Minerals of the triplite group were reported from the Krásno ore district in numerous publications from 19th century (see Beran 1999). Later on, Fisher (1957) studied the mineral in samples collected at the dumps near the Schnöd stock. The paper contains X-ray powder diffraction data and results of approximate, semiquantitative analysis. Fisher (1957) recognized two forms of triplite – dark and light triplite. Based on analogy with Hagendorf pegmatite (older dark triplite in feldspar, younger light triplite in quartz) he considered the possibility that the two forms of triplite may represent two independent generations. Beran (1999) described from samples of phosphate accumulations collected at the 5th level of the Huber shaft occurrence of zwieselite and triploidite in addition to predominating triplite. However, these descriptions are not confirmed by the present study.

We have studied a large number of samples of minerals from the triplite group, collected in the Huber open pit, in phosphate accumulation at the 5th level of the Huber shaft and for comparison several historical specimens collected before 1830, probably in the Gellnauer vein system. Triplite from the Huber stock forms irregular aggregates, up to 10 cm across, which are usually partly replaced by younger fluorapatite and isokite (open pit and

Fig. 83 Triplite aggregates with white quartz, 5th level of the Huber shaft, Krásno. Width of photo 9 mm. Microphotography Nicon SMZ1500 by J. & E. Sejkora.

Fig. 82 Purple-red strengite crystal on aggregates of light-coloured fluorapatite. 5th level of the Huber shaft, Krásno. Width of photo 3.1 mm. Nicon SMZ1500 microphotography by J. & E. Sejkora.

Table 29 Unit-cell parameters of strengite (for orthorhombic space group *Pbca*)

	this paper	Taxer – Bartl (2004)
a [Å]	8.750(6)	8.722(3)
b [Å]	9.821(7)	9.878(2)
c [Å]	10.126(7)	10.119(1)
V [Å^3]	870.2(6)	871.79

Fig. 84 Aggregates of Mn-rich zwieselite; Gellnauer vein system, Krásno. Width of photo 9 cm. Macrophotography Canon DS1 by J. & E. Sejkora.

5th level) or fluorapatite and minerals of the series rockbridgeite – frondelite (only 5th level of the Huber shaft). Triplite aggregates are light or dark brown (Fig. 83), they have a characteristic vitreous to greasy lustre and are partly transparent with red colour in small splinters. The differences in colour of triplite do not indicate existence of two generations, but rather the extent of alteration or weathering of individual samples. Dark triplite is coloured by oxides and hydroxides of Fe and Mn. All triplite occurrences are associated with compact or coarse-grained quartz in greisens. Samples from the Gellnauer vein system contain Mn-rich zwieselite in dark brown aggregates larger than 10 cm (Fig. 84). The aggregates are strongly replaced by compact fluorapatite from margin (Fig. 85) and this fluorapatite is succesively strongly replaced by fine-grained isokite. Triplite (or zwieselite) in all samples studied is compositionaly quite homogeneous, except rare and weak zoning in Fe/Mn ratio. During late alteration, resulting in corrosion cavities in phosphate accumulations, triplite appeared to be one of the most stable minerals. Various samples show fresh triplite aggregates and minute, lustrous triplite grains protruding into the cavities.

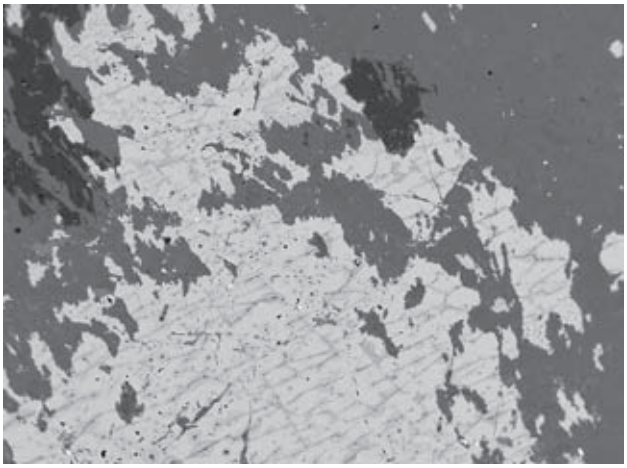

Fig. 85 Zwieselite aggregates (light) intensively replaced by fluorapatite (grey), fluorapatite is in turn replaced by isokite aggregates (dark). Gellnauer vein system, Krásno. Width of photo 1.2 mm. Cameca SX100, BSE photograph by J. Sejkora and R. Škoda.

X-ray powder diffraction data for triplite from Krásno correspond to the published data for minerals of the triplite – zwieselite series. Owing to chemical composition falling in between triplite and zwieselite (see below), it is not possible to recognize these minerals by X-ray patterns. Refined unit-cell parameters (Table 30) correspond to minerals of this group. With regard to extensive substitutions in *M*- and *Z*-sites and polytypism (Chopin *et al.* 2004), it is not possible to separate intermediate members of this group on the basis of unit-cell parameters.

The chemical composition of minerals of the triplite group can be expressed by the general formula $M_2(TO_4)(Z)$. Mn^{2+}, Fe^{2+}, Mg and Ca enter the octahdral *M*-sites, tetrahedra TO_4 are occupied by P, As, V and Si and *Z*-site is dominated by F or OH (Waldrop 1969). Triplite (Mn_2PO_4F) is isostructural with zwieselite (Fe_2PO_4F) and wagnerite (Mg_2PO_4F) and it is structurally related to triploidite (Mn_2PO_4OH) and wolfeite (Fe_2PO_4OH). The triplite group shows a wide (probably unlimited) isomorphism among all above given end-members.

The chemical composition of the studied minerals of the triplite group (Table 31) is relatively uniform within individual localities, but there is considerable variation in Mn, Fe a Mg contents among the localities (Fig. 86). Samples from the Gellnauer vein system correspond to Mn-rich and Mg-poor zwieselite. Samples from the Huber stock contain uniform Mn and Fe abundances and correspond to Fe-rich triplite (Fig. 87), but they show variation in Mg content. Triplite samples from the 5th level of the Huber shaft are Mg-poor (max. 0.01 *apfu*), but triplites from the Huber stock contain 0.28 to 0.31 *apfu* Mg. All the studied samples contain nearly constant quantity of Ca in *M*-site, 0.04 to 0.08 *apfu*. The tetrahedral *T*-site is occupied almost exclusively by P, contents of As, S and Si are low and irregular, always less than 0.004

Table 30 Unit-cell parameters for minerals of triplite group (for monoclinic space group *C*2/*c*)

	triplite*1 this paper	triplite*2 this paper	zwieselite*3 this paper	triplite*4 Waldrop (1968)	zwieselite*5 Yakubovich *et al.* (1978)	wagnerite*6 Tadini (1981)
a [Å]	13.276(4)	13.219(8)	13.233(8)	13.185(1)	13.641(3)	12.942(5)
b [Å]	6.487(1)	6.461(2)	6.492(2)	6.454(1)	6.489(1)	6.432(4)
c [Å]	10.020(3)	9.987(2)	9.995(6)	9.937(1)	9.890(3)	9.799(2)
β [°]	119.51(1)	119.33(2)	119.38(3)	119.00(6)	118.40(2)	117.90(2)
V [Å^3]	750.9(5)	743.6(9)	748.2(9)	739.6	733.5	720.9

*1 Fe-rich triplite, 5th level of the Huber shaft, Krásno – $(Mn_{1.05}Fe_{0.85}Ca_{0.07}Mg_{0.01})_{\Sigma 1.98}(PO_4)(F_{0.67}(OH)_{0.31})_{\Sigma 0.98}$
*2 Fe- and Mg-rich triplite, Huber open pit, Krásno – $(Mn_{0.88}Fe_{0.70}Mg_{0.29}Ca_{0.06})_{\Sigma 1.93}(PO_4)(F_{0.67}(OH)_{0.32})_{\Sigma 0.99}$
*3 Mn-rich zwieselite, Gellnauer vein system, Krásno – $(Fe_{1.06}Mn_{0.84}Ca_{0.06})_{\Sigma 1.96}(PO_4)(F_{0.66}(OH)_{0.32})_{\Sigma 0.98}$
*4 Mg-rich triplite $(Mn_{0.88}Mg_{0.70}Fe_{0.32}Ca_{0.10})_{\Sigma 2.00}(PO_4)F$
*5 zwieselite, synthetic Fe end-member
*6 wagnerite (= formerly magniotriplite) $(Mg_{0.89}Fe_{0.88}Mn_{0.23})_{\Sigma 2.00}(PO_4)F$

Table 31 Chemical composition of triplite group minerals from Krásno (in wt. %)

	1	2	3	4	5	6	7	8	9
Na_2O	0.06	0.00	0.01	0.00	0.01	0.05	0.01	0.00	0.00
K_2O	0.04	0.00	0.00	0.00	0.26	0.19	0.01	0.00	0.02
CaO	1.80	1.87	1.75	1.89	1.02	1.70	1.68	1.46	1.65
SrO	0.00	0.00	0.02	0.04	0.00	0.02	0.00	0.03	0.01
BaO	0.00	0.00	0.06	0.08	0.00	0.29	0.00	0.15	0.00
MgO	0.09	0.06	0.03	0.19	5.56	5.46	0.00	0.03	0.02
MnO	32.51	33.69	33.34	32.27	29.34	29.14	27.44	27.54	25.21
FeO	27.96	27.53	27.40	27.96	24.85	24.04	33.21	33.43	35.69
CuO	0.00	0.00	0.02	0.00	0.00	0.00	0.00	0.07	0.00
ZnO	0.23	0.10	0.00	0.42	0.29	0.18	0.24	0.14	0.15
PbO	0.07	0.02	0.17	0.08	0.01	0.14	0.00	0.00	0.23
Al_2O_3	0.00	0.02	0.00	0.04	0.00	0.01	0.00	0.02	0.02
TiO_2	0.09	0.05	0.06	0.07	0.11	0.18	0.03	0.06	0.41
SiO_2	0.07	0.03	0.00	0.03	0.04	0.00	0.02	0.00	0.05
P_2O_5	32.09	31.27	31.84	31.40	32.91	33.83	31.88	31.74	31.02
As_2O_5	0.00	0.04	0.00	0.11	0.09	0.00	0.00	0.09	0.00
SO_3	0.03	0.01	0.09	0.00	0.02	0.02	0.00	0.03	0.00
Cl	0.00	0.00	0.01	0.00	0.02	0.00	0.01	0.00	0.01
F	6.37	6.28	6.44	5.40	6.76	6.77	5.80	5.75	5.31
O=F	-2.68	-2.64	-2.71	-2.27	-2.85	-2.85	-2.44	-2.42	-2.23
O=Cl	0.00	0.00	0.00	0.00	0.00	0.00	0.00	0.00	0.00
H_2O*	1.48	2.39	1.58	2.98	1.76	1.13	2.04	2.27	3.47
total	100.19	100.71	100.11	100.70	100.18	100.27	99.92	100.38	101.04
Na^+	0.004	0.000	0.001	0.000	0.001	0.003	0.001	0.000	0.000
K^+	0.002	0.000	0.000	0.000	0.012	0.008	0.000	0.000	0.001
Ca^{2+}	0.071	0.076	0.069	0.076	0.039	0.064	0.067	0.058	0.067
Sr^{2+}	0.000	0.000	0.001	0.001	0.000	0.000	0.000	0.001	0.000
Ba^{2+}	0.000	0.000	0.001	0.001	0.000	0.004	0.000	0.002	0.000
Mg^{2+}	0.005	0.004	0.001	0.010	0.296	0.284	0.000	0.002	0.001
Mn^{2+}	1.011	1.075	1.045	1.025	0.889	0.861	0.861	0.866	0.812
Fe^{2+}	0.858	0.868	0.848	0.877	0.743	0.702	1.028	1.038	1.135
Cu^{2+}	0.000	0.000	0.001	0.000	0.000	0.000	0.000	0.002	0.000
Zn^{2+}	0.006	0.003	0.000	0.012	0.008	0.005	0.007	0.004	0.004
Pb^{2+}	0.001	0.000	0.002	0.001	0.000	0.001	0.000	0.000	0.002
Al^{3+}	0.000	0.001	0.000	0.002	0.000	0.000	0.000	0.001	0.001
Ti^{4+}	0.003	0.001	0.002	0.002	0.003	0.005	0.001	0.002	0.012
M-site	1.960	2.027	1.970	2.006	1.991	1.937	1.964	1.974	2.034
Si^{4+}	0.002	0.001	0.000	0.001	0.001	0.000	0.001	0.000	0.002
P^{5+}	0.997	0.998	0.998	0.997	0.997	1.000	0.999	0.997	0.998
As^{5+}	0.000	0.001	0.000	0.002	0.002	0.000	0.000	0.002	0.000
S^{6+}	0.001	0.000	0.002	0.000	0.000	0.000	0.000	0.001	0.000
T-site	1.000	1.000	1.000	1.000	1.000	1.000	1.000	1.000	1.000
F^-	0.739	0.748	0.753	0.640	0.764	0.748	0.679	0.675	0.638
Cl^-	0.000	0.000	0.001	0.000	0.001	0.000	0.001	0.000	0.001
*OH^-	0.178	0.309	0.192	0.376	0.209	0.125	0.247	0.278	0.452
Z-site	0.917	1.057	0.946	1.016	0.975	0.873	0.928	0.953	1.091

Representative spot analyses: 1–4 – triplite, 5th level of the Huber shaft; 5–6 – Huber open pit; 7–9 – zwieselite, Gellnauer vein system.
H_2O* and (OH)* calculated on the basis of charge balance, empirical formulas were calculated on the basis of (P+As+S+Si) = 1.

apfu. There is a limited variation in *Z*-site occupancy among individual localities (Fig. 88). Fluorine is always the dominant anion (0.53 to 0.77 *apfu*), irregular Cl contents do not exceed 0.002 *apfu*. The empirical formulas calculated on the basis of (P+As+S+Si) = 1 for representative spot analyses of triplite group minerals from Krásno are given in Table 31.

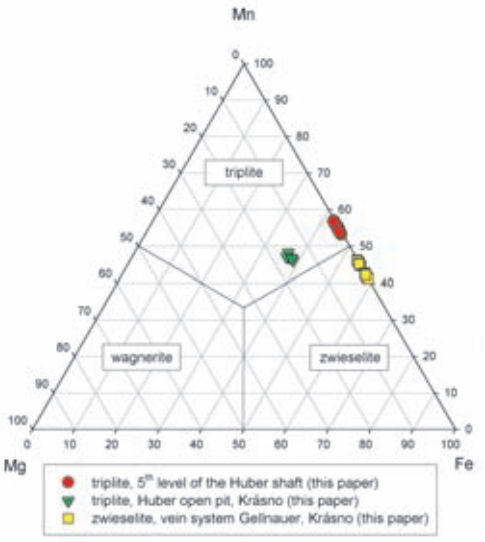

Fig. 86 Ternary plot of *M*-site occupancy (atomic ratio) in triplite group minerals from Krásno.

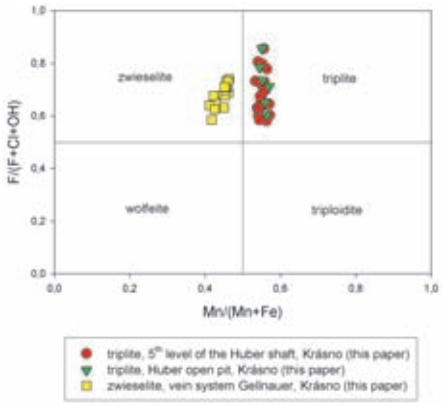

Fig. 87 Diagram Mn/(Mn+Fe) *vs*. F/(F+Cl+OH) (*pfu*) for minerals of the triplite group from Krásno.

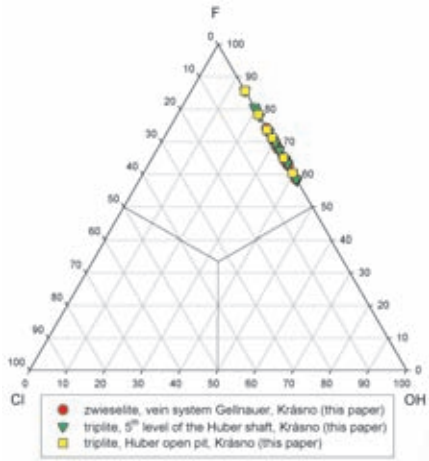

Fig. 88 Ternary plot of *Z*-site occupancy in triplite group minerals from Krásno.

Turqouise

see chalcosiderite

Vivianite $Fe^{2+}_3(PO_4)_2 . 8 H_2O$

This mineral has been found in the Huber open pit as blue grey spheroidal aggregates of lens-shaped crystals deposited on crystals of hydrothermal quartz. The size of the aggregates is up to 5 mm. In this case, no other secondary minerals accompany vivianite. The mineral was identified by X-ray powder diffraction.

Wavellite $Al_3(PO_4)_2(OH,F)_3 . 5 H_2O$

Presence of wavellite in the Krásno ore district is known for a long time (see Beran 1999). Korbel (1991) gave a spectral analysis and X-ray powder diffraction data. He identified two forms of wavellite in material from the Huber stock. The first type forms white radiating aggregates with fibers, up to 5 mm long. The second type occurs as grey white radiating spheroidal aggregates, up to 3 mm in diameter.

The present study confirmed the existence of both morphological types of wavellite described by Korbel (1991) in samples from the Huber open pit. Radiating aggregates of wavellite, rarely up to 1 cm long, occur in cavities together with beraunite, fluellite and siderite. In addition, radiating aggregates of wavellite longer than 1 cm (Fig. 89) with a weak colour zoning across the fibres have been found. The occurrence of wavellite was confirmed by X-ray powder diffraction.

Fig. 89 Radiating aggregate of wavellite. Huber open pit, Krásno. Width of photo 16 mm. Nicon SMZ1500 microphotography by J. & E. Sejkora.

Waylandite

see minerals of the crandallite group

Whitmoreite

see earlshannonite and whitmoreite (arthurite group)

Zwieselite

see minerals of the triplite – zwieselite series

Formation of mineral associations in phosphate accumulations in the Huber stock

Mineral associations and chemical composition of minerals at two localities in Krásno, i.e., Huber open pit and the 5th level of the Huber shaft, show numerous similarities, but there are also some differences. Consenquently, their evolution is discussed separately. In addition to the minerals described in this paper the discussion concerns also probable new mineral species (Sejkora *et al.* 2006) occurring in these associations.

Huber open pit

Phosphates exposed in the Huber open pit evolved in the apical part of the stock, which was probably completely greisenized and contains local bodies of coarse-grained or compact quartz. The studied samples come from level c. 20 to 40 m below the contact of the upper part of the stock with host rocks. This corresponds approximately to the position about 50-80 m below the original land surface. Accurate vertical positions are difficult to determine, as the structure was affected by extensive collapse caused by historical mining. The primary phosphates occur in masses of white compact quartz in greisens, whereas younger re-mobilized phosphates originated in cavities of coarse-grained quartz gangue.

Abundant triplite and compact fluorapatite I (Fig. 90) were identified as the primary phosphates. Replacement of triplite by younger fluorapatite II, starting from margins of aggregates and along fractures, was initiated probably in early hydrothermal stage. During the following stage, this newly formed fluorapatite II and partly primary fluorapatite I were extensively replaced by aggregates of isokite. Isokite formation is preferentially restricted on in fluorapatite domains. At the rarely observed isokite/triplite boundary triplite shows no replacement features.

The formation of abundant isokite aggregates requires import of Mg, because solubility of Mg in highly evolved peraluminous systems is low (Puziewicz – Johannes 1988, 1990). Magnesium was likely imported by aqueous fluids from rocks of the metamorphic envelope or perhaps from altered micas in underlying granite. Opening of the system as early as the beginning stage of phosphate accumulation is indicated by the increased contents

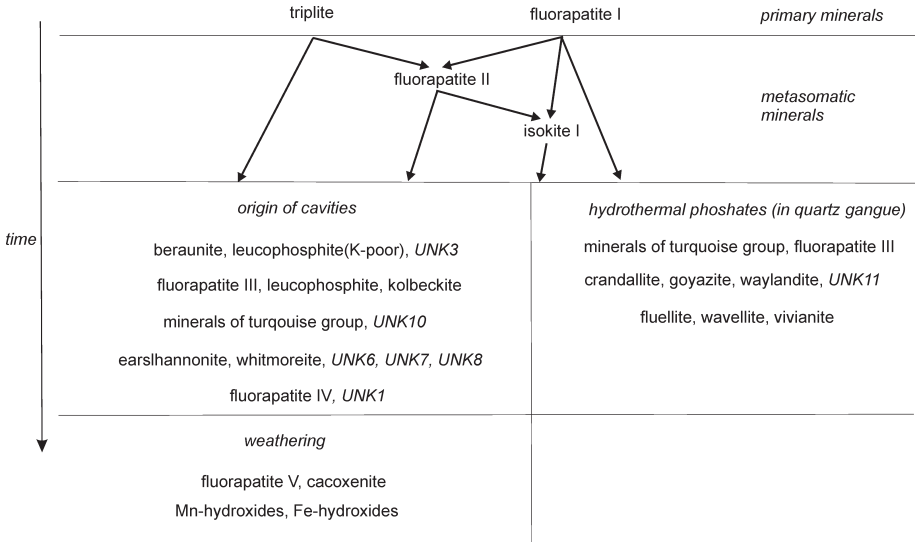

Fig. 90 Schematic presentation of the evolution of phosphate mineral associations in the Huber open pit, Krásno.

of Mg in primary triplite from the Huber open pit (Mg/(Mg+Fe+Mn) about 0.16), whereas triplite formed at a minimal depth of 200 m of the contact (5th level of the Huber shaft) has Mg/(Mg+Fe+Mn) only about 0.004. The high fluorine contents in fluorapatite, triplite and isokite suggest F-rich environment. The following stage of the evolution of phosphate accumulations is characterized by selective dissolution of fine-grained or compact fluorapatite associated with formation of incoherent isokite aggregates and abundant corrosion cavities from several mm up to 10 cm in size. In the process of fluorapatite dissolution, isokite remains stable, or may be partly dissolved and removed; however, triplite was not affected by these processes.

During the next stage crystallization of beraunite, K-poor leucophosphite and *UNK3*, fluorapatite, leucophosphite and kolbeckite in corrosion cavities took place. Later on, minerals of the turqouise group (chalcosiderite, turquoise, *UNK10*) and arthurite group (earlshannonite, whitmoreite, *UNK6, UNK7, UNK8*) crystallized. Remarkable compositional zoning on microscale is characteristic for this stage. The youngest minerals in cavities include fluorapatite in finely crystallized aggregates and locally abundant phase *UNK1*. The crystallization of these cavity minerals was accompanied by local introduction of As^{5+}, Sc^{3+}, Zn^{2+} a Cu^{2+}, i.e. elements, which are probably derived from altered primary sulphides, arsenides (chalcopyrite, sphalerite, arsenopyrite, tetrahedrite, tennantite) and wolframite, abundant in the apical part of the stock (Beran – Sejkora 2006).

Specific mineral association includes re-mobilized phosphates in cavities of coarse-grained quartz gangue, which are not related in their distribution to phosphate accumulations described above. Minerals of the turqouise group (chalcosiderite – turquoise), fluorapatite, minerals of the crandallite group (dominant goyazite, crandallite, waylandite and *UNK11*), vivianite, fluellite and wavellite are involved. Phosphates in cavities are accompanied by fluorite, topaz and minerals of kaolinite group. The relative time of crystallization of this association is somewhat uncertain. Based on indirect indications we assume that it may be approximately coeval with crystallization of younger phosphates in corrosional cavities of phosphate accumulations.

The latest stage of phosphate formation in the Huber open pit domain (filling of corrosion cavities and re-mobilized phosphates in cavities of quartz gangue) was characterized by exceptionally high fluorine activity as well. This is indicated by crystallization of the youngest fluorapatites and the abundant occurrence of a F-analogue of perhamite – mineral *UNK1* in cavities of phosphate accumulations, or the high F content in minerals of the crandallite group and locally rich occurrence of fluellite in quartz gangue cavities. Elevated contents of Sr, derived probably from dissolution of older generations of fluorapatite containing minor Sr, are interesting. Sr-dominated goyazite is the most common species among minerals of the crandallite group and Sr is also important as a regular minor element in *UNK1*.

5th level of the Huber shaft

The mineral association of phosphates at the 5th level of the Huber shaft evolved (Fig. 91) in the environment of greisenized granite stock with local development of extensive horizons of compact quartz, c. 200 m below contact with overlying gneisses and at about a similar depth below the present land surface.

The primary phosphates occur as large aggregates of triplite and compact fluorapatite. During the early hydrothermal stage triplite was extensively replaced by younger fluorapatite. This fluorapatite (together with a part of primary fluorapatite) was extensively selectively replaced by isokite, replacement of triplite by isokite was not observed. Subsequent extensive replacement of both generations of fluorapatite, and less commonly triplite, by

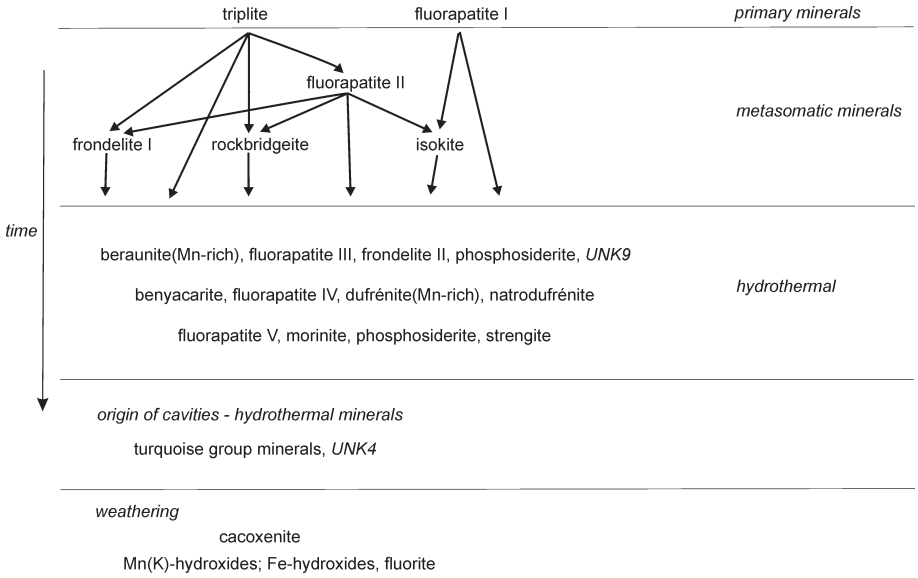

Fig. 91 Schematic presentation of the evolution of phosphate mineral associations at the 5th level of the Huber shaft, Krásno.

minerals of the rockbridgeite – frondelite (I) series resulted in formation of their large accumulations, up to 10 cm in size. Formation of abundant isokite aggregates during this stage indicates significant import of Mg (probably from rocks of the metamorphic envelope – see above). Fluorine contents in triplite, fluorapatite and isokite and their abundance indicate F-rich environment. Formation of minerals of the rockbridgeite – frondelite series points to locally significant import of Fe, Mn and some Zn.

During a later hydrothermal stage (or several overlapping stages) extensive alteration of Fe-Mn phosphates proceeded, whereas older triplite, fluorapatite and isokite were altered only exceptionally. The aggregates of Fe-Mn phosphates (predominating frondelite I and rare rockbridgeite) were first replaced by frondelite II, *UNK9*, Mn-rich beraunite and to a lesser extent by fluorapatite and phosphosiderite. This stage was followed by formation of Mn-rich dufrénite, natrodufrénite, fluorapatite and rare benyacarite crystals in small cavities. During the latest stage aggregates of abundant phosphosiderite formed in addition to fluorapatite, less common morinite and strengite as one of the latest phases.

The hydrothermal phosphates contain remarkably increased Mn, frondelite is more abundant than rockbridgeite, and *UNK9*, Mn-rich beraunite and dufrénite-related minerals occur, all indicating environment with a high Mn/Fe ratio. This high ratio is probably one of the general geochemical characteristics of the Huber stock. The increased Mn content in the studied apatites is remarkable. The enrichment in Mn is even higher in the nearby Schnöd stock as indicated by the occurrences of carpholite, rodochrosite, hübnerite etc.

During a following stage, dissolution of compact fluorapatite and its removal, accompanied by partial removal of isokite, resulted in formation of corrosion cavities 5–10 cm across, within the phosphate accumulations. However, the extent of this process and abundance of corrosion cavities at the 5th level of the Huber shaft is significantly lower, relative to the situation in the Huber open pit. Minerals of the turquoise group (chalcosiderite and turquoise), fluorapatite and local rich aggregates of *UNK4* crystallized in the cavities.

The environment during all stages of evolution of the phosphate accumulations was rich in fluorine. This is indicated by several successive generations of fluorapatite, the presence of F-rich morinite, *UNK4* and by abundance of small fluorite aggregates in the mineral associations.

Acknowledgements. We thank the following colleagues for their cooperation – Jiří Litochleb (National Museum, Prague), František Veselovský and Stanislav Vrána (Czech Geological Survey, Prague), Miroslava Novotná and Jana Ederová (Institute of Chemical Engineering, Prague), Jakub Plášil, Martin Mazuch and Oldřich Fatka (Faculty of Science, Charles University, Prague) and Jaromír Tvrdý and Zdeněk Mach (Karlovy Vary).

This work was supported by Grants from the Ministery of Culture of the Czech Republic (Project MK00002327201) and the Granting Agency of the Czech Republic (Grant No. 205/03/D004).

Submitted June 9, 2006

References

Anthony, J. W. – Bideaux, R. A. – Bladh, K. W. – Nichols, M. C. (2000): Handbook of Mineralogy. Volume IV. Arsenates, Phosphates, Vanadates. Mineral Data Publishing, Tucson, 680 pp.

Baldwin, J. R. – Hill, P. G. – von Knorring, O. – Oliver, G. J. H. (2000): Exotic aluminium phosphates, natromontebrasite, brazilianite, goyazite, gorceixite and crandallite from rare-element pegmatites in Namibia. – Min. Mag., 64: 1147–1164.

Bayliss, P. (1986): X-ray powder data for nissonite and waylandite. – Powder Diffr., 1: 331–333.

Beran, P. (1999): Minerals of tin-tungsten deposits in the Slavkovský les area. – Regional Museum and Library in Sokolov, Sokolov, 287 pp., (in Czech).

Beran, P. – Sejkora, J. (2006): The Krásno Sn-W ore district near Horní Slavkov: mining history, topographical, geological and mineralogical characteristics. – J. Czech Geol. Soc., 51: 3–42

Blass, G. – Witternn, A. (1994): Neue Mineralien von der Rubocin Mine bei Karibib, Namibia. – Mineral. Welt, 5:25–31.

Borensztajn, J. (1966): Structure cristallines de la metavariscite et de la metastrengite. – Bull. Soc. Franc. Min. Crist., 89: 428–438.

Clark, A. M. – Couper, A.G. – Embrey, P. G. – Fejer, E. E. (1986): Waylandite: new data, from an occurrence in Cornwall, with a note of agnesite. – Miner. Mag., 50: 731–733.

Chen, N. – Pan, Y. – Weil, J., A. (2002): Electron paramagnetic resonance spectroscopic study of synthetic fluorapatite: Part I. Local structural environment and substitution mechanism of Gd^{3+} at the Ca2 site. – Amer. Mineral., 87: 37–46.

Chopin, C. – Armbruster, T. – Baronnet, A. – Grew, E. S. (2004): Polytypism in the wagnerite-triplite group, $(Mg,Fe,Mn)_2PO_4(F,OH)$, and discreditation of magniotriplite. – 5th International conference "Mineralogy and Museums", Paris. Collected abstracts.

Deans, T. – McConnell, J. D. C. (1955): Isokite, a new mineral from Nothern Rhodesia. – Miner. Mag., 30: 681–691.

Demartin, F. – Gay, H. D. – Gramaccioli, C. M. – Pilati, T. (1997): Benyacarite, a new titanium-bearing phosphate mineral species from Cerro Blanco, Argentina. – Can. Mineral., 35: 707–712.

Demartin, F. – Pilati, T. – Gay, H. D. – Gramaccioli, C. M. (1993): The crystal structure of a mineral related to paulkerrite. – Zeit. Krist., 208: 57–71.

Dick, S. – Zeiske, T., (1997): Leucophosphite $K[Fe_2(PO_4)_2(OH)(H_2O)].H_2O$: Hydrogen Bonding and Structural Relationships. – Journ. Solid State Chemistry, 133: 508–515.

di Cossato, M. F. Y. – Orlandi, P. – Pasero, M. (1989): Manganese-bearing beraunite from Mangualde, Portugal: mineral data and structure refinement. – Can. Mineral., 27: 441–446.

Fanfani, L. – Zanazzi, P. F. (1966): La struttura cristallina della metastrengite. – Atti della Accademia Nazionale dei Lincei, Classe di Scienze Fisiche, Matematiche e Naturali, Rendiconti, 8, 40: 889–889.

– (1967): The crystal structure of beraunite. – Acta Cryst. 22: 173–181.

Farmer, V. C. (ed.) (1974): The infrared spectra of minerals. – Mineralogical Society Monograph., 4: 1–539.

Fischer, J. D. (1957): Isokite and triplite from Bohemia. – Miner. Mag., 31: 587–602.

– (1960): Morinite-apatite-whitlockite. – Amer. Mineral., 45: 645–667.

Fischer, J. D. – Runner, Ju. J. (1958): Morinite from the Black Hills. – Amer. Mineral., 43: 585–594.

Fontan, F. – Pillard, F. – Permingeat, F. (1982): La natrodufrénite $(Na,\square)(Fe^{+++},Fe^{++})(Fe^{+++},Al)_5(PO_4)_4(OH)_6.2H_2O$, une nouvelle espece minérale du groupe de la dufrenite. – Bull. Minéral., 105: 321–326.

Foord, E. E. – Taggart, J. E. Jr. (1998): A reexamination of the turquoise group: the mineral aheylite, planerite (redefined), turquoise and coeruleolactite. – Miner. Mag., 62: 93–111.

Fransolet, A.-M. – Oustriere, P. – Fontan, F. – Pillard, F. (1984): La mantiennéite, une nouvelle espece minérale du gisement de vivianite d'Anloua, Cameroun. – Bull. Minéral., 107: 737–744.

Guy, B. B. – Jeffrey, G. A (1966): The crystal structure of fluellite, $Al_2PO_4F_2(OH)(H_2O)_7$. – Amer. Mineral., 51: 1579–1592.

Hawthorne, F. C. (1979): The crystal structure of morinite. – Can. Mineral., 17: 93–102.

Hey, M. H. – Milton, C. – Dwornik, E. J. (1982): Eggonite (kolbeckite, sterrettite), $ScPO_4 . 2H_2O$. – Mineral. Mag., 46: 493–497.

Hochleitner, R. – Fehr, K. T. (2005): Isokite, $CaMg[F|PO_4]$, from Senhora de Assunçao, Portugal: new find and new data. – N. Jb. Miner. Abh., 182: 103–108.

Hughes, J. M. – Ertl, A. – Bernhardt, H., J. – Rossman, R. – Rakovan, J. (2004): Mn-rich fluorapatite from Austria: Crystal structure, chemical analysis, and spectroscopic investigations. – Amer. Mineral., 89: 629–632.

Isaacs, M. A., Peacor, D. P. (1981): Panasqueiraite, a new mineral: the OH-equivalent of isokite. Can. Mineral., 19: 389–392.

Jaffe, H. W. – Hall, L. M. – Evans, H. T. (1992): Wagnerite and isokite from Benson Mines, west-central Adirondack Highlands, New York. – Miner. Mag., 56: 227–233.

Knorring von, O. – Lehtinen, M. – Sahama, T. G. (1977): Burangaite, a new phosphate mineral from Rwanda. – Bull. Geol. Soc. Finland, 49:33–36.

Knorring von, O. – Mrose, M. E. (1963): Westgrenite and waylandite, two new bismuth minerals from Uganda. – Geol. Soc. Amer. Spec. Paper 73, 256A.

Korbel, P. (1991): Supergene minerals from Horní Slavkov. – Sbor. Nár. Muz. (Praha); B47: 1–24.

Kydryashova, V. I. – Rozhdestvenskaya, I. V. (1991): New minerals XLV. – Zap. Vses. Mineral. Obshch., 120: 100-115 – reference of book *Chesnokov, B. V. – Vilisov, V. A. – Polakov, V. O. – Bushmakin, A. F.*: Mineraly i mineralnoe syre gorno-promyshlennykh rajonov Urala; see also – *Vasil´ev, E., Chesnokov, B*. (1991): Institute of the Earth´s crust, Lermontov, Irkutsk, Russia, private communication in ICDD card No. 44–1404.

Leroy, N. – Bres, E. (2001): Structure and substitutions in fluorapatite. – European Cells and Materials, 2: 36–48.

Lindberg, M. L. (1949): Frondelite and frondelite-rockbridgeite series. – Amer. Mineral., 34: 541–549.

– (1957): Leucophosphite from the Sapucaia pegmatite mine, Minas Gerais, Brazil. – Amer. Mineral., 42: 214–221.

Lindberg, M. L. – Frondel, C. (1950): Zincian rockbridgeite. – Amer. Mineral., 35: 1028–1034.

Lottermoser, B. G. – Lu, J. (1997): Petrogenesis of rare-element pegmatites in the Olary Block, South Australia, part 1. Mineralogy and chemical evolution. – Mineral. Petrol., 59: 1–19.

Mach, Z. (1979): Chalkosiderite and Ba-pharmacosiderite from Krásno near Horní Slavkov – a find report. – Čas. Mineral. Geol., 79: 90–91, (in Czech).

Marincea, Ş. – Dumitras, D. – Gibert, R. (2002): Tinsleyite in the "dry" Cioclovina Cave (Sureanu Mountains, Romania): the second occurrence. – Eur. J. Mineral., 14: 157–164.

McKie, D. (1962): Goayzite and florencite from two African carbonatites. – Miner. Mag. 33: 281–297.

Medrano, M. D. – Piper, D. Z. (1997): Fe-Ca-phosphate, Fe-silicate, and Mn-oxide minerals in concretion fron the Monerey Formation. – Chemical Geology, 138, 9–23.

Moore, P. B. (1970): Crystal chemistry of the basic iron phosphates. – Amer. Mineral., 55: 135–169.

– (1972): Octahedral tetramer in the crystal structure of leucophosphite, $K_2[Fe^{3+}_4(OH)_2(H_2O)_2(PO_4)_4] . 2H_2O$. – Amer. Mineral., 57, 397–410.

Moore, P. B. (1982): Pegmatite minerals of P(V) and B(III). – *In:* Černý, P. ed.: Granitic pegmatite in science and industry. – MAC Short course, 8: 267–291.

Moore, P. B. – Kampf, A. R. (1992): Beraunite: refinement, comparative crystal chemistry, and selected bond valences. – Zeit. Krist., 201: 263–281.

Mrázek, Z. (1981): Crandallite and mixite from Horní Slavkov. – Sbor. Vys. Šk. chem.-technol., mineral., G 20: 43–47, (in Czech).

Novák, F. – Jansa, J. – Prachař. I. (1994): Classification and nomenclature of alunite – jarosite and related mineral groups. – Věst. Čes. geol. úst., 69: 51–58.

Novák, F. – Pauliš, P. – Süsser, C. (2001): Chemical composition of crandallite, goyazite and waylandite from Krásno near Horní Slavkov. – Bull. mineral. – petrolog. Odd. Nár. Muz. (Praha), 9: 230–234, (in Czech).

Ondruš, P. (1993): ZDS – A computer program for analysis of X-ray powder diffraction patterns. – Materials Science Forum, 133–136: 297–300, EPDIC-2. Enchede.

Ondruš, P. – Skála, R. (1997): New quasi-empirical channel Search/Match algorithm for ICDD PDF2 Database: A tool for qualitative phase analysis integrated in the ZDS-System software package for X-ray powder diffraction analysis – Fifth European Powder Diffraction Conference EPDIC-5, 193. Parma.

Palache, Ch. – Berman, H. – Frondel, C. (1951) Dana's System of Mineralogy. 7th edition, vol. II, J. Wiley and Sons, 920 pp.

Peacor, D. R. – Dunn, P. J. – Simmons, W. B. (1984): Paulkerrite, a new titanium phosphate from Arizona. – Min. Record: 303–306.

Pe-Piper, G. – Dolansky, L. M. (2005): Early diagenetic origin of Al phosphate-sulfate minerals (woodhouseite and crandallite series) in terrestrial sandstones, Nova Scotia, Canada. – Amer. Mineral., 90: 1434–1441.

Pollmann, H. – Witzke, T. – Keck, E. – Steins, M. – Friese, K. – Goske, J. (1998): Martin-Luther-Univ. Halle, Wittenberg, Germany; ICDD Grant-in-Aid (ICDD card 50-1552).

Pouchou, J. L. – Pichoir, F. (1985): "PAP" procedure for improved quantitative microanalysis. – Microbeam Analysis, 20: 104–105.

Povarennykh, A. S. (1972): Crystal Chemical Classification of Minerals. (English Edition). Plenum Press, New York. pp 349.

Puziewicz, J. – Johannes, W. (1988): Phase equilibria and composition of Fe-Mg-Al minerals and melts in water-saturated peraluminous granitic system. – Contr. Miner. Petr., 100: 156–168.

– (1990): Experimental study of biotite-bearing granitic system under water-saturated and water-unsaturated conditions. – Contr. Miner. Petr., 104: 397–406.

Raudsep, M. (1995): Recent advances in the electron-probe analysis of minerals for the light elements. – Can. Mineral., 33: 203–218.

Roda-Robles, E. – Fontan, F. – Pesquera Pérez, A. – Keller, P. (1998): The Fe-Mn phosphate associations from the Pinilla de Fermoselle pegmatite, Zamora, Spain: occurrence of kryzhanovskite and natrodufrénite. – Eur. J. Mineral., 10: 155–167.

Rodríguez-Carvajal, J. (2005): Computer Program FullProf, ver. December 2005. – Laboratoire Leon Bril-louin (CEA-CNRS), France.

Scott, K. M. (1987): Solid solution in, and classification of, gossan-derived members of the alunite-jarosite family, northwest Queensland, Australia. – Amer. Mineral., 72: 178–187.

Sejkora, J. – Škoda, R. – Ondruš, P. (2006d): New naturally occurring mineral phases from the area Krásno – Horní Slavkov, western Bohemia, Czech Republic. – Journ. Czech Geol. Soc., 51: 159–188

Selway, J. B. – Cooper, M. A. – Hawthorne, F. C. (1997): Refinement of the crystal structure of burangaite. – Can. Mineral., 35:1515–1522.

Schwab, R. G. – Pimpl, T. – Schukow, H. – Stolle, A. – Breitinger, D. K. (2004): Compounds of the crandallite-type: Synthesis, properties and thermodynamic data of pure crandallite and woodhouseite. – N. Jb. Miner. Mh., 385–409.

Tadini, C. (1981): Magniotriplite: its crystal structure and relation to the triplite-triploidite group. – Bull. Soc. Franc., Miner. Crist., 104: 677–680.

Taxer, K. – Bartl, H. (2004): On the dimorphy between the variscite and clinovariscite group: refined finestructural relationship of strengite and clinostrengite, $Fe(PO_4)$. $2(H_2O)$. – Crystal Research Technol., 39: 1080–1088.

Waldrop, L. (1968): The crystal structure of triplite. – Naturwissenschaften, 55: 178.

– (1969): Study of minerals with the formula type $ABXO_4(Z)$, with special attention to the crystal structures of the triplite-triploidite group. – PhD. thesis, Massachusetts Institute of Technology. 136 pp.

Wambeke van, L. (1975): La zairite, un nouveau minéral appartenant à la série de la crandallite. – Bull. Soc. fr. Minéral., 98: 351–353.

Wilson, M. J. – Bain., D. C. (1976): Occurence of leucophosphite in a soil from Elephant Island, Brithis Antarctic Territory. – Amer. Mineral., 61, 1027–1028.

– (1986): Sphenicsidite, a new phosphate mineral from Elephant Island, British Antarctic Territory. – Miner. Mag., 50, 291–293.

Yakubovich, O. V. – Simonov, M. A. – Matvienko, E. N. – Belov, N. V. (1978): The crystal structure of the synthetic finite Fe-term of the series triplite – zwieselite $Fe_2(PO_4)F$. – Dokl. Akad. Nauk SSSR, 238, 576–579.

Mineralogie akumulací fosfátů oblasti Huberova pně, rudní revír Krásno, Slavkovský les, Česká republika

Podrobný výzkum byl zaměřen na minerály fosfátových akumulací, zjištěných v povrchovém lomu na Huberově pni a na 5. patře dolu Huber v Sn-W rudním revíru Krásno, Slavkovský les (Česká republika). Na studovaných lokalitách byly zjištěny výskyty benyacaritu, beraunitu, chalkosideritu, crandallitu, dufrénitu, earlshannonitu, fosfosideritu, fluellitu, fluorapatitu, frondelitu, goyazitu, isokitu, kakoxenu, kolbeckitu, leukofosfitu, morinitu, natrodufrénitu, rockbridgeitu, strengitu, triplitu, tyrkysu, vivianitu, wavellitu, waylanditu, whitmoreitu a zwieselitu. Pro jednotlivé zjištěné minerální druhy je podána makro- i mikroskopická charakteristika, rentgenová prášková data a/nebo vypřesněné parametry základní cely a výsledky kvantitativních chemických analýz. Zjištěná data jsou podrobně diskutována v porovnání s publikovanými údaji pro jednotlivé minerální druhy.

Součástí článku je i přehled vývoje minerálních asociací fosfátů na obou studovaných lokalitách.